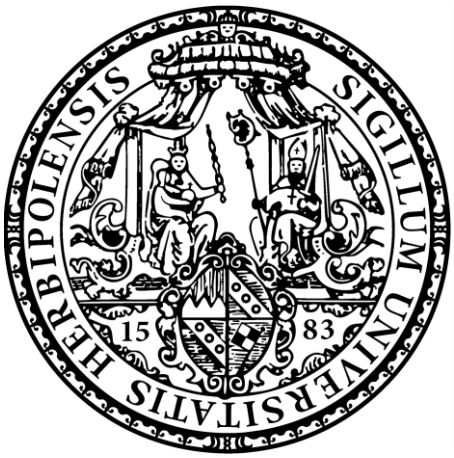


# Activation of the integrated stress response induces remodeling of cardiac metabolism in Barth Syndrome

# Aktivierung der "Integrated Stress Response" führt zur Umstellung des kardialen Metabolismus im Barth Syndrom

Doctoral thesis for a doctoral degree
at the Graduate School of Life Sciences,
Julius-Maximilians-Universität Würzburg,
Section: Biomedicine

submitted by

**Ilona Kutschka**

from

**Munich**

Würzburg, 2023

**Submitted on**:……..……..

Office stamp

## Members of the Thesis Committee

**Chairperson:** Prof. Dr. David Stegner

**Primary Supervisor:** Prof. Dr. Christoph Maack

**Supervisor (Second):** Prof. Dr. Almut Schulze

**Supervisor (Third):** Prof. Dr. Alma Zernecke-Madsen

**Supervisor (Fourth):** Dr. Jan Dudek

**Date of Public Defense: ……..……**

**Date of Receipt of Certificates:…….**

# Abstract

Barth Syndrome (BTHS) is an inherited X-chromosomal linked disorder, characterized by early development of cardiomyopathy, immune system defects, skeletal muscle myopathy and growth retardation. The disease displays a wide variety of symptoms including heart failure, exercise intolerance and fatigue due to the muscle weakness. The cause of the disease are mutations in the gene encoding for the mitochondrial transacylase Tafazzin (*TAZ*), which is important for remodeling of the phospholipid cardiolipin (CL). All mutations result in a pronounced decrease of the functional enzyme leading to an increase of monolysocardiolipin (MLCL), the precursor of mature CL, and a decrease in mature CL itself. CL is a hallmark phospholipid of mitochondrial membranes, highly enriched in the inner mitochondrial membrane (IMM). It is not only important for the formation of the cristae structures, but also for the function of different protein complexes associated with the mitochondrial membrane. Reduced levels of mature CL cause remodeling of the respiratory chain supercomplexes, impaired respiration, defects in the Krebs cycle and a loss of mitochondrial calcium uniporter (MCU) protein. The defective $Ca^{2+}$ handling causes impaired redox homeostasis and energy metabolism resulting in cellular arrhythmias and defective electrical conduction. In an uncompensated situation, blunting mitochondrial $Ca^{2+}$ uptake provokes increased mitochondrial emission of $H_2O_2$ during workload transitions, related to oxidation of NADPH, which is required to regenerate anti-oxidative enzymes. However, in the hearts and cardiac myocytes of mice with a global knock-down of the *Taz* gene (*Taz*-KD), no increase in mitochondrial ROS was observed, suggesting that other metabolic pathways may have compensated for reduced Krebs cycle activation.

The healthy heart produces most of its energy by consuming fatty acids. In this study, the fatty acid uptake into mitochondria and their further degradation was investigated, which showed a switch of the metabolism in general in the *Taz*-KD mouse model. *In vivo* studies revealed an increase of glucose uptake into the heart and decreased fatty acid uptake and oxidation. Disturbed energy conversion resulted in activation of retrograde signaling pathways, implicating overall changes in the cell metabolism. Upregulated integrated stress response (ISR) was confirmed by increased levels of the downstream target, i.e., the activating transcription factor 4 (ATF4). A *Tafazzin* knockout mouse embryonal fibroblast cell model ($Taz^{KO}$) was used to inhibit the ISR using siRNA transfection or pharmaceutical inhibition. This verified the central role of

the ISR in regulating the metabolism in BTHS. Moreover, an increased metabolic flux into glutathione biosynthesis was observed, which supports redox homeostasis. *In vivo* PET-CT scans depicted elevated activity of the xCT system in the BTHS mouse heart, which transports essential amino acids for the biosynthesis of glutathione precursors. Furthermore, the stress induced signaling pathway also affected the glutamate metabolism, which fuels into the Krebs cycle via $\alpha$-ketoglutarate and therefore supports energy converting pathways. In summary, this thesis provides novel insights into the energy metabolism and redox homeostasis in Barth syndrome cardiomyopathy and its regulation by the integrated stress response, which plays a central role in the metabolic alterations. The aim of the thesis was to improve the understanding of these metabolic changes and to identify novel targets, which can provide new possibilities for therapeutic intervention in Barth syndrome.

# Zusammenfassung

Barth Syndrome (BTHS) ist eine X-chromosomal vererbbare Erkrankung, welche sich in der frühen Entstehung von Kardiomyopathie, Störungen des Immunsystems, Skelettmuskelschwäche und Wachstumsverzögerungen manifestiert. Das Krankheitsbild ist sehr variabel mit milden Symptomen bis hin zu sehr schwerwiegenden Fällen, bei denen die schnelle Verschlechterung der Kardiomyopathie bereits in jungen Jahren eine Herztransplantation erfordern kann. Betroffenen Patienten zeigen eine deutliche Intoleranz gegenüber körperlicher Anstrengung, welche mit schneller Müdigkeit einhergeht. Die Krankheit wird durch verschiedene Mutationen auf dem Gen für die mitochondriale Transacylase Tafazzin (TAZ) ausgelöst. Die Mutationen führen zu einem Funktionsverlust des Enzyms, welches in der Biosynthese des Phospholipids Cardiolipin (CL) eine entscheidende Rolle spielt. Die Vorstufe des Lipids, das sogenannte Monolysocardiolipin (MLCL), reichert sich dadurch an, wohingegen die Menge an reifem CL entscheidend verringert ist. CL ist ein bedeutendes Phospholipid in den Mitochondrien, wo es vor allem in der inneren Mitochondrien Membran vorkommt. CL ist einerseits wichtig für die Ausbildung der Cristae Strukturen der inneren Mitochondrien Membran. Darüber hinaus ist es notwendig für die Struktur und Funktion verschiedenster Proteinkomplexe in der Membran, welche dadurch erst ihre volle Funktionsfähigkeit erhalten. Es wurde bereits gezeigt, dass der Verlust von reifem CL in BTHS zu einer Dissoziation der Superkomplexe der Atmungskette führt, welche dadurch in ihrer Funktion beeinträchtigt ist. Zusätzlich sind Störungen im Krebs Zyklus und der Kalziumaufnahme durch den mitochondriellen Kalzium ($Ca^{2+}$) -Uniporter (MCU) Komplex bekannt. Die beeinträchtigte mitochondriale $Ca^{2+}$ Aufnahme beeinflusst sowohl die Redox Homöostase als auch den Energie Metabolismus, was zu Arrhythmien und einer Störung der elektrischen Weiterleitung im Herzen führt. Im gesunden Herzen gewinnen die Herzmuskelzellen den Hauptanteil ihrer Energie aus dem Abbau von Fettsäuren. In dieser Studie wurde durch die Untersuchung des Fettsäurestoffwechsels im *Taz* knockdown Mausmodell (*Taz*-KD) gezeigt, dass eine deutliche Reduktion in Proteinen vorliegt, welche für die Aufnahme und die Verstoffwechselung der Fettsäuren in den Mitochondrien verantwortlich sind. Diese Veränderungen führten *in vivo* zu einer verringerten Aufnahme und Verstoffwechselung von Fettsäuren und einer Erhöhten Aufnahme von Glucose. Dysfunktionale Mitochondrien aktivieren retrograde Signalwege, welche eine generelle

Umstellung des Metabolismus zur Folge haben. Eine erhöhte Menge des Transkriptionsfaktors ATF4, welcher sowohl Fettsäure- als auch Aminosäuremetabolismus beeinflusst, zeigte die Aktivierung der sogenannten „Integrated stress response“ (ISR). Ein Zellmodel embryonaler Fibroblasten aus der Maus mit einem *Taz* knockout ($Taz^{KO}$) wurde verwendet um die ISR durch siRNA Transfektion oder einem pharmakologischen Inhibitor zu blockieren. Dadurch konnte die zentrale Rolle der ISR in der Umstellung des Metabolismus bestätigt werden. Zusätzlich konnte eine erhöhte metabolische Aktivität in Richtung der Glutathion Biosynthese beobachtet werden, welche für die Redox Homöostase in den Mitochondrien von Bedeutung ist. *In vivo* PET-CT Untersuchungen zeigten eine erhöhte Aktivität des xCT Systems im Herzen des BTHS Mausmodells auf. Dies dient der Aufnahme von Aminosäuren, welche für die Glutathion Biosynthese benötigt werden. Hinzu kommt, dass die Aktivierung des Stresssignalweges den Glutamat Stoffwechsel in der Zelle beeinflusste. Über $\alpha$-Ketoglutarat trägt Glutamat so vermehrt zur Energiegewinnung bei. Das Ziel dieser Doktorarbeit war es, die metabolischen Veränderungen in BTHS zu untersuchen, um die veränderten Vorgänge besser zu verstehen und so neue mögliche Angriffspunkte für Therapiemöglichkeiten zu identifizieren.

# Table of contents

Abstract ..... I

Zusammenfassung ..... III

1. Introduction ..... 1

1.1 Mitochondrial function in energy metabolism ..... 1

1.1.1 Cardiolipin – a hallmark phospholipid in mitochondrial membranes ..... 2

1.1.2 The role of cardiolipin in energy production at the electron transport chain 3

1.1.3 Mitochondrial homeostasis of reactive oxygen species and its effects on cardiolipin ..... 5

1.1.4 The role of cardiolipin in fatty acid metabolism in mitochondria ..... 6

1.1.5 Additional functions of cardiolipin ..... 8

1.2 Barth Syndrome ..... 10

1.2.1 Clinical characteristics of Barth Syndrome ..... 10

1.2.2 Model organisms for Barth Syndrome research ..... 12

1.2.3 Treatment approaches for Barth Syndrome ..... 14

1.3 The integrated stress response ..... 15

1.4 The one-carbon metabolism ..... 17

1.5 Aim of the thesis ..... 19

2. Materials ..... 21

2.1 Model organisms and biopsy samples ..... 21

2.2 Chemicals ..... 21

2.3 Antibodies ..... 26

2.4 Oligonucleotides ..... 27

2.5 Kits ..... 30

2.6 Buffers and solutions ..... 31

2.7 Media for cell culture ..... 33

2.8 Consumables ..... 34

2.9 Equipment ..... 35

2.10 Softwares ..... 36
3. Methods ..... 38
3.1 *Taz*-KD mouse ..... 38
3.2 Cultivation of mouse embryonal fibroblasts ..... 38
3.3 Cultivation of induced pluripotent stem cells and their differentiation into cardiac myocytes ..... 39
3.4 siRNA mediated knockdown ..... 40
3.5 *In vitro* ISRIB treatment ..... 40
3.6 RNA isolation from tissue or cells ..... 41
3.7 Digestion of genomic DNA ..... 41
3.8 RNA transcription into cDNA ..... 41
3.9 quantitative real-time PCR ..... 42
3.10 Whole tissue lysate of mouse tissue ..... 42
3.11 Whole tissue lysates of mouse embryonal fibroblasts ..... 43
3.12 Mitochondria isolation of heart tissue ..... 43
3.13 Mitochondria isolation of MEF cells ..... 44
3.14 SDS-polyacrylamide gel electrophoresis (SDS-PAGE) and Western Blotting 44
3.15 Respiration measurements using the Oroboros Oxygraph-2k ..... 45
3.16 Protein determination ..... 46
3.17 Glutathione assay ..... 46
3.18 Enzymatic formate assay ..... 46
3.19 $^{13}C_6$ glucose labeling in mouse embryonal fibroblasts ..... 47
3.20 *In vivo and in vitro* radiotracer experiments and PET-CT scan ..... 47
3.21 RNaseq analyses ..... 47
3.22 Data analysis ..... 47
4. Results ..... 48
4.1 Defective fatty acid metabolism in Barth Syndrome ..... 48

4.2 Conversions in the mitochondrial intermediate metabolism in Barth Syndrome .....53
4.3 The integrated stress response signaling regulates metabolic changes in Barth syndrome .....59
4.4 Remodeling of glutamate metabolism in Barth Syndrome .....65
5. Discussion .....74
5.1 Metabolic switch from fatty acid oxidation to glycolysis in Barth Syndrome .....74
5.2 Activation of the integrated stress response causes metabolic remodeling in Barth Syndrome .....76
5.3 Remodeling of the mitochondrial metabolism supports glutathione synthesis and anaplerosis .....80
5.4 Outlook .....84
6. Bibliography .....89
7. Appendix .....109
7.1 Abbreviations .....109
7.2 List of figures .....111
7.3 List of tables .....112
7.4 Acknowledgement .....113
7.5 Curriculum vitae .....114
7.6 Publications in peer reviewed journals .....116
7.7 Affidavit .....117
7.8 Eidesstattliche Erklärung .....117

# 1. Introduction

## 1.1 Mitochondrial function in energy metabolism

Mitochondria were first of all described as granular structures in muscle cells by Albert von Koelliker in 1856 (as cited in [1]). In the late 20$^{th}$ century Richard Altmann referred to so called “Bioplasts” as “autonomous elementary organisms responsible for metabolic and genetic functions” (as cited in [2]). In 1927 Ivan Emmanuel Wallin, already using the term mitochondria, claimed their origin from endosymbiosis of a bacterial progenitors [3]. This theory is supported by the structural characteristics of mitochondria consisting of a double membrane structure, own mitochondrial DNA, and the ability for autonomous translation of proteins due to own ribosomes. The outer mitochondrial membrane (OMM) not only encloses the organelle to separate it from the cytosol, but is also important for the mitochondrial interplay with other cellular components such as the plasma membrane, the endoplasmic reticulum, lysosomes or peroxisomes [4-6]. The inner mitochondrial membrane (IMM) further separates the organelle into an intermembrane space (IMS) between the two membranes and the mitochondrial matrix (MM). Cristae formation of the IMM [7] leads to an enlargement of the membrane surface. The proper organization of these invaginations is ensured by the mitochondrial contact site and cristae organizing system (MICOS) [8]. Cristae structures harbor the complexes of the electron transport chain and the ATP synthase that are integrated in the IMM [9].

Mitochondria play a crucial role in various cellular processes and are often referred to as the “powerhouse of the cell” as one of their main function is energy conversion and production of adenosine triphosphate (ATP). In addition, mitochondria are also important organelles for $Ca^{2+}$ homeostasis [10-12] and the regulation of reactive oxygen species (ROS) balance by its production and elimination [13-16], which triggers different signaling pathways such as autophagy, necrosis and apoptosis [17]. Furthermore, mitochondrial structures and products are involved in the activation of an immune response [18, 19]. High mitochondrial dynamics enable the organelle to respond to environmental changes. Mitochondria can change their shape as a result of fusion and fission events. In mammals the main important components for proper mitochondrial fusion are mitofusins (Mfn1 and Mfn2) [20] as well as the dynamin-

related GTPase OPA1 [21], whereas the dynamin-related GTPase DRP1 is required for mitochondrial fission [22].

### 1.1.1 Cardiolipin – a hallmark phospholipid in mitochondrial membranes

Cell organelles are not only surrounded by membranes for their compartmentalization, but also crucial processes need the membrane structures for proper function of their proteins. Cardiolipin (CL) is a phospholipid almost exclusively present in mitochondrial membranes and was first isolated from beef heart [23, 24]. It is more abundant in the inner- than in the outer mitochondrial membrane [25]. Most phospholipids are synthesized in the endoplasmic reticulum (ER) and subsequently incorporated into their final location, such as mitochondria. In contrast, CL is already synthesized at the inner mitochondrial membrane. The precursor molecule phosphatidic acid (PA) is transported from the ER to the IMM with the help of the protein complex PRELID-TRIAP1 [26] and under the use of cytidine triphosphate (CTP), the phosphatidate cytidylyltransferase TAMM41 catalyzes its conversion to cytidine diphosphate diacylglycerol (CDP-DAG) [27]. Together with glycerol-phosphate, the CDP-diacylglycerol-glycerol-3-phosphate 3-phosphatidyltransferase PGS1 transforms CDP-DAG to phosphatidylglycerol phosphate (PGP) following a dephosphorylation by the phosphatidylglycerophosphatase and protein-tyrosine phosphatase 1 (PTPMT1) [28, 29]. Phosphatidylglycerol then reacts with a second molecule of CDP-DAG forming premature CL. This reaction is catalyzed by the CL synthase (CLS1) [30]. The acyl-chain composition of CL varies in different tissues. Therefore, after the biosynthesis of premature CL, it undergoes a two-step remodeling process. With the removal of one of the four acyl chains, the de-acetylation reaction forms monolysocardiolipin (MLCL), which is followed by the maturation of CL, a re-acetylation reaction that adds the required acyl-chains [31]. The de-acetylation is catalyzed by phospholipases, though the specific enzymes for the de-acetylation of premature CL is not identified yet. Enzymes with CL hydrolyzing activity are $iPLA_2\beta$, $iPLA_2\gamma$, $cPLA_2$, and $sPLA_2$ [32-34]. For the re-acetylation reaction, three different enzymes were identified, including the MLCL acyltransferase (MLCLAT1), acyl-CoA:lysocardiolipin acyltransferase (ALCAT1) or Tafazzin (TAZ) [35-38]. TAZ is considered to be the major enzyme contributing to CL remodeling, as defects in TAZ result in functional defects causing Barth Syndrome [39]. Mature CL consists of a double glycerophosphate backbone and four different fatty acyl chains, giving it a cone like shape [40]. The fatty

acids bound to CL differ in their properties and can build up different CL pools depending on the tissue. For instance, in heart and skeletal muscle, the CL pool contains more than 90 % of tetralinoleoyl-CL, whose four acyl residues consist of linoleic acid molecules, a fatty acid composed of eighteen carbons and two unsaturated bonds [41]. The characteristics of mature CL are relevant for many different functions in the mitochondria and it is therefore essential for the cell organelle.

### 1.1.2 The role of cardiolipin in energy production at the electron transport chain

The mitochondrial electron transport chain (ETC) is part of the OXPHOS system and the final step of energy production in mitochondria. It receives the reducing equivalents nicotinamide adenine dinucleotide (NADH) and flavin adenine dinucleotide ($FADH_2$) from the Krebs cycle, which oxidizes acetyl-CoA derived from different nutrients such as proteins, carbohydrates and fats. The ETC consists of five protein complexes (complex I, II, III, IV and V), that are embedded in the IMM (**Figure 1**) and are highly associated which each other [42]. The electron transfer, which takes place between complexes I to IV of the ETC, is coupled to proton export across the IMM at complexes I, III and IV, establishing a proton gradient between the intermembrane space and the mitochondrial matrix. The electron carrier NADH emits its electron into complex I, which is therefore called NADH dehydrogenase. Containing 45 subunits, complex I is the biggest complex of the ETC [43] and its distinctive L-shaped structure was described in several organisms using electron microscopy [44-47] and later on, higher resolution images were obtained by using X-ray [48, 49]. For each transferred electron, complex I pumps two protons across the IMM [50-52]. Complex II, the succinate dehydrogenase, is besides the ETC also part of the Krebs cycle. This complex consists of four proteins, the flavoprotein, iron-sulfur protein and two membrane anchor proteins [53]. During its reaction to form fumarate from succinate, the covalently bound cofactor FAD is reduced to $FADH_2$, which consequently transfers electrons via three iron-sulfur centers onto ubiquinone in the ETC [53, 54]. Interestingly, complex II doesn´t directly pump protons across the membrane during this process. The electrons from complex I and II are transmitted to complex III, the cytochrome *c* reductase, via ubiquinone. The electrons from complex III are transferred onto cytochrome *c*, which is then oxidized by complex IV, the cytochrome *c* oxidase. Here, the electrons are finally passed onto oxygen to form $H_2O$. The property of the IMM, to be impermeable to protons, allows the generation of an electrical ($\Delta\Psi_m$) and chemical ($\Delta pH$) potential that together

constites the proton-motive force (ΔμH). This proton-motive force is utilized by complex V, the $F_1$-$F_o$ ATP synthase, to phosphorylate adenosine diphosphate (ADP) producing the energy storage molecule ATP [55].

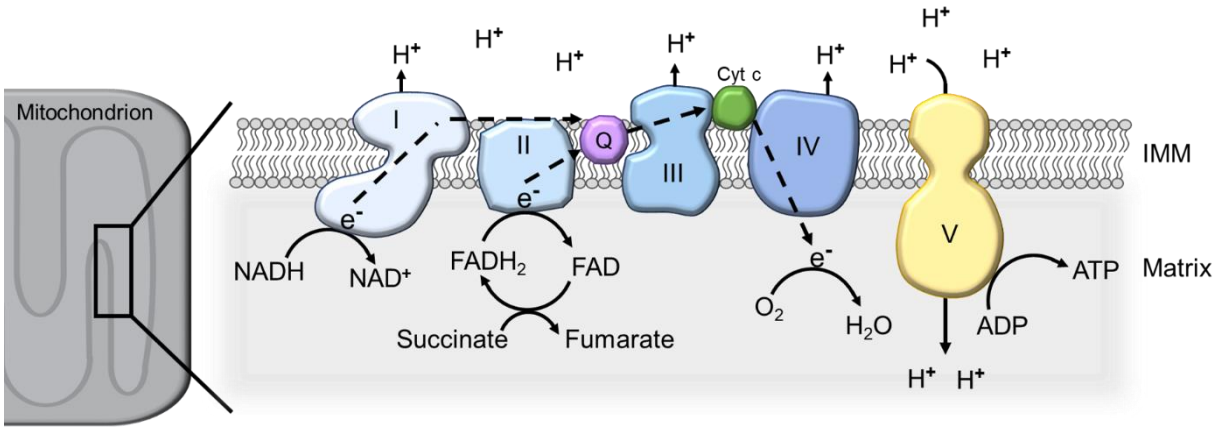


**Figure 1: Schematic overview of the electron transport chain at the inner mitochondrial membrane.** Electrons ($e^-$) provided by electron donors from the Krebs cycle are transported across different protein complexes onto their final acceptor $O_2$ to form $H_2O$. The released energy is used to pump protons ($H^+$) from the matrix into the intermembrane space, creating an electrochemical gradient. This gradient is used by the ATP synthase to synthesize ATP under the consumption of ADP. Numbers I to V represent the different complexes in the ETC. ADP: Adenosine diphosphate, ATP: Adenosine triphosphate, $NAD^+$/NADH: oxidized/ reduced nicotinamide adenine dinucleotide, FAD/ $FADH_2$: oxidized/ reduced flavin adenine dinucleotide, Cyt c: cytochrome c, Q: ubiquinone

Lack of mature CL also affects protein complexes of the ETC and impairs the transport of electrons and hence respiration [56-58]. CL is tightly associated with different complexes of the ETC. Extensive studies with bovine heart cytochrome *c* oxidase (complex IV) demonstrate the necessity of CL for not only the enzymatic function, but also the sustainability of the protein structure [59-63]. Similar requirements for CL are known for complexes I, II and III. Loss of CL leads to destabilization of the ETC structure and loss of enzymatic activity of the different ETC complexes [56, 64-67]. In 2000, Schägger and Pfeiffer described a tight association of the single ETC complexes to form so-called supercomplexes [42]. The formation of these respirasomes ensures a quick and efficient electron transport. These supramolecular structures consist of one copy of complex I, two copies of complex III and different copy numbers of complex IV [68-72]. Different models of the respiratory chain arrangements have been discussed

in the past, considering a more “fluid” or “liquid state” model, a “solid-state mode” as well as a combination of both [73]. The importance of CL in this assembly process becomes apparent by looking at diseases with altered CL composition or decreased amounts of mature CL. In BTHS, the reduction of mature CL leads to disassembly of the ETC and impaired oxidative phosphorylation [58, 74]. In complexes I, II and IV, specific CL binding sites have been discovered [75] and several bound CLs are required for their stability [76, 77].

### 1.1.3 Mitochondrial homeostasis of reactive oxygen species and its effects on cardiolipin

Aerobic metabolism not only produces energy but also ROS as by-products. At the ETC, the main part of $O_2$ is reduced to $H_2O$, however, there is also the possibility for an incomplete reduction of $O_2$ by accepting only one electron, creating the superoxide radical ($\cdot O_2^-$). Superoxide is converted to hydrogen peroxide ($H_2O_2$) by the superoxide dismutase (SOD). The production of ROS in mitochondria occurs at many different proteins and the contribution of the different enzymes to the ROS level is dependent on the substrate that is metabolized [78]. In this context, complex I and III of the ETC are often referred to as the main producers of ROS in mitochondria [79-81]. Complex I contains flavin in the NADH-oxidizing site (site $I_F$) and the ubiquinone-reducing site, which both produce superoxide [82]. In complex III, superoxide is generated at the quinol-oxidizing site (site IIIQo) [83, 84]. ROS in mitochondria not only arise from proteins of the ETC, but there are other enzyme complexes that contribute to their production such as the $\alpha$-ketoglutarate dehydrogenase ($\alpha$-KGDH) and the pyruvate dehydrogenase (PDH) [85, 86], although the $\alpha$-KGDH under physiological conditions rather contributes to ROS elimination than to ROS production [87]. ROS can cause damage to cellular biomolecules, including lipids, proteins and DNA. Accumulation of ROS can be critical to the cell due to its toxicity and therefore, the organelle harbors different antioxidant systems to inactivate the generated oxidants, thus preventing mitochondrial damage and balancing the amount of ROS. The family of SODs performs the dismutation of $\cdot O_2^-$ to $H_2O_2$ (and $O_2$) with copper and zinc-dependent SODs in the intermembrane space, and a manganese-dependent SOD (MnSOD) in the mitochondrial matrix [88]. $H_2O_2$ is subsequently inactivated afterwards by its conversion into $H_2O$. This process is catalyzed by different matrix peroxidases

including the glutathione peroxidase [89]. This peroxidase uses the electron donor glutathione (GSH) to reduce $H_2O_2$, while GSH itself is oxidized to the dimer GSSG. Several reactions recycle the oxidized GSSG under the usage of reduction equivalents provided by NADPH. Mitochondria not only play a role in production and elimination of ROS, but they are also prone to damage caused by ROS. Lipid peroxidation is one major target of free ROS and CL is highly susceptible to peroxidation [90]. Reduction of CL itself, changes in the acyl-chain compositions of CL and its peroxidation are suggested to play a role in mitochondrial dysfunction and different diseases such as ischemic reperfusion injury and the aging heart by affecting the oxidative metabolism [91-96]. Moreover, metabolic diseases, e.g. diabetes and apoptotic signaling due to cytochrome *c* release, are connected to CL peroxidation [97-100]. Under oxidative stress, ROS induces ALCAT1 activity that remodels CL leading to CL composed of long and polyunsaturated acyl chains, which are subjected to peroxidation. Upregulated ALCAT1 activity is related to diabetes and cardiomyopathy [97].

### 1.1.4 The role of cardiolipin in fatty acid metabolism in mitochondria

The heart requires a high ATP turnover for the proper function of the organ. To cope with this enormous energy demand, almost all ATP consumed in the healthy heart derives from oxidation of fatty acids. After their import into the cell, fatty acids are bound to fatty acid binding proteins [101]. Fatty acids need to be transported into mitochondria, where the catabolic reactions take place. The outer mitochondrial membrane can be freely passed by small, uncharged molecules and ions through porins such as the voltage-dependent anion channel (VDAC) [102]. Very long-chain and long-chain fatty acids cannot cross the inner mitochondrial membrane by just diffusing into the mitochondrial matrix but need the help of other transporter proteins. For fatty acid import, the mitochondrial outer and inner membranes harbor different proteins to facilitate the entry into the mitochondria. A central molecule of the uptake system is carnitine. Therefore, the whole process is also known as the carnitine shuttle system (**Figure 2**). Before fatty acids can enter the mitochondria, they are activated by acyl-CoA synthetases, which transfers the acyl group to coenzyme-A [103]. Activated fatty acids are a substrate for the carnitine palmitoyltransferase 1 (CPT1), which removes the CoA-SH group from the fatty acyl molecule and fuses it with carnitine to form fatty acyl-carnitines. After the transport across the OMM, the carnitine/acylcarnitine translocase (CACT) facilitates the transport across the IMM

[104, 105]. CACT belongs to the mitochondrial protein carrier family (Slc25 genes) like the ADP/ATP carrier (AAC), which are known to tightly bind CL and essentially require it for proper enzymatic activity [106, 107]. Mutation in ACC are related to different diseases such as Senger´s syndrome and external ophthalmoplegia [108]. The carnitine palmitoyltransferase 2 (CPT2) resides in the IMM [109], where the carnitine is hydrolyzed from the acyl-carnitine and the fatty acyl residue is bound again to Coenzyme-A. CPT2 is reportedly stabilized and more efficient with CL [110]. Carnitine itself is transported back outside the mitochondrial matrix, where it can be reused.

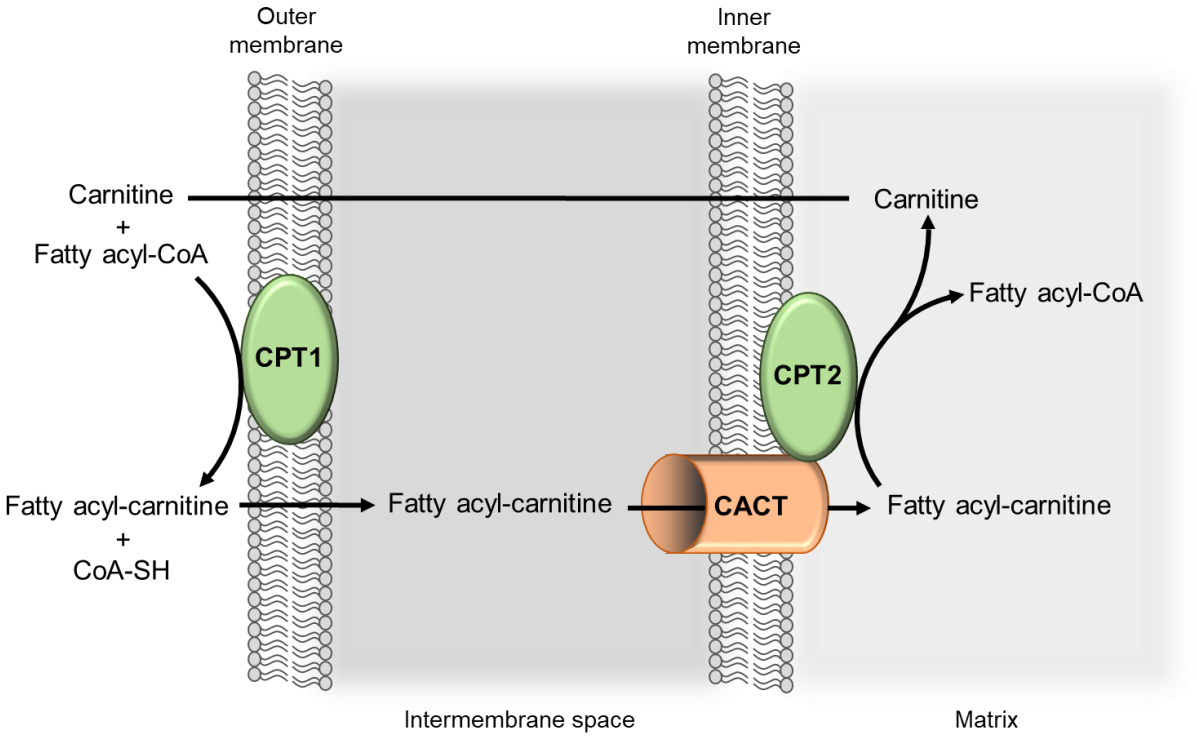


**Figure 2: Schematic representation of the carnitine shuttle system for fatty acid uptake into mitochondria.** Activated fatty acids are coupled to carnitine by the carnitine palmitoyltransferase 1 (CPT1) and shuttled across the mitochondrial membranes into the mitochondrial matrix via the carnitine-acylcarnitine translocase (CACT). The carnitine palmitoyltransferase 2 (CPT2) converts the fatty acyl-carnitine back to fatty acyl-CoA and the released carnitine is transported outside the mitochondria again, where it can be reused.

The carnitine-mediated entry of fatty acids is also the rate limiting step for fatty acid oxidation, as it may limit the supply of the substrate. CPT1 can be inhibited by malonyl-CoA, in contrast to CPT2, which is not affected [109]. Inside the mitochondrial matrix,

fatty acids are degraded during the β-oxidation, which consists of four consecutive reaction steps. Each reaction cycle shortens the acyl-CoA by two carbons, which are released as acetyl-CoA. Dependent on their length, fatty acids run through multiple oxidation cycles for full degradation. The first step of the fatty acid oxidation of very long chain fatty acids is controlled by the very-long-chain acyl-CoA dehydrogenase (ACADVL or VLCAD) for breakdown of acyl-CoAs with 14 to 20 carbons [111]. Membrane binding of ACADVL and consequently its activity is regulated by sirtuins (SIRT3 and SIRT5) that de-acetylate and de-succinylate lysine sites of ACADVL, which affects its binding on CL in the mitochondrial membrane [112]. A cardiac specific ACADVL knockout in mice revealed its important role for cardiac function. ACADVL deficiency induced dilated cardiomyopathy concomitant with reduced ATP production. These mice also early developed hypothermia, bradycardia and diminished cardiac function [113]. In the β-oxidation an acyl-CoA ester is dehydrogenated resulting in trans-2-enoyl-CoA. Secondly the double bond is hydrated producing L-3-hydroxy-acyl-CoA, which is afterwards dehydrogenated generating 3-keto-acyl-CoA. The final step produces an acyl-CoA with two less carbon atoms and acetyl-CoA due to thiolytic cleavage. Additionally, the reaction releases one NADH and one $FADH_2$ as electron carriers. Acetyl-CoA can now fuel into the Krebs cycle and the reducing equivalents provide electrons for the ETC. The remaining acyl-CoA re-enters the β–oxidation until it is fully degraded into acetyl-CoA [114].

### 1.1.5 Additional functions of cardiolipin

The previous sections of the introduction already covered very important functions of CL, which were relevant for the work on this thesis. However, there are more processes in the cell, which also require CL. Figure 3 gives a short overview of the different processes where CL plays a significant role in the function.

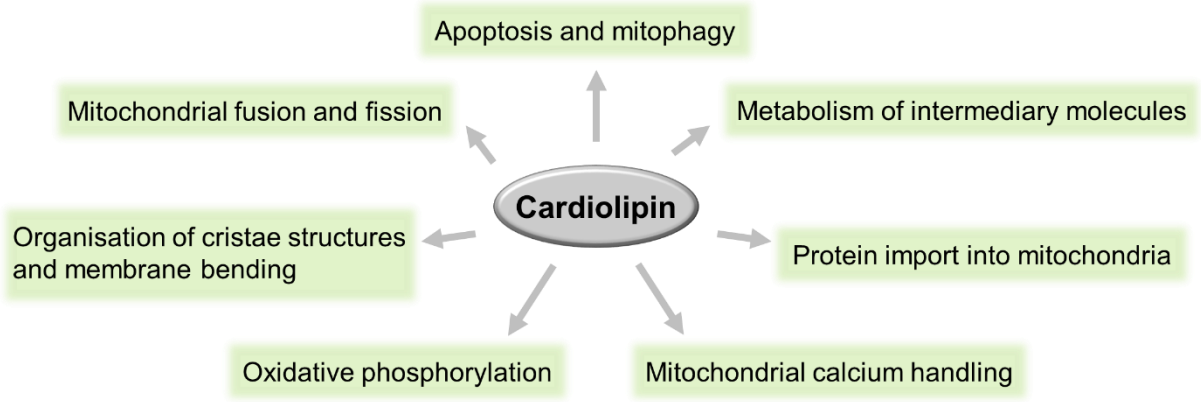


**Figure 3: Overview of mitochondrial processes that require cardiolipin for correct function.** Detailed information and references are given in the text.

CL supports the dynamics of mitochondria by interacting with different proteins that are necessary for fusion and fission such as DRP1 and OPA1 (or Mgm1 in yeast) [115-118]. It is also reported that CL regulates the MICOS system for the cristae formation [119], moreover, the conical shape of CL and its interaction with the protein DRP1 might be conductive to the curvature formation in the highly bent areas supporting the distinct shape of the IMM [120, 121]. It is also tightly associated with different protein complexes, which need the integration of CL for the correct embedding into the membrane to ensure their function and prevent the degradation of the proteins. Import of proteins into mitochondria is mediated by different protein complexes, which were shown to require CL for their receptor-channel associations, such as the TIM23 complex [122]. With CL depletion or dysfunction, not only the respiratory chain itself is malfunctioning, but also proteins from the intermediary metabolism that break down different substrates to fuel the respiratory chain are disturbed. The succinate dehydrogenase requires CL for its structural arrangement and activity [74], as well as the pyruvate dehydrogenase [123]. Moreover, CL plays a role in the regulation of apoptosis. Paradies et al. showed that age-dependent decline in cytochrome *c* oxidase activity correlates with the reduction of CL levels [124] and the released cytochrome *c* activates apoptotic programs [125]. In addition, CL recruits and binds proteins of the pro-apoptotic Bcl-2 family on the OMM [126, 127]. Lastly, CL is also involved in $Ca^{2+}$ signaling in heart mitochondria. Loss of CL leads to the reduction of the MCU complex and therefore impaired $Ca^{2+}$ uptake into the mitochondria, which consequently disturbs the Krebs cycle [128].

## 1.2 Barth Syndrome

Barth Syndrome (BTHS) is a rare X-chromosomal inheritable disease, first described by Peter G. Barth et al. in 1983, who described high infant mortality in a large pedigree caused by heart failure and infections [39]. BTHS can even lead to fetal loss or stillbirth [129]. The main symptoms of this disease are very early development of cardiomyopathy, skeletal myopathy, neutropenia and growth retardation [130]. Over ten years later, mutations in a gene that is highly expressed in cardiac and skeletal muscle was discovered to cause BTHS and the putative protein was called Tafazzin (TAZ) [37]. The authors described insertions of stop codons into the open reading frame of the gene due to the mutations and therefore prohibited translation of the complete protein [37]. Until now, over 100 different mutations have been identified including frameshift, missense, non-sense and splice site mutations [131]. Even though there is a high variety in mutations and clinical severance, there is no correlation between the genetic mutation and the phenotypical presentation of the disease [132]. The functional loss of TAZ leads to increased MLCL and decreased mature CL levels, which can be used as diagnostic markers to confirm the disease [31]. The following sections outline the predominant clinical characteristics of BTHS in human, give an overview of different model organisms that are used in the research field of BTHS and describe current strategies for BTHS treatment.

### 1.2.1 Clinical characteristics of Barth Syndrome

As mentioned above, BTHS patients display a variety of symptoms. The major clinical characteristic and cause of death from the disease is early onset cardiomyopathy, although its manifestation can be very diverse. Cardiomyopathy caused by BTHS can be present already at the fetal stage [133]. Patients show different forms of cardiomyopathy such as dilated or hypertrophic cardiomyopathy [134-136]. Moreover, up to 50% of patients exhibit criteria for left ventricular non-compaction due to the development of left ventricular hypertrabeculation; endomyocardial fibroelastosis is less commonly present [134, 137, 138]. BTHS cardiomyopathy is mostly diagnosed very early in life. In severe cases, the cardiomyopathy is lethal or requires very early heart transplantation, whereas mild cases can be controlled over years with standard heart failure therapy. In a study performed by Spencer et al. including 31 BTHS patients, the mean left ventricular ejection fraction (LVEF) was 50±10% [138]. 16 of

these patients have preserved (≥50%) LVEF and their condition remained unchanged over two years [138]. Later Roberts at al. confirmed in their study including 73 BTHS patients that the LVEF was only mildly abnormal in the majority of patients [137]. Systolic dysfunction is observed primarily in the first days to weeks and months after birth, while beyond the first year of life, LVEF is rather preserved and LV volume is normal, showing characteristic of a phenotype of heart failure with preserved ejection fraction (HFpEF) [137]. However, BTHS patients with a HFpEF phenotype (mean LVEF 51 ± 7%) are unable to increase their cardiac output under exercise conditions and show a distinct decrease in cardiac contractile reserve [139]. Furthermore, independent of the severity of the cardiac dysfunction, patients with BTHS are at higher risk of ventricular arrhythmia and sudden cardiac death [138].

Besides the cardiac muscle, also skeletal muscles are affected by myopathy. This affects the development of motor ability in BTHS patients, which is often delayed and accompanied by reduced exercise capacity and impaired motion reaction time [137, 138, 140]. Connected to this, patients also suffer from fatigue, which is probably caused by the inability of skeletal and cardiac muscle to normally utilize oxygen [139]. The disease not only affects muscles but also the immune system. One of the prevalent symptoms of BTHS is neutropenia, which can potentially be lethal [39]. Patients are susceptible to infections and fever, which is one of the main causes for hospitalization [137]. Furthermore, elevated levels of 3-methylglutaconate (3-MGA) in the urine is present in the majority of patients [141], but the excreted levels can be highly variable including delayed secretion of 3-MGA and there is even a case report of a patient without increased 3-MGA levels in urine [142, 143]. 3-MGA originates from the degradation of the amino acid leucine and patients with 3-MGA-uria type I display even higher 3-MGA levels in their urine after leucine-rich meals [144, 145]. However this was not observed in BTHS, suggesting another origin than leucine degradation [135, 141] that may be connected to amino acid metabolism, but the exact underlying mechanisms are still unknown. In addition, growth delay is reported in infants with BTHS, which adapts later in their lifetime and does not influence the ultimate body size of patients [137, 138]. Also, changes in the facial features that lessen with age are described consisting of a round face with large cheeks and a prominent chin, broad tall fore head, large ears and deep set eyes [146].

### 1.2.2 Model organisms for Barth Syndrome research

From the first description of the disease until now, the research field around BTHS has highly expanded. Even though the CL compositions vary in different species, the steps of CL synthesis and its impairment due to TAZ mutations are highly conserved throughout eukaryotes. This enabled the development of many different model organisms ranging from yeast to human derived cells.

#### Cellular model systems

Different cellular systems are used to investigate the disease, including cells from rats and mice. Major observations in TAZ deficient rat neonatal ventricular myocytes and fibroblasts were the reduction in ATP production, activation of the AMPK pathway and increased ROS production [147, 148]. This was additionally reported in mouse myoblasts with a CRISPR/Cas9 induced *Taz* knockout [149]. The CRISPR method was also used to generate a *Taz* knockout cell line from mouse embryonic fibroblasts (MEFs) [150]. Under hypoxic conditions, the loss of functional TAZ in these cells caused reduced ROS production which prevented the activation of hypoxia-induced factor-1α (HIF-1α) signaling. A doxycycline inducible TAZ depletion in MEFs resulted in mitochondrial dysfunction, oxidative stress and defective mitophagy [151].

#### Human derived cellular model systems

Several different cell lines from patients were used to study BTHS including lymphoblasts, skin fibroblasts, induced pluripotent stem cells and their differentiation into cardiomyocytes (iPSC-CMs). Patient derived lymphoblasts confirmed phenotype changes of patients including altered CL pattern, reduction in the mitochondrial membrane potential, and destabilized supercomplex formation of the ETC [57, 152, 153], which was also found in patient derived skin fibroblasts [130, 154]. iPSC-derived cardiac myocytes reflect the alterations in the ETC complexes and impaired respiration [58, 74]. Interestingly Wang et al. showed that TAZ deficiency hinders sarcomere assembly, which contributes to contractile dysfunction of the generated iPSC cardiac myocytes [155]. By repressing the ROS formation, they demonstrated a normalization of the metabolic phenotype, sarcomere assembly and contractile phenotypes in the BTHS iPSC-derived cardiac myocytes [155].

#### Mouse

Mice (mus musculus) are a commonly used model organism for human diseases. A genetically modified mouse expressing a small hairpin RNA under the control of a

doxycycline inducible promotor was the first mammalian animal model for BTHS with *Taz* mRNA reduced by over 90% [156, 157]. As main characteristic findings of the *Taz*-KD mouse compared to WT mice at eight months of age, Acehan et al. reported altered CL composition with increases in MLCL, severe cardiac abnormalities in its morphology and function including dilation of the left ventricle, reduced fractional shortening and LVEF [156]. In our laboratory, *Taz*-KD mice developed heart failure with a HFpEF phenotype, age-dependent diastolic dysfunction with reduced LVEF, but no fibrosis [128]. In connection with heart failure the expression level of the atrial natriuretic peptide starts to increase at the age of ten weeks [128]. Moreover, impaired $Ca^{2+}$ signaling triggered arrhythmias in isolated cardiac myocytes from these mice [128]. The work from Acehan et al. used a mouse strain with the C57BL/6J genetic background. Naturally occurring mutations in the *Nnt* gene were identified in this mouse strain resulting in a loss of functional NNT enzyme [158]. The mouse model used in our previous study [128] and in this thesis had the genetic background C57BL/6N and therefore contained a functional NNT. Furthermore, cellular abnormalities were revealed using electron microscopy such as alterations in mitochondria composition in cardiac and skeletal muscle as well as abnormal sarcomere structure in cardiac ventricles [156]. Similar observations were described in several other studies [157, 159, 160]. In accordance with skeletal muscle impairments in BTHS patients, the *Taz*-KD mouse displayed a markedly reduction in exercise capacity. Additionally, some studies describe changes in mitochondrial respiration, while others observe no changes [159, 161-163]. Increased ROS emission in BTHS is still widely discussed [128, 159, 162, 164]. Goncalves et al. analyzed eleven superoxide production sites in isolated heart mitochondria reporting no ROS increase in *Taz*-KD mitochondria in any analysis [164]. In skeletal muscle mitochondria, solely one production site showed increased $H_2O_2$ production compared to WT [164]. Recently, *Taz* knockout mouse lines have been developed, either inducing a global knockout of *Taz* or specific to cardiac myocytes [165]. The global knockout mice had a high embryonic and neonatal lethality, surviving mice resembled many of the clinical features of BTHS such as growth retardation, altered MLCL:CL ratios, cardiac dysfunction and dilatation, reduced motor performance and lower amount of circulating neutrophils [165]. In contrast, no higher lethality occurred in the cardiac myocyte specific knockout, where only a cardiac phenotype was observed that included left ventricular dilatation and dysfunction and myocardial fibrosis [165].

**Miscellaneous model systems**

Besides mammal derived model systems also Yeast (*Saccharomyces cerevisiae)*, zebrafish (*danio rerio*) and fruit flies (*drosophila melanogaster)* were extensively used for BTHS research. Yeast strains with *Δtaz* showed overall reduction of CL, reduction in unsaturated acyl chains, whereas the MLCL levels increase and growth defects under elevated temperature conditions[166, 167]. Interestingly, the growth defect was rescued by deletion of the enzyme CLD1 that catalyses the deacylation in yeast of CL to MLCL, increasing the overall CL levels with saturated acyl chains [168], which emphasizes the importance of overall CL levels independent of its saturation [169]. This presents a possible therapeutic approach to stabilize the CL pool with CLD1 inhibition, however, the human homologue of CLD is currently unknown. Additionally, different studies in yeast described the influence of CL in the intermediary metabolism including the Krebs cycle [170, 171]. Morpholino mediated knockdown of *TAZ* in zebrafish led to developmental abnormalities including abnormal heart morphology compared to WT embryos [172]. Loss of full length TAZ in fruit flies caused reduction in the CL pool, abnormal mitochondria in muscle tissue, low motor performance and decreased endurance [173]. In addition, affected animals were not able to improve their endurance with exercise [174]. This reflects the clinical phenotype in BTHS patients with skeletal myopathy and reduced exercise capacity.

### 1.2.3 Treatment approaches for Barth Syndrome

At the current stage, treatment of BTHS is restricted to treatment of the clinical symptoms presented in the patients. Patients with severe cardiomyopathy may undergo heart transplant surgery [175], in milder cases the cardiomyopathy is managed with common heart failure medication [176]. For improvement of skeletal muscle weakness and exercise intolerance, a study including four patients was performed, where the regular endurance exercise was implemented over a period of twelve weeks [177]. This however, showed no significant improvement. Due to neutropenia, there is also a higher risk for bacterial infections, which might be decreased with application of the granulocyte colony stimulating factor (G-CSF) according to a study from Steward et al. [178]. In addition, they suggested simultaneous prophylactic treatments with antibiotics such as low dose daily penicillin or trimethoprim-sulfamethoxazole [178]. Its beneficial usage has already been

described in patients with severe, chronic neutropenia [179]. However, it needs to be considered that other diseases with neutropenia had a higher risk for developing acute myeloid leukaemia if treated with G-CSF [180]. Even though this was not reported in BTHS [178], the long term effects and toxicity of G-CSF in BTHS are mostly unknown. Currently, two small molecules are in clinical trial that are not only for symptomatically treatment but should prevent or attenuate the disease manifestation. The first compound is Benzafibrate, which regulates transcription factors of the oxidative metabolism and has already been tested in diseases of mitochondrial metabolism describing controversial results concerning the efficacy [181-184]. In the mouse *Taz*-KD model Benzafibrate treatment resulted in improvement of the cardiac function [185], a placebo randomized clinical study including eleven participants is still ongoing [186].

Elamipretide (SS-31) is the second compound. This four amino acids-containing peptide localizes in the IMM and binds CL, which presumably leads to enhanced cristae structures and improved mitochondrial function [187, 188]. In rat liver mitochondria, the treatment with Elamipretide showed improvement in the ETC and ATP synthesis [189]. In adults with primary mitochondrial myopathy, Elamipretide improved the 6 minutes walking test (6MWT) [190]. This was also observed in BTHS patients after Elamipretide treatment, moreover BTHS patients reported improved overall well-being and less fatigue, and enhanced cardiac function was described [191]. A possible future therapy approach could be gene therapy based on gene delivery by a recombinant adeno-associated virus (AAV). This has recently been tested in mice with *Taz* knockdown and knockout [165, 192]. In the *Taz*-KD mice, the AAV plasmid contained either desmin or CMV promotors, but also a TAZ promotor was used. The gene therapy improved general activity of the mice, enhanced cardiac function and improved soleus muscle strength and fatigue dependent on the different promotors. In addition, defective mitochondrial structures were restored [192]. In the constitutive *Taz*-KO mice, AAV mediated gene replacement prevented neonatal death and fibrosis, moreover, it reversed cardiac dysfunction, which was also observed in the cardiomyocyte-specific *Taz*-KO [165].

## 1.3 The integrated stress response

The integrated stress response (ISR) is a signaling pathway in eukaryotic cells activated upon different stress factor such as hypoxia, amino acid or glucose

deprivation, viral infection and ER stress [193-197]. Until now, there are four sensor kinases identified in mammals that are triggered by different stress factors. The PKR-like ER kinase (PERK) is mainly activated, if unfolded proteins accumulate in the ER [198]. The double-stranded RNA-dependent protein kinase (PKR) reacts on the one hand to viral infections [199] but is also activated by cytokine signaling or growth factors [200, 201]. Another kinase is the heme-regulated eIF2α kinase (HRI), which responds to iron deficiency [202, 203] but also to arsenite or cytoplasmic stress such as heat shock, osmotic and oxidative stress [204, 205]. The last kinase is the general control non-derepressible 2 (GCN2). This kinase is primarily triggered by amino acid and glucose shortage [206, 207]. All four kinases phosphorylate the central molecule of the ISR, the alpha subunit of the eukaryotic translation initiation factor 2 (eIF2α) at the serine 51 position [196]. This leads to a general reduction in protein translation, however, there are specific mRNAs, which are preferentially translated upon ISR activation. This is suggested to be regulated by an upstream open reading frame (uORF) mediated mechanism. uORFs are localized at the 5´-leader of mRNAs and occur in over 40% of mammalian mRNAs [208]. They are usually known to be inhibitors of downstream translation of protein coding sequences, however, they are also reported to initiate translation as a response to environmental stress [208].

The best-described stress response transcription factor with increased translation during stress is the basic leucine zipper (bZIP) transcription factor ATF4 [209], which is part of the activating transcription factor/cyclic AMP response element binding protein (ATF/CREB) family [210]. Studies using a *Atf4* knockout mouse revealed the central role of ATF4 in many different cellular processes such as lipid metabolism and energy consumption, and it also influences physiological processes, such as thermoregulation [211-213]. Elevated ATF4 levels during stress induce the transcription of stress-responsive genes through binding to C/EBP-ATF response element (CARE) sequences of its target genes [214]. In context of amino acid starvation, these sequences are called amino acid response elements (AARE), and ATF4 is the only described transcription factor which is able to bind all of these sequences [215-217]. ATF4 is also known to interact with other transcription factors such as the C/EBP homology protein (CHOP) to intensify their signal [216, 218]. Upregulation of key enzymes from several metabolic pathways is reported including the serine biosynthesis, the one-carbon metabolism, cysteine biosynthesis and the glutathione cycle [219]. Dysregulation of the ISR is observed in the context of

numerous diseases including diabetes [220-222], neurodegenerative diseases including Alzheimer´s disease [223, 224], as well as heart, brain and liver ischemia [225-227] and heart failure [228]. Moreover, the upregulation of typical ISR-target genes, such as MTHFD2, was observed in animal models of mitochondrial related diseases including Familial progressive external ophthalmoplegia (PEO), which is caused by mutations in the mitochondrial helicase Twinkle, leading to deletions in mitochondrial DNA and cytochrome *c* oxidase deficiency [229, 230]. ISR activation in different cardiac diseases displays very contrary results. Therapeutically, activation of the ISR in rat models with induced myocardial infarction was protective for the cardiac myocytes [231, 232]. Another study, however, showed that ISR activation via PKR promotes myocardial inflammation, apoptosis of cardiac myocytes and the development of congestive heart failure [233]. Additionally, preventing the activation of the ISR via GCN2 was reported to protect the cardiac function and diminish congestive heart failure development [234, 235]. The same controversial effects of ISR activation were observed in cancer, where an active ISR either supports survival of tumor cells and tumor progression [207, 236-238] or in contrast, repressed tumor growth [239]. Overall, the effect of an activated ISR on the different diseases is still controversially discussed.

## 1.4 The one-carbon metabolism

The concept of the one-carbon metabolism combines several pathways that are connected with each other, including the folate cycle, the methionine cycle and the trans-sulfuration pathway (**Figure 4**). Multiple biological processes benefit from the one-carbon metabolism such as nucleotide biosynthesis, amino acid homeostasis, epigenetic modifications and redox defense mechanisms [240-242]. Mitochondria play an important role in the folate cycle, as this pathway consists of a cytosolic and mitochondrial branch [243]. However, animals are not capable to synthesize folate themselves and therefore, it needs to be taken up with their diet [244]. The folate is further converted into tetrahydrofolate (THF), which is the central backbone of the one-carbon reactions and drives the cycle in both compartments, the cytosol and the mitochondria [242]. Serine is one of the major one-carbon donors in the one-carbon metabolism and can be synthesized from intermediates of glycolysis [245]. The one-carbon unit from serine is transferred onto THF by two different serine hydroxyl-methyltransferases (SHMT1 and SHMT2) depending on the compartment, generating

5,10 methyleneTHF (5,10-meTHF) [246]. Serine is thereby converted into glycine, however, this reaction step is reversible. By the consumption of one-carbon units, glycine may be converted back to serine [247]. Following the mitochondrial side of the cycle, 5,10-meTHF is further converted to either 10-formylTHF if it stays in the folate cycle, or it is used as a cofactor in pyrimidine synthesis, where it serves as a one-carbon donor for the conversion of deoxyuridine monophosphate (dUMP) to deoxythymidine monophosphate (dTMP) [248]. The generation of 10-formyl-THF is catalyzed by the methylenetetrahydrofolate dehydrogenase 2 (MTHFD2) and its further transformation into formate is catalyzed by the mitochondrial monofunctional tetrahydrofolate synthase (MTHFD1L) [246]. Formate is now able to shuttle into the cytosol where it is used in the cytosolic part of the format cycle and converted back to 10-formylTHF by the enzyme methylenetetrahydrofolate dehydrogenase 1 (MTHFD1). This enzyme additionally functions as a cyclohydrolase and formyltetrahydrofolate synthetase 1, as it is also responsible for the conversion of 10-formylTHF to 5,10-me-THF in the cytosol. However, 10-formylTHF can also leave the folate cycle and is utilized in purine synthesis as donor of C2 and C8 units [248]. 5,10-meTHF on the one hand is converted to THF by SHMT1, closing the folate cycle, on the other hand it is converted into 5-meTHF by the methylenetetrahydrofolate reductase (MTHFR). Then, its methyl group is used to generate methionine from homocysteine, which links the folate cycle to the methionine cycle [249].

In the following reaction steps of the methionine cycle, methionine is transformed to S-adenosylmethionine (SAM) and S-adenosylhomocysteine (SAH), which is finally converted back to homocysteine. In addition, the intermediate SAM plays an important role in epigenetics as a methyl donor, suggesting a connection between the one-carbon metabolism and histone methylation [250]. Additionally, homocysteine can fuel into the trans-sulfuration pathway instead of forming methionine again. Several reactions of the trans-sulfuration pathway with the intermediates cystathionine, cysteine and γ-glutamylcysteine lead to the synthesis of GSH under the consumption of glutamate and glycine [249, 251]. Besides GSH for redox defense the one-carbon metabolism also generates NADPH at several reaction sides, which plays an important role in the redox balance of the cell [252].

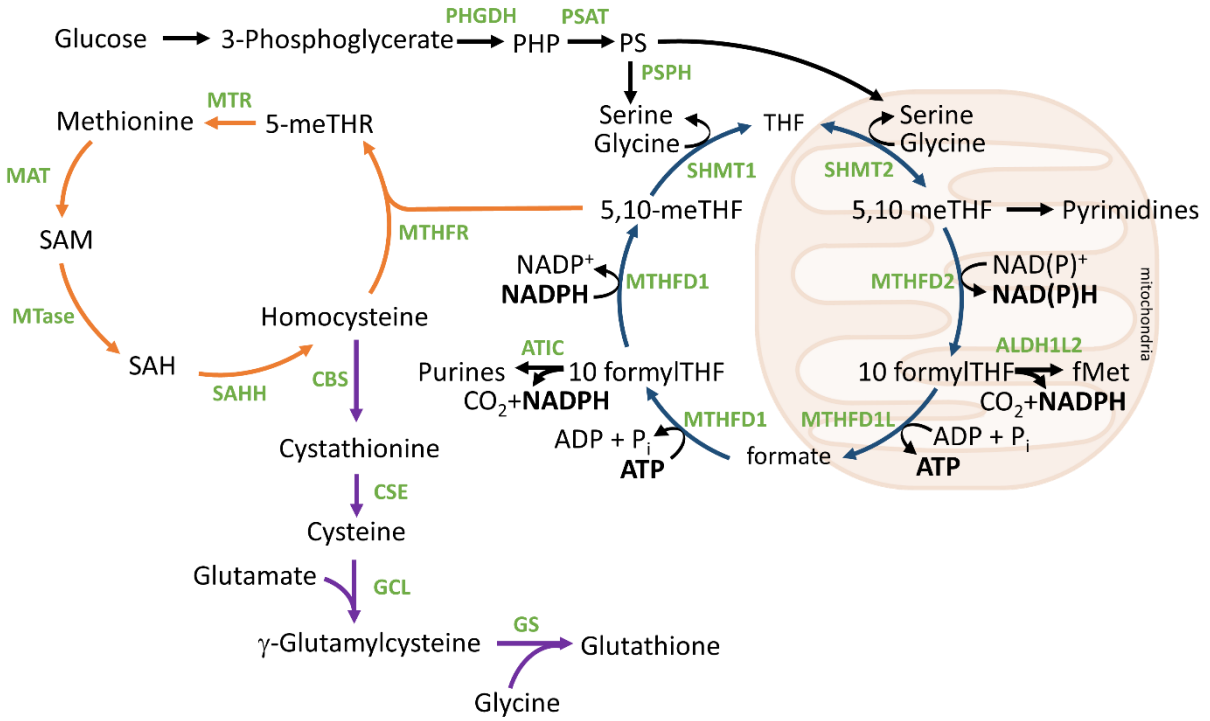


**Figure 4: Overview of the one-carbon metabolism.** The one-carbon metabolism combines pathways including the folate cycle (blue), the methionine cycle (orange) and the trans-sulfuration pathway (purple). Its central function is the transfer of one carbon units. Details of the pathways are described in the text. Enzymes involved in the different reactions are highlighted in green. PHGDH: D-3-phosphoglycerate dehydrogenase, PSAT: Phosphoserine aminotransferase, PSPH: Phosphoserine phosphatase, SHMT1/2: serine hydroxyl-methyltransferase 1/2, MTHFD1/2: methylenetetrahydrofolate dehydrogenase 1/2, MTHFD1L: mitochondrial monofunctional tetrahydrofolate synthase, ALDH1L2: mitochondrial 10-formyltetrahydrofolate dehydrogenase, ATIC: Bifunctional purine biosynthesis protein, MTHFR: methylenetetrahydrofolate reductase, MTR: methionine-synthetase, MAT: methionine adenosyltransferase, MTase: methyltransferase, SAHH: S-adenosyl-L-homocysteine hydrolase, CBS: Cystathionin-beta-Synthase, CSE: Cystathionine gamma-lyase, GCL: glutamate cysteine ligase, GS: Glutathione synthetase. Further abbreviations used in the figure: PHP: phosphohydroxypyruvate, PS: phosphoserine, THF: tetrahydrofolate, 5,10-meTHF: 5,10-methylenetetrahydrofolate, 10-formylTHF: 10-formyltetrahydrofolate, 5-me-THF: 5-methylenetetrahydrofolate, SAM: S-adenosyl methionine, SAH: S-adenosyl-homocysteine, ADP: Adenosine diphosphate, ATP: Adenosine triphosphate, NAD(P)+/NAD(P)H: nicotinamide adenine dinucleotide (phosphate) oxidized/ reduced.

## 1.5 Aim of the thesis

Therapeutic treatment of BTHS is very limited so far and concentrates on the clinical symptoms using already existing medications rather than treating the cause itself, which is still a prevalent issue in genetic diseases. For the development of efficient treatments that improve or at best, cures the disease, it is essential to obtain a better

understanding of the underlying mechanisms of the disease. Healthy hearts derive their energy mostly from fatty acid metabolism, a strictly mitochondrial process, which is affected in BTHS due to dysfunctional mitochondria. Uptake of fatty acids into mitochondria requires a specific shuttle system. Certain enzymes of this transport system belong to the family of carrier proteins which are known to be affected in CL deficient cells [108]. Therefore, loss of mature CL might impair this process in BTHS. Investigating the fatty acid metabolism in different models resembling BTHS was therefore a major aim of this thesis, as TAZ deficiency concomitant with altered CL composition might affect the fatty acid metabolism and consequently the generation of energy by oxidative phosphorylation. Fatty acid metabolism refuels energy and plays an important role in redox homeostasis in the heart. In BTHS patients, the cardiac energy deficiency can be measured by evaluating the PCr/ATP ratio, which is significantly lower in BTHS patients compared to a control group [253]. Cade et al. reported a correlation between reduced PCr/ATP ratio and cardiac dysfunction with lower myocardial FA utilization at rest and exercise-induced FA oxidation rates [254, 255]. Altered redox homeostasis with increased ROS production was already reported in different BTHS models [155, 256], however, this was not observed in the *Taz*-KD mouse model used in this thesis [128]. Metabolic remodeling might act as a compensatory mechanism and could help with rebalancing the redox homeostasis in BTHS, hence increased ROS cannot be detected. This indicates the existence of retrograde signaling pathways that are responsible for the altered metabolism. In heart failure and cancer cells, which require adaptation of their metabolism under stressful conditions, the activity of the ISR was already reported as described in section 1.3. Hence, the extensive study of the ISR and the identification of possible mechanisms that activate this retrograde signaling pathway was another major aim of this thesis. Thereby the focus was set on alterations in the cellular metabolism in TAZ deficient cells including the amino acid metabolism, as changes in the amount of different amino acids have already been reported in BTHS patients [257]. In summary, the overarching aim of this thesis was to further investigate the effect of TAZ deficiency in different model organisms and provide new insights in substantial metabolic alterations in TAZ deficient cells, which possibly arise from an activation of stress responses. This might reveal new pathways, which could be used as targets for the development of novel therapeutic strategies in BTHS.

# 2. Materials

## 2.1 Model organisms and biopsy samples

Mice were purchased from Jackson Laboratories (B6.Cg-Gt(ROSA)26Sor$^{tm37(H1/tet0-RNAi:Taz)Arte}$/ZkhuJ (stock No. 014648). This mouse strain expresses a small hairpin RNA against *Taz* mRNA in the ROSA26 locus under control of the tetracycline-response element (Tet-On). The generation and characterization of this mouse line has been described in Acehan et al. [156]. The genetic background of mice used in this thesis was C57BL/129S6 containing a functional NNT (nicotinamide nucleotide transhydrogenase).

Mouse embryonal fibroblasts containing a CRISPR/Cas9 mediated *Tafazzin* knockout and the corresponding WT cell line as well as induced pluripotent stem cells from a BTHS patient (TAZ10) and control cells were kindly provided by Prof. Peter Rehling, Universitätsmedizin Göttingen, and described elsewhere [58, 74, 150].

Biopsy samples from human hearts (three without heart failure, non-failing; one patient with dilated cardiomyopathy, DCM; and one patient with ischemic cardiomyopathy, ICM) were kindly provided by Prof. Christoph Maack, Comprehensive Heart Failure Center Würzburg, and approved by the Ärztekammer des Saarlandes (131/00) [258, 259].

A heart biopsy sample from a male BTHS patient was kindly provided by Dr. Marcus Fischer, Klinikum der Universität München, with the patient's consent given concomitant with the consent for heart transplantation surgery.

## 2.2 Chemicals

All Chemicals and reagents used in this thesis are listed in Table 1.

**Table 1:** Chemicals and reagents.

| **Chemical** | **Manufacturer** |
|---|---|
| Accutase solution | Sigma-Aldrich, Steinheim |

| | |
|---|---|
| Acetic acid | Carl Roth GmbH + Co. KG, Karlsruhe |
| Amersham ELC™ Western blotting detection reagents | GE Healthcare GmbH, Solingen |
| Ammonium peroxodisulphate (APS) | Carl Roth GmbH + Co. KG Karlsruhe |
| B-27™ Supplement with insulin | Thermo Fisher Scientific, Waltham, USA |
| B-27™ Supplement without insulin | Thermo Fisher Scientific, Waltham, USA |
| Bovine serum albumin (BSA) | Sigma-Aldrich, Steinheim |
| Bromophenol blue | Carl Roth GmbH + Co. KG, Karlsruhe |
| 2,3-Butanedione monoxime (BDM) | Alfa Aesar, Haverhill (USA) |
| Calcium chloride ($CaCl_2$) | Honeywell fluka, Charlotte (USA) |
| CHIR99021 (GSK-3 Inhibitor XVI) | Merck KGaA, Darmstadt |
| Chloroform | Carl Roth GmbH + Co. KG, Karlsruhe |
| Coomassie Brilliant Blue G-250 | Carl Roth GmbH + Co. KG, Karlsruhe |
| Coomassie Brilliant Blue R-250 | Carl Roth GmbH + Co. KG, Karlsruhe |
| Dimethyl sulfoxide (DMSO) | Sigma-Aldrich, Steinheim |
| 2,4-Dinitrophenol (DNP) | Sigma-Aldrich, Steinheim |
| Disodium hydrogen phosphate ($NA_2HPO_4$) | Sigma-Aldrich, Steinheim |
| DL-lactate solution | Sigma-Aldrich, Steinheim |
| Doxycycline hyclate | Sigma-Aldrich, Steinheim |

| | |
|---|---|
| Dulbecco´s modified eagle medium, high glucose (DMEM) | Thermo Fisher Scientific, Waltham (USA) |
| Dulbecco's MEM (DMEM) w/o Glucose, Glutamine, Serine, Glycine, Sodium Pyruvate (Powder) | US Biological Life Science, Marblehead (USA) |
| Ethanol (denatured) | Carl Roth, Karlsruhe |
| Ethanol (technical purity grade) | Sigma-Aldrich, Steinheim |
| Ethylenediaminetetraacetic acid (EDTA) | Sigma-Aldrich, Steinheim |
| Ethyleneglycoltetraacetic acid (EGTA) | Sigma-Aldrich, Steinheim |
| Fetal calve serum (FCS) | Sigma-Aldrich, Steinheim |
| Glucose | Sigma-Aldrich, Steinheim |
| Glutathione reductase | Sigma-Aldrich, Steinheim |
| Glutathione, reduced (GSH) | Sigma-Aldrich, Steinheim |
| Glycine | Carl Roth, Karlsruhe |
| HEPES solution | Sigma-Aldrich, Steinheim |
| Hydrochloric acid, 37% (HCl) | Sigma-Aldrich, Steinheim |
| Integrated stress response inhibitor (ISRIB) | Selleckchem, Houston (USA) |
| Invitrogen™ UltraPure™ DNase/RNase-Free Distilled Water | Thermo Fisher Scientific, Waltham (USA) |
| Isopropanol | VWR International GmbH, Darmstadt |
| IWP2 (Wnt antagonist II) | Merck KGaA, Darmstadt |
| KnockOut™ Serum Replacement | Thermo Fisher Scientific, Waltham (USA) |
| L-Glutamine (200mM) | Thermo Fisher Scientific, Waltham (USA) |
| Lipofectamine RNAiMAX | Sigma-Aldrich, Steinheim |

| | |
|---|---|
| Magnesium sulfate ($MgSO_4$) | Sigma-Aldrich, Steinheim |
| Malic acid (sodium malate) | Sigma-Aldrich, Steinheim |
| Mannitol | Sigma-Aldrich, Steinheim |
| Matrigel®, Growth factor reduced | Corning Inc, Corning (USA) |
| β-Mercaptoethanol | Sigma-Aldrich, Steinheim |
| Methanol | Carl Roth, Karlsruhe |
| mTeSR™1 medium | Stemcell technologies (Vancouver, Canada) |
| N-2-Hydroxyethylpiperazine-N'-2-ethane sulfonic acid (HEPES) | Sigma-Aldrich, Steinheim |
| Natriumpyruvate | AppliChem GmbH, Darmstadt |
| Oligomycin | Sigma-Aldrich, Steinheim |
| OptiMEM™ | Thermo Fisher Scientific, Waltham (USA) |
| Penicillin-Streptomycin (10.000 U/ml) | Thermo Fisher Scientific, Waltham (USA) |
| Phenylmethylsulfonyl fluoride (PMSF) | Carl Roth, Karlsruhe |
| Phosphate buffered saline (PBS) | PAN-Biotech GmbH, Aidenbach |
| Phosphatase Inhibitor Cocktail Tablets | Roche, Penzberg |
| potassium bicarbonate ($KHCO_3$) | Sigma-Aldrich, Steinheim |
| Potassium chloride (KCl) | Sigma-Aldrich, Steinheim |
| Potassium phosphate ($KH_2PO_4$) | Merck KGaA, Darmstadt |
| Precision Plus Protein™ All Blue Prestained Protein Standards | Bio-Rad Laboratories GmbH, München |
| Protease Inhibitor Complete EDTA free | Roche, Penzberg |
| Protein Assay Reagent A | Bio-Rad Laboratories GmbH, München |

| | |
|---|---|
| Protein Assay Reagent B | Bio-Rad Laboratories GmbH, München |
| Protein Assay Standard I | Bio-Rad Laboratories GmbH, München |
| RNase/DNase- free water | Thermo Fisher Scientific, Waltham (USA) |
| Rotiphorese®Gel 30 | Carl Roth, Karlsruhe |
| RPMI 1640 (HEPES/GlutaMax) | Thermo Fisher Scientific, Waltham (USA) |
| RPMI 1640 without glucose/HEPES | Thermo Fisher Scientific, Waltham (USA) |
| SensiMix™ SYBR Low-ROX | Bioline, London (UK) |
| Sodium chloride (NaCl) | Sigma-Aldrich, Steinheim |
| sodium bicarbonate ($NaHCO_3$) | Sigma-Aldrich, Steinheim |
| Sodium dodecyl sulfate pellets (SDS) | Carl Roth, Karlsruhe |
| StemMACS™Y27632 | Miltenyi Biotec, Bergisch Gladbach |
| Sucofin skimmed milk powder | TSI GmbH, Zeven |
| Sucrose | Sigma-Aldrich, Steinheim |
| Tetramethylethylenediamine (TEMED) | Carl Roth, Karlsruhe |
| Trehalose | Carl Roth, Karlsruhe |
| Tris(hydroxymethyl)aminomethane (Tris) | Carl Roth, Karlsruhe |
| TRIzol™ Reagent | Life technologies, Eugene (USA) |
| Trypan blue dye 0.4% | Bio-Rad Laboratories, Watford (UK) |
| Trypsin-EDTA (0.05 %) | Thermo Fisher Scientific, Waltham (USA) |
| Tween 20 | Carl Roth, Karlsruhe |

## 2.3 Antibodies

All antibodies used in this thesis are listed in Table 2. Non commercially bought antibodies were kindly provided by Prof. Peter Rehling, Universitäsmedizin Göttingen. These antibodies were diluted in milk solution. Commercially bought antibodies were diluted in 2% BSA dissolved in 1x TBST.

**Table 2:** Primary and secondary antibodies for Western Blot.

| **Primary antibodies** | | | |
|---|---|---|---|
| **Name** | **Dilution** | **Supplier** | **Identifier** |
| ACADVL Polyclonal antibody | 1:1000 | Proteintech | 14527-1-AP |
| Anti-ALDH18A1 antibody (P5CS) | 1:250 | Sigma | HPA012604 |
| Anti-beta Tubulin antibody (TUBULIN) | 1:10000 | Abcam | ab6046 |
| Anti-CPT1B antibody | 1:2000 | Abcam | ab134988 |
| Anti-Glyceraldehyd-3-phosphat-dehydrogenase antibody (GAPDH) | 1:1000 | Sigma-Aldrich | MAB374 |
| ATF4 Antibody | 1:1000 | Cell Signaling | 11815 |
| SLC25A20 Polyclonal antibody (CACT) | 1:2000 | Proteintech | 19363-1-AP |
| CPT2 Polyclonal antibody | 1:1000 | Thermo Fisher | PA5-12217 |
| eIF2a Antibody | 1:1000 | Cell Signaling | 9722 |
| GAC-specific Polyclonal antibody | 1:1000 | Proteintech | 19958-1-AP |
| GPT2 Polyclonal antibody | 1:1000 | Proteintech | 167577-1-AP |
| GSS Polyclonal antibody | 1:2000 | Proteintech | 15712-1-AP |
| MTHFD2 Polyclonal antibody | 1:1000 | Proteintech | 12270-1-AP |
| Phospho-eIF2α Antibody | 1:1000 | Cell Signaling | 9721 |
| PHGDH Polyclonal antibody | 1:3000 | Proteintech | 14719-1-AP |
| PSAT1 Polyclonal antibody | 1:1000 | Proteintech | 10501-1-AP |
| SHMT1 Polyclonal antibody | 1:3000 | Proteintech | 14149-1-AP |
| SHMT2 Polyclonal antibody | 1:3000 | Proteintech | 11099-1-AP |
| SLC7A5 Polyclonal antibody | 1:6000 | Proteintech | 28670-1-AP |
| TMLHE Polyclonal antibody | 1:400 | Proteintech | 16621-1-AP |
| VDAC | 1:3000 | Prof. Rehling | |

| Secondary antibodies | | | |
|---|---|---|---|
| **Name** | | **Producer** | **Identifier** |
| Peroxidase AffiniPure Goat Anti-Mouse IgG | 1:10000 | Jackson ImmunoReasearch | 115-035-146 |
| Peroxidase AffiniPure Goat Anti-Rabbit IgG | 1:10000 | Jackson ImmunoReasearch | 111-035-144 |

## 2.4 Oligonucleotides

All primers used for qPCR analysis were purchased from Microsynth, Balgach (Swizerland). Primer sequences for the different target genes are listed in Table 3 for samples from mice and in Table 4 for human derived samples. Primers were dissolved in 10 mM Tris pH 7.4 with 1 mM EDTA to reach a stock concentration of 100 µM. For usage they were further diluted to 10 µM in 10 mM Tris pH 7.4.

**Table 3:** Primer sequences for qPCRs with samples from mice.

| **Target genes** | **Primer sequence 5´→ 3´** | |
|---|---|---|
| *Acadvl* | forward | TATCTCTGCCCAGCGACTTT |
| | reverse | reverse TGGGTATGGGAACACCTGAT |
| *Aldh18a1* | forward | TGTAATGCCCTGGAGACGTT |
| | reverse | GACTTCACTTCTGAGGGGCT |
| *Asns* | forward | TACAACCACAAGGCGCTACA |
| | reverse | AAGGGCCTGACTCCATAGGT |
| *Atf4* | forward | GCCGGTTTAAGTTGTGTGCT |
| | reverse | CTGGATTCGAGGAATGTGCT |
| *Cact* | forward | GGATGAACTTAGCTACCCA |
| | reverse | ACTGGCAGGAACATCTC |
| *Chop* | forward | TATCTCATCCCCAGGAAACG |
| | reverse | GGGCACTGACCACTCTGTTT |
| *Cpt1b* | forward | GTCGCTTCTTCAAGGTCTGG |
| | reverse | AAGAAAGCAGCACGTTCGAT |
| *Cpt2* | forward | ACCTGCTCGCTCAGGATAAA |
| | reverse | TGTCTTCAGAAACCGCACTG |

| | | |
|---|---|---|
| *Cth* | forward | CCCAGGGATGGTCAGTTTCT |
| | reverse | TCTAGGCCCACAGAAAGTCG |
| *Gadd45* | forward | GCTCAACGTAGACCCCGATA |
| | reverse | GTTCGTCACCAGCACACAGT |
| *Gapdh* | forward | CATCACTGCCACCCAGAAGACTG |
| | reverse | ATGCCAGTGAGCTTCCCGTTCAG |
| *Gpt2* | forward | GTGGCAGCCTTTATCACCAG |
| | reverse | AGCCCAGCAGTTCTCTTCA |
| *Gss* | forward | GTGACGTATGCCCCATTCA |
| | reverse | CGGGCAGTATAGTCGTCCTT |
| *mS12* | forward | GAAGCTGCCAAGGCCTTAGA |
| | reverse | AACTGCAACCAACCACCTTC |
| *Mthfd1l* | forward | TGAAACTGCAGCCTCTCTCA |
| | reverse | TCCCAGCAACCAAGACGTAT |
| *Mthfd2* | forward | CAGAGGAGCTGGAAGTGTTCAA |
| | reverse | TGGCTCAGAGTGCTGCTAGTTG |
| *Pgc1$\alpha$* | forward | TGATGTGAATGACTTGGATACAGACA |
| | reverse | GCTCATTGTTGTACTGGTTGGATA |
| *Phgdh* | forward | GACCCCATCATCTCTCCTGA |
| | reverse | GCACACCTTTCTTGCACTGA |
| *Ppar$\alpha$* | forward | CCACGAAGCCTACCTGAAGA |
| | reverse | GGACCTCTGCCTCTTTGTCT |
| *Psat1* | forward | CAGGTCAGTGGGAGGCATTC |
| | reverse | GGCCGCCAGCTTCTCAA |
| *Pycr1* | forward | GCTGGCCCAAGACATCGT |
| | reverse | CAGTGCCTAGGGAATCATTGC |
| *Shmt1* | forward | GTGATGCCGAGGTTTACAGC |
| | reverse | AATGCACGCTTCTGACACAG |
| *Shmt2* | forward | CGCCGGGCCTTGGAA |
| | reverse | CTGAGTATGGCTGCACATTGACT |
| *Slc7a5* | forward | CTTTGTACAGCGGCCTCTTC |
| | reverse | CAGGACATGACACCCAAGTG |

| | | |
|---|---|---|
| *Slc7a11* | forward | GTCTGCCTGTGGAGTACTGT |
| | reverse | ATTACGAGCAGTTCCACCCA |
| *Slc25a39* | forward | GCGAATTGACAACTCCCTCC |
| | reverse | TGCCGCACAATCTTCACAAA |
| *Slc38a1* | forward | GTGTTGGTGGTGATGGTGAC |
| | reverse | CGTCGGTCACATTAGCACTG |
| *Tmlhe* | forward | TACAGCACACCGAACCCTAA |
| | reverse | CATGAAGACCCAGGAGACGA |

**Table 4:** Primer sequences for qPCRs with human derived samples.

| **Target genes** | **Primer sequence 5´→ 3´** | |
|---|---|---|
| *ACADVL* | forward | CCTTTGCAACACCCAGTA |
| | reverse | CCACAGTCTCCCCAGAT |
| *ACTIN* | forward | GGACTTCGAGCAAGAGATGG |
| | reverse | AGCACTGTGTTGGCGTACAG |
| *ALDH18A1* | forward | CCTTGGAACCTGAGCAGAGA |
| | reverse | GCCAGGCTGTTCAATTTGGA |
| *ASNS* | forward | GTTGCTGCCACTCTGTTGAA |
| | reverse | AGAGCCTGAATGCCTTCCTC |
| *CACT* | forward | TACAGATTCAGGCTTCTTCAG |
| | reverse | CTCACTGACCCTCTTTCC |
| *CPT1b* | forward | TCAGCGGTACCTAGAGTC |
| | reverse | TAGTTGCTGTTCACCATGAG |
| *CPT2* | forward | CTGTAGCACTGCCGCATTCA |
| | reverse | AGAGCAAACAAGTGTCGGTCAA |
| *L28* | forward | GCAATTCCTTCCGCTACAAC |
| | reverse | TGTTCTTGCGGATCATGTGT |
| *MTHFD2* | forward | GAGGTGATGCCACTGTT |
| | reverse | ACTCCTTCAAAATCCACATC |
| *PPAR$\alpha$* | forward | ACG GAC ACG CTT TCA C |
| | reverse | AAG AAG CCC TTG CAG C |

| | | |
|---|---|---|
| SLC7A5 | forward | GAAGGCACCAAACTGGATGT |
| | reverse | GAAGTAGGCCAGGTTGGTCA |
| SLC7A11 | forward | ACCTTTTCTGAGCGGCTACT |
| | reverse | GTGCTTGCGGACATGAATCA |

Table 5 represents the siRNA sequences used for knockdown experiments in MEF cells.

**Table 5:** siRNA sequences for knockdown experiments.

| **Target gene** | **siRNA sequences** | **supplier** |
|---|---|---|
| ATF4 | CCAUCUCCCAGAAAGUUUA dTdT | Eurogentec, Seraing (Belgium) |
| GADD45 | GGAUCCUGCCUUAAGUCAA dTdT<br>GAUCCAUUUCACCCUCAUC dTdT<br>GACGAACCCACAUUCAUCA dTdT | Eurogentec, Seraing (Belgium) |
| Negative control (scrRNA) | AGGUAGUGUAAUCGCCUUG | Microsynth, Balgach (Swizerland) |

## 2.5 Kits

The different Kits used in this thesis are listed in Table 6.

**Table 6:** Kits.

| **Name** | **Application** | **Company** |
|---|---|---|
| DNAse I, Rnase-free | Digestion of genomic DNA | Thermo Fisher Scientific, Waltham, USA |
| First strand cDNA Synthesis Kit | Transcription of RNA into cDNA | Thermo Fisher Scientific, Waltham, USA |
| Monarch™ Total RNA Miniprep Kit | RNA isolation | New England Biolabs GmbH, Frankfurt am Main |
| Formate assay kit | Measurement of formate in cell lysates | Sigma-Aldrich, Steinheim |

## 2.6 Buffers and solutions

The composition of different buffers and solutions used in this thesis are listed in Table 7.

**Table 7:** Composition of different buffers and solutions.

| Name | contents |
|---|---|
| Buffer B | 20 mM Hepes pH 7.6<br>220mM Mannitol<br>70 mM Sucrose<br>1 mM EDTA |
| Destainer | 50 % $H_2O$<br>40 % EtOH<br>10 % Acetic acid |
| Isolation solution | 225 mM Mannitol<br>75 mM Sucrose<br>2 mM HEPES<br>1 mM EGTA<br>pH 7.4 |
| Milk solution | 5% Sucofin skimmed milk powder 1x TBST |
| Mitochondrial suspension solution | 225 mM Mannitol<br>75 mM Sucrose<br>2 mM HEPES<br>pH 7.4 |
| PBS | 95.5 g/l PBS powder<br>pH 7.4 |
| Respiration buffer | 137 mM KCl<br>2 mM KH2PO4<br>2.5 mM MgCl<br>20 mM HEPES<br>0.5 mM EGTA<br>pH 7.2 |
| RIPA buffer | 50mM Tris pH 7.4 with HCl<br>1 % NP-40<br>0.5 % NA-deoxycholate |

| | |
|---|---|
| | 0.1 % SDS<br>150 mM NaCl<br>2 mM EDTA<br>50 mM NaF |
| SDS running gel buffer | 1.8 M Tris<br>pH adjusted to 8.8 with HCl |
| SDS running buffer (10x) | 250 mM Tris<br>1.91 M Glycine<br>10% (w/v) SDS |
| SDS sample buffer | 2% SDS<br>10 % Glycerol<br>60 mM Tris pH6.8<br>0.2-1 % β-mercaptoethanol<br>0.01 % Bromphenolblau |
| SDS stacking gel buffer | 0.8M Tris<br>pH adjusted to 6.8 with HCl |
| Stainer | 0.1 % Coomassie R250 in destainer |
| TBS (10x) | 200 mM Tris<br>1.25 M NaCl<br>→ adjust pH to 7.4 with HCl |
| TBST | 0.1 % Tween20 in 1x TBS |
| THE buffer | 10 mM KCL<br>10 mM HEPES/KOH pH 7.4<br>300 mM Trehalose<br>1 mM EDTA<br>1mM EGTA |
| Western Blot buffer | 20 mM Tris<br>150 mM Glycin<br>0.02 % SDS<br>20% Ethanol |

## 2.7 Media for cell culture

The composition of the different media required for cultivation of MEF cells, iPSCs and iPSC-derived cardiac myocytes are described in Tables 8 and 9.

**Table 8:** Composition of different media for MEF cell cultivation.

| Name | Components | Amount |
|---|---|---|
| Normal DMEM | DMEM, High glucose (4,5 g/l) | 500 ml |
| | Fetal calve serum | 50 ml |
| | Penicillin-Streptomycin | 5 ml |
| | L-Glutamine | 5 ml |
| Serine/Glycin free medium | DMEM w/o Glucose, Glutamine, Serine, Glycine, Sodium Pyruvate (Powder) | 4.13 g in 500 ml |
| | Glucose | 2.25 g |
| | Sodium bicarbonate | 1.85 g |
| | Fetal calve serum | 50 ml |
| | Penicillin-Streptomycin | 5 ml |
| | L-Glutamine | 5 ml |
| Freezing medium | Normal DMEM | 4,5 ml |
| | Fetal calve serum | 4,5 ml |
| | DMSO | 1 ml |

**Table 9:** Composition of different media for cultivation of iPS cells and their differentiation into cardiac myocytes .

| Name | Components | Amount |
|---|---|---|
| mTE1 Medium | mTeSR™1 medium | 500 ml |
| | Included supplement | 10 ml |
| Differentiation medium 1 | RPMI 1640 (HEPES/GlutaMax) | 500 ml |
| | B-27™ Supplement without insulin | 10 ml |
| Differentiation medium 2 | RPMI 1640 (HEPES/GlutaMax) | 500 ml |
| | B-27™ Supplement with insulin | 10 ml |
| Selection medium | RPMI 1640 without glucose/HEPES | 500 ml |
| | 1 M HEPES solution | 1713 µl |
| | DL-lactate solution | 287 µl |

## 2.8 Consumables

Consumables used in this thesis are listed in Table 10.

**Table 10:** Consumables.

| Name | Company |
|---|---|
| BD™ Needle, 30G | Beckton Dickinson, Franklin Lakes, USA |
| Biosphere® Filter Tips (200 µl) | Sarstedt AG & Co. KG, Nümbrecht |
| Bottle top filtration unit (0.2 µm pore size) | VWR International GmbH, Darmstadt |
| Blotting paper (0,35 mm, 195 g / m²) | A. Hartenstein GmbH, Würzburg |
| Cell Counting Slides; Dual Chamber | Bio-Rad Laboratories GmbH, München |
| CELLSTAR® cellculture dish, 145/20 mm | Greiner Bio-One GmbH, Frickenhausen |
| CELLSTAR® cellculture flask 25 $cm^2$ | Greiner Bio-One GmbH, Frickenhausen |
| CELLSTAR® cellculture flask 75 $cm^2$ | Greiner Bio-One GmbH, Frickenhausen |
| CELLSTAR® cellculture multiwell plate (6-well/12-well) | Greiner Bio-One GmbH, Frickenhausen |
| CELLSTAR® tubes (15 ml/ 50 ml) | Greiner Bio-One GmbH, Frickenhausen |
| Cutfix™ surgical disposable scalpel | B. Braun SE, Melsungen |
| Gel-Loadertips (1-200 µl) | A. Hartenstein GmbH, Würzburg |
| Immobilon®-P Transfermembran, PVDF, 0,45 µM | Merck KGaA, Darmstadt |
| Injekt® Solo, disposable syringes | B. Braun SE, Melsungen |
| Micro tube 1.5 ml | Sarstedt AG & Co. KG, Nümbrecht |
| Microseal 'B' PCR Plate Sealing Film | Bio-Rad Laboratories GmbH, München |
| NunclonTM delta surface dish, 100/21 mm | Thermo Fisher Scientific, Waltham (USA) |
| Pasteur-Plast pipet 3ml | Ratiolab, Dreieich |
| PCR plate low profile, 96-well | A. Hartenstein GmbH, Würzburg |
| PCR plate sealing film | A. Hartenstein GmbH, Würzburg |
| PCR® plate, 96-well | Bio-Rad Laboratories GmbH, München |
| Pipet tips (10µl) | Eppendorf AG, Hamburg, Deutschland |
| Pipet tips (200 µl, 1000 µl) | Sarstedt AG & Co. KG, Nümbrecht |
| Safe seal micro tube 2 ml | Sarstedt AG & Co. KG, Nümbrecht |

| | |
|---|---|
| Safe seal tube 1.5 ml | Sarstedt AG & Co. KG, Nümbrecht |
| Serological pipet (5 ml, 10 ml, 25 ml, 50 ml) | Greiner Bio-One GmbH, Frickenhausen |
| SurPhob SafeSeal® low binding filter tips (10 µl, 100 µl, 1000 µl) | Biozym Scientific GmbH, Oldendorf |
| Syringe filter, 0.2 µM | VWR International GmbH, Darmstadt |
| TissueRuptor Disposable Probes | Qiagen N.V. Hilden |

## 2.9 Equipment

All equipment used in this thesis is listed in Table 11.

**Table 11:** Equipment.

| **Name** | **Company** |
|---|---|
| accu-jet® pro | Brand GmbH & Co. KG, Wertheim |
| Analytical scale ABS 120-4 | Kern & Sohn GmbH, Balingen-Frommern |
| Analytical scale PLJ 600-2GM | Kern & Sohn GmbH, Balingen-Frommern |
| Analytical scale SE622 | VWR International GmbH, Darmstadt |
| Automated cell counter TC20TM | Bio-Rad Laboratories GmbH, München |
| Centrifuge Micro 220R | Andreas Hettich GmbH & Co. KG. Tuttlingen |
| Centrifuge Rotina 380R | Andreas Hettich GmbH & Co. KG. Tuttlingen |
| Centrifuge Rotina 420R | Andreas Hettich GmbH & Co. KG. Tuttlingen |
| CFX96 Touch™Real-Time PCR | Bio-Rad Laboratories GmbH, München |
| ChemiDocTM Touch Imaging System, Detection System | Bio-Rad Laboratories GmbH, München |
| Eppendorf Research® plus pipet (0,1-2,5 µL, 0,5-10 µl, 2-20 µl, 10-100 µl, 100-1000 µl, 1000-5000 µl) | Eppendorf AG, Hamburg |
| Eppendorf ThermoStat™ C | Eppendorf AG, Hamburg |
| HERAcell 240i CO2 Incubator | Thermo Fisher Scientific, Waltham (USA) |

| | |
|---|---|
| Mini-PROTEAN Tetra Vertical Electrophoresis Cell | Bio-Rad Laboratories GmbH, München |
| MyBlockTM mini dry bath | Benchmark Scientific, Inc.,Edison (USA) |
| MyFugeTM mini centrifuge | Benchmark Scientific, Inc.,Edison (USA) |
| NanoDrop$^{TM}$ One$^{C}$ | Thermo Fisher Scientific, Waltham (USA) |
| neoLab Rocking Shaker | neoLab MiggeGmbH, Heidelberg |
| Oroboros O2k Fluorespirometer | Oroboros Instruments GmbH, Innsbruck, Austria |
| Peqlab semi dry blotting device | VWR International GmbH, Darmstadt |
| Sunlab® magnetic stirrer with heating | neoLab MiggeGmbH, Heidelberg |
| Shaker DRS-12 | neoLab MiggeGmbH, Heidelberg |
| PowerPac™ Basic Power Supply | Bio-Rad Laboratories GmbH, München |
| TC10TM Automated cell counter | Eppendorf AG, Hamburg |
| TECAN infinite M200 Pro | Tecan Trading AG, Männedorf, Swizerland |
| Thermo ScientificTM safe2020, biological safety hood | Thermo Fisher Scientific, Waltham (USA) |
| TissueRuptor II | Qiagen N.V. Hilden |
| Vornado™ Vortex Mixer | Benchmark Scientific, Inc.,Edison (USA) |
| Waterbath WNE14 | Memmert GmbH und Co. KG, Schwabach |

## 2.10 Softwares

The different softwares used for data analysis and graphical presentation in this thesis are listed in Table 12.

**Table 12:** Softwares.

| **Name** | **Company** |
|---|---|
| BioRad Image Lab 6.0 | Bio-Rad Laboratories GmbH, München |
| GraphpadPrism 7.05 | GraphPad Software, La Jolla California, USA |

| | |
|---|---|
| Microsoft Office 2016 (Word, Excel PowerPoint) | Microsoft Corporation, Redmond, USA |

# 3. Methods

## 3.1 *Taz*-KD mouse

Animal breeding and procedures were conducted according to the institutional guidelines and approved by the local animal ethics committees. The generation and characterization of this mouse line has been described in Acehan et al [156]. The mice were keept under 12 h light/darkness cycles with controlled temperature and humidity in an pathogen-free animal facility. On the bottom shelf of each ventialted rack, two senitnal animals per cage were housed and routinely controled for pathogens using either serology tests or PCR on pelt swabs, feces or tissue. Sentinel animals were exposed to animal bedding for six to eight consecutive months. Mice were fed with standard rodent chow supplemented with 625 mg/kg doxycycline (ssniff Spezialdiäten GmbH, Soest). To prevent male infertility the doxycycline supplement was stopped during mating. Non transgenic offspring was used as WT control and also fed with doxycycline supplemented chow as described above. The genotype of the pups was determined by PCR under stadardized conditions. Since there was no gender specific differences in cardiac function *in vivo* or mitochondrial function *in vitro* observed in the working group before, male and female mice were used for experiments [128]. If not indicated otherwise animals included in the experiments were aged between 40 and 50 weeks. For tissue harvesting the animals were euthanized by cervical dislocation.

## 3.2 Cultivation of mouse embryonal fibroblasts

Frozen WT MEF cells and *Taz*$^{KO}$ MEF cells were placed in a 37 °C water bath for quick thawing and then transferred to 4 ml cold normal DMEM in a 15 ml falcon and centrifuged at 350 g for 5 min. Supernatant was discarded and cells were re-suspended in 12 ml normal DMEM and transferred to a new 75 ccm cell culture flask. Cells were kept at 37 °C and 5 % $CO_2$ in an incubator with constant air humidity. Cells were passaged every two to three days at 80 – 100 % confluence. For this purpose, cells were washed with 1x PBS to remove dead cells and culture medium. 2 ml Trypsin were added and cells were incubated at 37 °C for up to 10 min. Tapping the flask helped with detachment of the cells. To stop the Trypsin reaction, fresh medium was added to the cells. Cells were re-seeded with lower density and 12 ml of fresh medium were added for a 75 ccm cell culture flask. For experiments the cell

number was determined by using the automated cell counter from BioRad mixing the cells at a 1:1 ratio with Trypan blue dye. To generate stocks of the different cell lines, cells were seeded in 75 ccm cell culture flasks and cultured for 2 – 3 days. Confluent cells were detached with Trypsin as described above and transferred to a 15 ml falcon. Cells were centrifuged at 350 g for 5 min. Supernatant was discarded and the cell pellet was re-suspended in 2 ml freezing medium. Cell suspension was transferred to cryo tubes in 1 ml aliquots and placed in a freezing container for even freezing of the cells at -80 °C over night. Long term storage of cells was at 80 °C.

## 3.3 Cultivation of induced pluripotent stem cells and their differentiation into cardiac myocytes

Prior to cultivation of iPS cells, all used cell culture plates needed to be coated with Matrigel. The dilution factor of Matrigel in cold DMEM/F12 medium is dependent on the batch and can be looked up on the supplier´s webpage. For a 6-well plate 1 ml of Matrigel mix was added to the plate and for a 12-well plate 0.5 ml was added. Pipet tips and cell culture plates have been precooled at 4 °C to prevent early hardening of the Matrigel. Afterwards the coating was cured at 37 °C for 30 min. Coated plates were sealed with Parafilm and stored at 4 °C. The coating mixture from the plate was recycled once and discarded after the second usage. The cell stock was quickly thawed in a water bath at 37 °C and cells were transferred to cold mTE1 medium. Cells were centrifuged at 350 g for 5 min and the supernatant was discarded. The cell pellet was re-suspended with mTE1 medium and the cells were seeded onto pre-warmed 6-well plates. iPSCs were cultured at 37 °C, 5 % $CO_2$ supply and constant air humidity. Medium was changed every day with fresh mTE1 medium and before reaching 100 % confluence cells were passaged. To remove dead cells and medium the plates were washed with 1x PBS and afterwards 500 µl Accutase-solution was added to detach the cells for 3 to 5 min. To stop the detaching process 1-2 ml DMEM/F12 medium were added. After each passaging step, the culture medium was supplemented with 10 µM ROCK inhibitor. To generate iPS cell stocks, cells from one 6-well plate were pooled in a 15 ml falcon after detaching and centrifuged at 350 g for 5 min. Supernatant was discarded, pellet was re-suspended in 1 ml of iPSC freezing medium and transferred to a cryo tube. For even freezing the tube was placed in a freezing container at -80 °C. Long term storage of the cells was at -80 °C.

For differentiation of iPSCs into cardiac myocytes, cells were seeded in 12-well plates with Matrigel coating and differentiation was induced at 80 – 90% confluence by changing the medium to Differentiation medium 1. 12 µM of CHIR99021 (GSK-3 Inhibitor XVI) was added to the cells for 24 h. After 48 h 12 µM IWP2 (Wnt antagonist II) in Differentiation medium 1 was added to the cells for two days. At day seven the medium was changed to Differentiation medium 2, which was used from now on. Medium was changed every other day depending on the appearance. For selection and enrichment of cardiac myocytes, cells were incubated in Selection medium for 7 days starting at day 20. Afterwards cells were incubated in Differentiation medium 2 until harvesting at day 60 with medium change every 2 to 3 days. Every medium change during the differentiation hat to be conducted very gentle as cells tend to detach very easily during this process.

## 3.4 siRNA mediated knockdown

Transfection with siRNA was performed using the Lipofectamine RNAiMAX transfection reagent. Cells were seeded one day prior to transfection with an identical cell number (150000-250000 cells) in each well of a 6-well plate. For each well to be transfected 150µl OptiMEM were added to a sterile reaction tube and 9 µl Lipofectamine RNAiMAX was added. In a second sterile reaction tube 100 pmol of siRNA was added to 150 µl of OptiMEM. Both mixtures were combined and incubated at RT for 5 min. Afterwards the transfection mix was added dropwise to the cells. Plates were gently rocket to distribute the transfection mixture evenly. To exclude any alterations of the cell by the transfection process itself, additional samples were transfected with scrambled siRNA as a negative control.

## 3.5 *In vitro* ISRIB treatment

For *in vitro* experiments ISRIB was dissolved in DMSO. 200 nM ISRIB was added to the cells and incubated for 1 to 3 days. High ISRIB stock concentration ensured low volume of DMSO added to the cells to prevent toxicity.

## 3.6 RNA isolation from tissue or cells

RNA was isolated from tissue or cells using the Monarch™ Total RNA Miniprep kit according to the manufacturers protocols or TRIzol™ Reagent according to the following protocol. 1 ml TRIzol™ Reagent was added to cryo grinded mouse tissue or cell pellet and homogenized in a 1.5 ml reaction tube with small plastic pistils. The homogenized sample was incubated or 5 min at RT and then centrifuged at 12000 g for 10 min at 4 °C. The cleared supernatant was transferred to a new 1.5 ml reaction tube and 200 µl chloroform were added per 1 ml TRIzol™ Reagent. The tube was shaken for 15 s and incubated at RT for 2 to 3 min. The sample was centrifuged at 12000 g for 15 min at 4°C. The upper aqueous phase was transferred into a new 1.5 ml reaction tube without taking any of the lower phase. 500 µl of 100 % isopropanol were added per 1 ml TRIzol™ Reagent and gently mixed by inverting the tube two times. The sample was incubated at RT for 10 minutes and then centrifuged at 12000 g for 10 min at 4°C. Supernatant was removed leaving only the RNA pellet behind. The pellet was washed with 1 ml of 75 % ethanol and centrifuged at 7500 g for 5 min at 4 °C. The RNA pellet was air dried for 5 to 10 min and then re-suspended in 30 ml RNase-free water. The sample was finally incubated at 55 °C for 10 to 15 min. RNA concentration was determined by measuring at the NanoDrop™ One$^{C}$ with preset settings for RNA. RNase free water was used as blank reference. RNA was stored at -80 °C

## 3.7 Digestion of genomic DNA

If genomic DNA digestion was not included in the RNA purification, the isolated RNA was further treated with the RNase-free DNAse I kit. 1 µg of total RNA, 1 µl of 10x reaction buffer containing $MgCl_2$ and 1 µl DNaseI were pipetted in a 1.5 ml reaction tube and filled up with RNase-free water to 10 µl. The samples were incubated at 37 °C for 30 min. 1 µl 50 mM EDTA was added to the samples and they were incubated at 65°C for 10 minutes. Digested RNA was stored at -80 °C.

## 3.8 RNA transcription into cDNA

RNA was transcribed into cDNA using the first strand cDNA Synthesis kit. Therefore, 100 ng of digested RNA was mixed with 1 µl random primer and filled up to 11 µl with RNase-free water in a 1.5 ml reaction tube. The sample was incubated at 65 °C for 5

min and then put on ice for 2 min to cool down. 4 µl of 5x reaction buffer, 1 µl RNase inhibitor, 2 µl dNTPs and 2 µl Transcriptase were added to the sample shortly mixed and centrifuged down. The sample was incubated for 5 min at RT followed by 1 h incubation at 37 °C. The reaction was terminated with an incubation for 5 min at 70 °C. The cDNA concentration was determined by measuring at the NanoDrop$^{TM}$ One$^{C}$ with preset settings for single stranded DNA (ssDNA). The cDNA was stored at -20 °C.

## 3.9 Quantitative real-time PCR

The quantitative real-time PCR (qPCR) method was used for measuring expression levels of genes in mouse tissues and cells. For one reaction 500 ng cDNA of the sample were mixed with 12.5 µl SensiMix SYBR Lo-ROX, 200 nM of each primer and 9.5 µl $H_2O$. For each sample triplicates were measured. The PCR program is described in Table 13. The expression levels were calculated with the $\Delta\Delta C_t$ method and are displayed as a relative fold change (FC) of the WT or control for individual experiments and as 2($\Delta$ct) values for technical replicates. Gene expression was normalized to different housekeeping genes including *Gapdh* or *mS12* for mouse derived tissue and *L28* or *ACTIN* for human derived tissue.

**Table 13:** qPCR protocol settings.

| | **Temperature in °C** | **Duration in s** | **Cycles** |
|---|---|---|---|
| Amplification | 95 | 600 | 1 |
| | 95 | 30 | 40 |
| | 58 – 61 (dependent on primer) | 20 | |
| | 72 | 30 | |
| Melting curve | 95 | 60 | 1 |
| | 65 | 30 | |
| | 95 | 30 | |

## 3.10 Whole tissue lysate of mouse tissue

Tissue sample was placed in a 2 ml reaction tube and 500 µl RIPA buffer freshly supplemented with 0.5 mM PMSF, complete protease inhibitors and phosphatase inhibitors were added. Sample was homogenized with the TissueRuptor II in short pulses and kept on ice during the procedure. The sample was then incubated on ice for 5 min and vortexed at maximum speed for 30 s. After centrifugation for 10 min at 3000 rpm and 4°C the supernatant was stored at -80°C until used for further analysis.

## 3.11 Whole tissue lysates of mouse embryonal fibroblasts

Medium was removed from cell culture plates and cells were washed with cold PBS and removed from the plates in 1 ml PBS using a cell scraper. Cell suspension was transferred to a 1.5 ml reaction tube and centrifuged at 350 g for 5 min. Cell pellet was mechanically homogenized in 200–500 µl RIPA buffer freshly supplemented with 0.5 mM PMSF, complete protease inhibitors and phosphatase inhibitors using a small plastic pistil. The sample was then incubated on ice for 5 min and vortexed at maximum speed for 30 s. After centrifugation for 10 min at 3000 rpm and 4°C the supernatant was stored at -80°C until used for further analysis.

## 3.12 Mitochondria isolation of heart tissue

All steps from the mitochondria isolation were performed on ice and the centrifuge was precooled to 4°C. Frozen heart tissue was cryo grinded with a ceramic mortar and pistil and transferred to a manual homogenizer. The tissue was homogenized in 2 ml Buffer B with freshly added 0.5 mM PMSF, complete protease inhibitors and phosphatase inhibitors. Homogenized sample was transferred to a 2 ml tube and centrifuged 15 min at 800 g. The supernatant was transferred to a new 2 ml tube and kept on ice until further usage. The homogenization and centrifugation steps were repeated another two times with the pellet after the centrifugation. After the third homogenization and centrifugation the pellet was discarded and all collected supernatant was centrifuged at 10000 g for 10 min. Supernatant was transferred into a new reaction tube and stored at -80 °C until further usage. 1 ml Buffer B was added to the mitochondria pellet and centrifuged again at 10000 g for 10 min. Mitochondria were re-suspended in 150 µl Buffer B and stored at -80 °C in 25 µl aliquots.

For respiration measurements mitochondria had to be isolated from fresh heart tissue, which was shredded using scissors. Instead of Buffer B the tissue was homogenized in 1 ml isolation solution for 14 min. The heart homogenate was centrifuged for 5 min and 400 g. Afterwards the supernatant was centrifuged at 7700 g for 10 min. The mitochondria containing pellet was washed with 1ml mitochondrial suspension solution and centrifuged twice at 7700 g for 10 min. After the final centrifugation step, the mitochondria pellet was re-suspended in 100-150 µl mitochondria suspension solution and stored on ice until the respiration measurement.

## 3.13 Mitochondria isolation of MEF cells

For mitochondrial isolation of MEF cells, five confluent grown 15 cm cell culture plates per cell line were used. Cells were washed in cold 1x PBS and scraped in 2 ml THE buffer supplemented with 10 mg/ ml BSA and freshly added 0.5 mM PMSF, complete protease inhibitors and phosphatase inhibitors. All steps were performed on ice and the centrifuging steps were performed at 4 °C. The cells were transferred to a manually homogenizer and homogenized for approximately 1 min. The homogenate was transferred to a 2 ml reaction tube and centrifuged at 400 g for 10 min. The supernatant was transferred to a new reaction tube and the pellet was used for another homogenization. In total the homogenization steps were conducted three times. The collected supernatant was centrifuged at 800 g for 10 min to separate remaining cell debris. Afterwards the supernatant was centrifuged at 11000 g for 10 min to spin down the mitochondria. Mitochondria pellets were washed with 1 ml THE buffer without BSA and centrifuged again at 11000 g for 10 min. Mitochondria pellets were re-suspended in 100 µl THE buffer without BSA and stored at -80 °C.

## 3.14 SDS-polyacrylamide gel electrophoresis (SDS-PAGE) and Western Blotting

Polyacrylamide gels were prepared according to the details listed in Table 14 and stored at 4 °C for up to one week.

**Table 14:** Polyacrylamide gel recipe for two BioRad mini gels.

| | **Running gel** | | | **Stacking gel** |
|---|---|---|---|---|
| | **8 %** | **10 %** | **12.5 %** | **4%** |
| **$H_2O$** | 3 ml | 5 ml | 4.1 ml | 830 µl |
| **SDS running gel buffer** | 2.3 ml | 2.3 ml | 2.3 ml | - |
| **SDS stacking gel buffer** | - | - | - | 500 µl |
| **Rotiphorese gel (30%)** | 5.8 ml | 3.8 ml | 4.7 ml | 3.6 ml |
| **10 % SDS** | 113 µl | 113 µl | 113 µl | 50 µl |
| **10 % APS** | 67 µl | 67 µl | 67 µl | 80 µl |
| **TEMED** | 6.7 µl | 6.7 µl | 6.7 µl | 8 µl |

Samples containing SDS-sample buffer were incubated at 95 °C for 5 min before loading onto the gel. Equal loading of proteins in different samples was ensured due to protein determination. For size determination a protein standard was loaded onto every gel. Proteins were separated at 30 mA. Afterwards the proteins were transferred onto a PVDF membrane, which was prior activated with methanol, via the semi dry blot technique. Therefore, three Whatman paper were soaked with 1x Western Blot buffer and put onto the chamber. On top of that the membrane, polyacrylamide gel and another three Whatman paper were placed. Possible air bubbles were removed by gently rolling over the stack with a plastic tube. Proteins were transferred at 230 mA for 2 h. To visualize the proteins, the membrane was incubated in staining solution for 1 min and washed with destainer afterwards. Completely removal of the Coomassie was achieved by incubating the membrane in methanol. For the antibody incubation the membrane was then incubated in milk solution at RT for at least 1 h or at 4°C over night. Afterwards the membrane was placed into the first antibody and incubated at RT for at least 1 h or at 4°C over night. To remove the excess antibody, the membrane was washed with 1x TBST three times for approximately 10 min. The secondary antibody incubation was performed at RT for at least 1 h. Afterwards the three washing steps were repeated. Protein signals were visualized with ECL™ Western Blotting Detection Reagents using the ChemiDocTM Imager. For quantification of the western blot signals the software Image Lab 6.0 was used.

## 3.15 Respiration measurements using the Oroboros Oxygraph-2k

For the respiration measurements mitochondria were isolated from fresh heart tissue as described in 3.12. The mitochondria were kept on ice until added to the chamber. The measurement was performed at 37°C and constant stirring. Therefore, 200 µg – 400 µg of isolated mitochondria were added to 2 ml respiration buffer in the measuring chamber. Different substrates (5 mM Pyruvate + 5 mM Malate or 5 mM Malate + 50 µM Palmitoylcarnitine or 5 mM Malate + 200 µM Octanoylcarnitine) were added depending on the experiment, followed by 1 mM ADP addition. For subsequent blocking of mitochondrial respiration 1.25 µM Oligomycin were added to the chambers. To measure the maximal respiration capacity DNP was titrated to the chambers at 125 µM steps. The measurements were analyzed using the provided Microsoft Excel template from the Oroboros Company.

## 3.16 Protein determination

To ensure equal protein usage for all samples in the different protocols, a protein determination was performed. Therefore 4 µl of sample were diluted in 36 µl $H_2O$. First 50µl of Protein Assay Reagent A were added to the samples followed by 400 µl of Protein Assay Reagent B. After short mixing and centrifugation, the samples were incubated at RT between 15 and 60 min. Samples were measured in a 96-well Plate at 750 nm in duplicates using the TECAN reader system. For calculation of the protein concentration a new standard curve for each protein determination was measured using the Protein Standard I.

## 3.17 Glutathione assay

300 µl GSH buffer were added to mouse heart tissue and the tissue was homogenized mechanically with a tissue raptor. The sample was quickly frozen on dry ice and thawed twice for proper cell break up and was centrifuged afterwards for 10 min at 4°C and 8000 g. The pellet was discarded and the supernatant was used for measurements. Protein determination ensured equal protein amount for measurements. The measurement was performed at the TECAN plate reader at a wave length of 412 nm for 15 min measuring every minute. Triplicates were measured for every sample. A standard curve using commercially bought GSH was performed for calculating the GSH amount in the samples.

To measure glutathione in MEF cells, cells were cultured in serine/glycine free DMEM medium and seeded in 10 cm cell culture dishes. Cells were harvested in 300 µl GSH buffer and pushed through a syringe with a 0.3 mm needle for cell breakup. Centrifugation and following measurements were performed as described above.

## 3.18 Enzymatic formate assay

The formate amount in MEF cells was determined using the formate assay kit. An additional protein determination of the sample lysates was performed as described in 3.16.

## 3.19 $^{13}C_6$ glucose labeling in mouse embryonal fibroblasts

Labeling of MEF cells was performed in serine/glycine free DMEM medium without glucose supplemented with 25mM of $^{13}C_6$ labeled glucose. Cells were incubated for 6 h or 24 h at 37 °C and 5 % $CO_2$ with constant air humidity. Cells were washed with PBS and harvested using 0.05 % Trypsin-EDTA for detachment. Cell suspension was centrifuged at 350 g for 5 min. Supernatant was discarded and dry cell pellet was stored at -80 °C.

For analyzing the water soluble metabolites, a liquid chromatography and mass spectrometry was kindly performed by Dr. Werner Schmitz (Lehrstuhl für Biochemie und Molekularbiologie, Universität Würzburg).

## 3.20 *In vivo and in vitro* radiotracer experiments and PET-CT scan

All experiments and data acquisition using $^{18}$F-FDG, $^{18}$F-FTOa and $^{18}$F-FASu as well as the $^{3}$H-Glutamate uptake experiment were kindly performed by the group of Prof. Takahiro Higuchi (Department of Nuclear Cardiology, Comprehensive Heart Failure Center Würzburg).

## 3.21 RNaseq analyses

The transcriptome analysis of cardiac tissue and the related data processing was kindly performed by the group of Prof. Thomas Thum (Medizinische Hochschule Hannover).

## 3.22 Data analysis

Statistical analysis of the data was performed using GraphPad Prism version 7.05 for Windows. The Data are displayed as mean ± standard error of the mean (SEM). For the comparison of two groups the unpaired students t-test was performed. Three or more groups were compared using the One-way/two-way ANOVA followed by Bonferroni's, Tukey´s or Sidak´s multiple comparisons test. The applied statistical tests are stated in each figure legend.

# 4. Results

## 4.1 Defective fatty acid metabolism in Barth Syndrome

The healthy heart covers most of its energy demand from oxidizing fatty acids in mitochondria. In BTHS patients, the utilization of fatty acids is reduced accompanied by an increase in glucose metabolism that might contribute to the cardiac phenotype of the disease [255, 260]. In order to test if the mouse model reflects the metabolic alterations of the human phenotype, studies of fatty acid uptake *in vivo* using $^{18}$F-fluoro-4-thia-oleic acid ($^{18}$F-FTOa) [232] combined with a PET-CT scan were performed in collaboration with the working group of Prof. Takahiro Higuchi. The results in the *Taz*-KD mouse model were similar to the described effects in BTHS patients. *In vivo* fatty acid uptake and metabolism in 12 weeks old *Taz*-KD mice compared to WT showed impaired cardiac uptake and oxidation of fatty acids (**Figure 5A**). The usage of $^{18}$F-FTOa instead of the formerly often used tracer BMIPP [261] enables not only the tracking of fatty acid uptake into the cell itself, but also into the mitochondria. BMIPP cannot be transferred into the mitochondria via CPT1, whereas $^{18}$F-FTOa is able to enter the mitochondria via CPT1 and is metabolically trapped there [262, 263]. Furthermore, an increase in cardiac glucose uptake in *Taz*-KD mice was shown by using fluorodeoxyglucose ($^{18}$F-FDG), which was also performed in collaboration with the working group of Prof. T. Higuchi (**Figure 5B, 5C**).

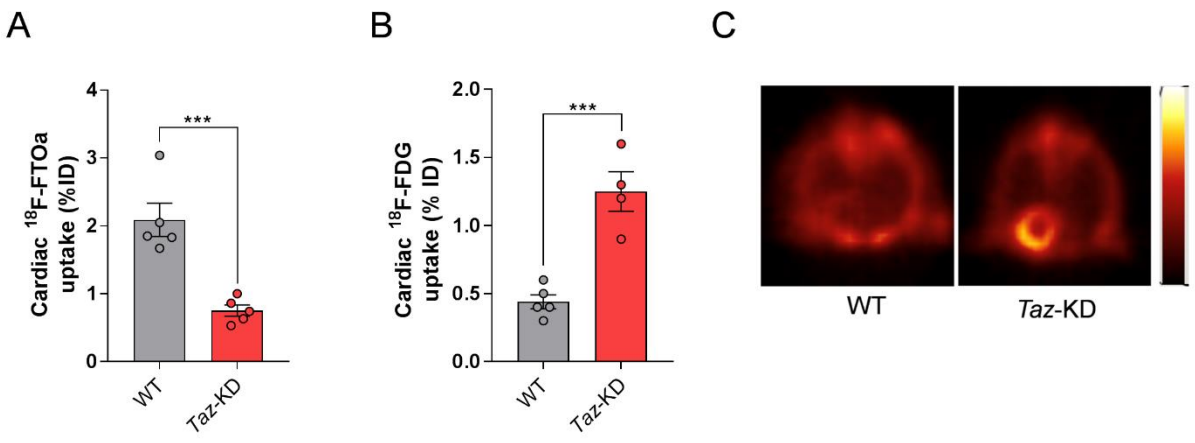


**Figure 5: *In vivo* measurement of cardiac glucose and fatty acid uptake. A)** Cardiac $^{18}$F-FTOa uptake normalized to blood levels of the tracer in 12 weeks old *Taz*-KD mice compared to WT, n= 5. **B)** Quantification of cardiac $^{18}$F-FDG uptake measured by PET-CT and normalized to lung uptake in 12

weeks old *Taz*-KD mice compared to WT, n= 5 for WT and n= 4 for *Taz*-KD. **C)** Representative images of cardiac $^{18}$F-FDG uptake in WT and *Taz*-KD hearts from 12 week old mice. Data are represented in mean +/- SEM, n-numbers represent individual animals. Statistical analysis was performed with two-tailed unpaired Student´s t-test. ***: *p*-value< 0.001; all Data in this figure were provided by the group of Prof. T. Higuchi.

In order to analyze if reduced respiration on fatty acids already originates at the level of mitochondria, mitochondria were isolated from cardiac mouse tissue. The Oroboros O2k respirometer allows the functional analysis of the respiration in isolated mitochondria by measuring the oxygen consumption rate (OCR). Chance and Williams defined in 1995 different states of respiration [264]. In State 1, mitochondria are added to the respiration medium that contains oxygen and inorganic phosphate, where ADP and respiration substrates are still absent. State 2 shows the respiration of the mitochondria with supplementation of the substrates but still without addition of ADP. In State 3, a saturating amount of ADP is added to stimulate the respiratory chain. During this step, the respiration capacity is coupled to the production of ATP from ADP and $P_i$ at the ATP-Synthase. The addition of oligomycin inhibits respiration due to the inhibition of the ATP-Synthase. Therefore, the remaining $O_2$ consumption (State 4 respiration) does not result from respiration connected to ATP production and is often roughly comparable to state 2 respiration. To measure the full respiratory capacity of the ETC, it needs to be uncoupled from ATP synthesis, which is a rate-limiting step in the electron transport. DNP functions as an uncoupler by creating pores for protons into the mitochondrial membrane [265]. Upon the depletion of the proton gradient, respiration is no longer dependent on the ATP-Synthase. The usage of different substrates provides conclusions about the ability of the mitochondria to metabolize these substrates for energy production at the respiratory chain.

Mitochondria from 22 to 23 weeks old *Taz*-KD and WT mice were stimulated with different substrates, and the OCR was measured with the Oroboros system. Adding different fatty acids as substrates allows the localization of the fatty acid metabolism defect more accurately. In contrast to octanoylcarnitine, which is a medium chain fatty acid (8C), palmitoylcarnitine, a long chain fatty acid (16C), is not able to enter the mitochondrial matrix without the carrier protein CACT; both however, need CPT2 for removal of the carnitine. Additionally, octanoylcarnitne can bypass some enzymes of the β-oxidation, such as ACADVL, due to its medium length of the fatty acid chain. In

mitochondria isolated from *Taz*-KD hearts, State 3 respiration was significantly reduced compared to WT mitochondria upon administration of both fatty acids (**Figure 6A**). No difference in respiration was observed using pyruvate as a substrate (**Figure 6B**). In all measurements, malate was added as an additional substrate to stimulate the Krebs cycle. These data indicate a specific defect in fatty acid oxidation in BTHS hearts.

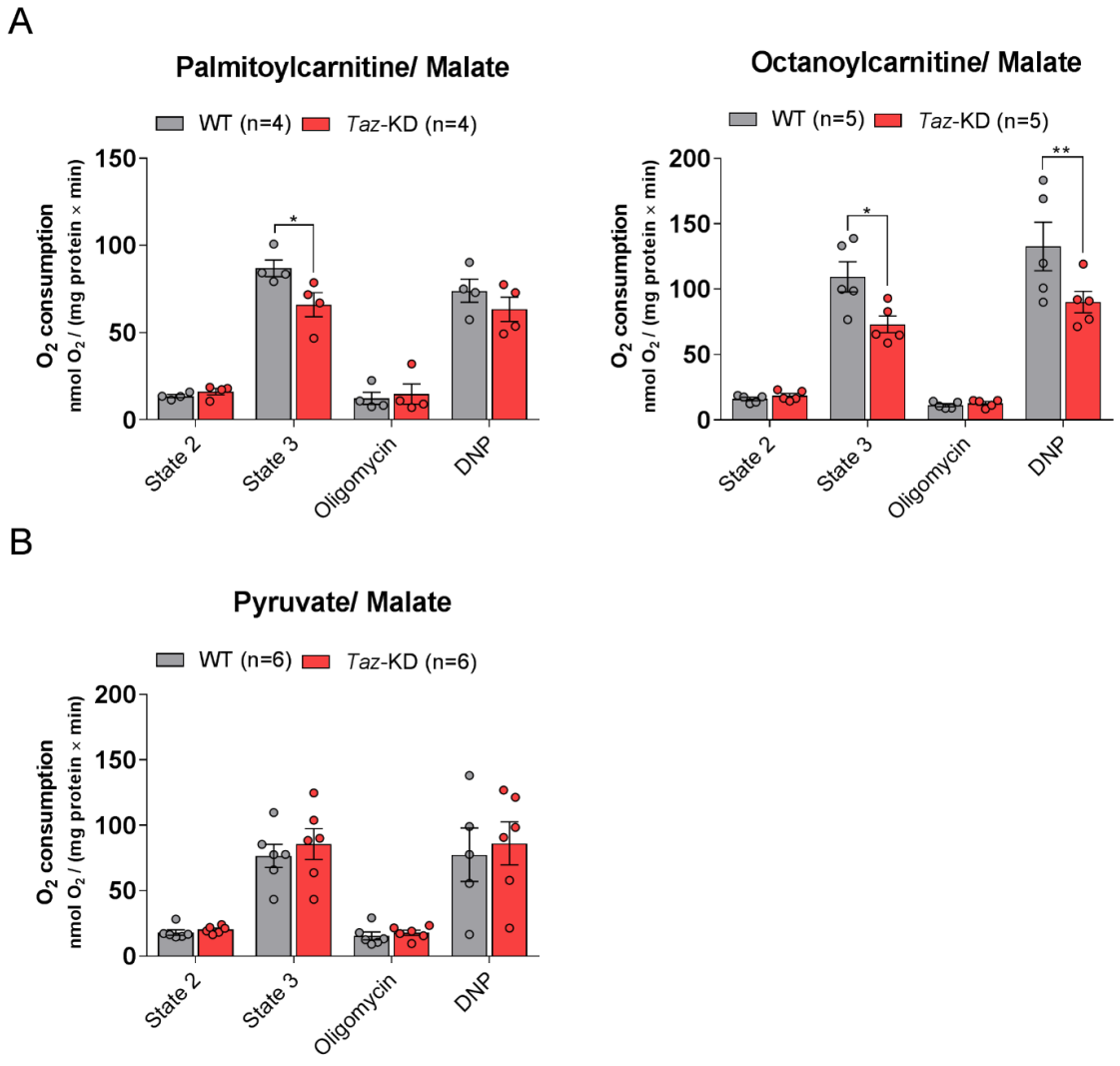


**Figure 6: Defective fatty acid supported respiration in cardiac *Taz*-KD mitochondria**. Oxygen consumption of isolated heart mitochondria from 22 to 23 weeks old *Taz*-KD and WT mice induced by administration of **A)** Palmitoylcarnitine/ Malate (left panel, n= 4), Octanoylcarnitine/ Malate (right panel, n= 5) and **B)** Pyruvate/ Malate, n= 6. Respiration is measured in the absence (State 2) and presence (State 3) of ADP. Respiratory control is induced by oligomycin and maximal respiratory rates are measured upon administration of DNP. Data are represented in mean +/- SEM, n-numbers represent

individual animals. Statistical analysis for this figure was performed by Edoardo Bertero, PhD, using the 2-way ANOVA followed by Bonferroni´s multiple comparisons test. *: *p*-value < 0.05, **: *p*-value< 0.01.

For a better understanding of the underlying molecular mechanisms, protein levels of carnitine shuttle proteins were analyzed by Western Blots. Reduced protein levels of enzymes involved in the fatty acid transport into mitochondria (CPT1b, CPT2) and the β-oxidation (ACADVL) were observed in isolated mitochondria from *Taz*-KD mice at different ages compared to WT (**Figure 7A-D**). Furthermore, the gene expression of these proteins was reduced in cardiac tissue from the *Taz*-KD mouse model compared to WT (**Figure 7E**). Induced pluripotent stem cells from a BTHS patient, which have already been described before [58, 74], were differentiated into cardiac myocytes, which allowed to validate the new insights from the mouse model in a patient derived system, supporting the investigation of the human disease. In patient iPSC-derived cardiac myocytes, the protein levels of CPT1b and CPT2 were also decreased and the same genes as in the mouse model showed reduced expression (**Figure 7I, 7J**). The first enzyme of the carnitine synthesis, the Trimethyllysine dioxygenase (TMLHE), exhibited reduced protein levels on Western Blot analysis from *Taz*-KD isolated heart mitochondria compared to WT, as well as significantly reduced gene expression in the cardiac tissue (**Figure 7F, 7G**). Additionally, reduction of the two key regulators of fatty acid metabolism PPARα and PGC1α indicated a major change of the energy metabolism in the BTHS (**Figure 7H**).

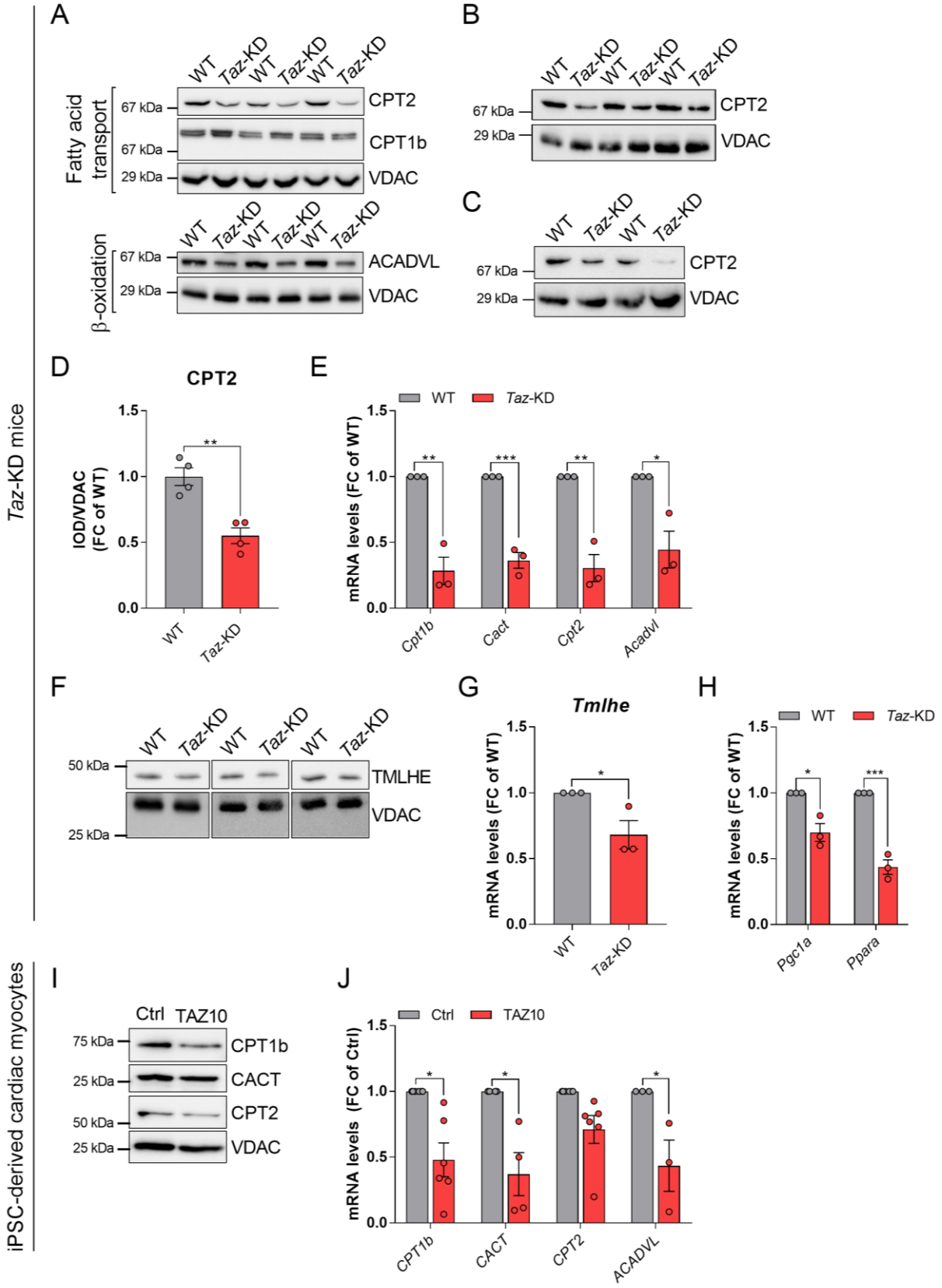


**Figure 7: Altered gene expression and protein levels of fatty acid metabolism enzymes in Barth Syndrome. A)** Western Bot analysis of indicated proteins in isolated mouse heart mitochondria from 50 weeks old *Taz*-KD mice compared to WT with VDAC as loading control, n= 3. **B)** CPT2 Western Blot

analysis of isolated mouse heart mitochondria from 32 weeks old *Taz*-KD mice compared to WT with VDAC as loading control, n= 3. **C)** CPT2 Western Blot analysis from isolated mouse heart mitochondria from 10 weeks old *Taz*-KD mice compared to WT with VDAC as loading control, n= 2. **D)** Quantification of CPT2 Western Blot analysis of isolated mouse heart mitochondria from 10 weeks old *Taz*-KD mice compared to WT normalized to VDAC n= 4 for *Taz*-KD and n= 5 for WT. **E)** mRNA levels of indicated genes in mouse cardiac tissue from *Taz*-KD mice compared to WT normalized to *mS12*, n= 3. **F)** Western Blot analysis of TMLHE in isolated mouse heart mitochondria from *Taz*-KD mice compared to WT with VDAC as loading control, n= 3. **G)** mRNA levels of *Tmlhe* expression in cardiac tissue from *Taz*-KD mice compared to WT normalized to *Gapdh*, n= 3. **H)** mRNA levels of indicated genes in mouse cardiac tissue compared to WT normalized to *Gapdh*, n= 3. **I)** Western Blot analysis of indicated proteins in TAZ10 iPSC-derived cardiac myocytes relative to control with VDAC as loading control, n= 1. **J)** mRNA levels of indicated genes in TAZ10 iPSC-derived cardiac myocytes relative to control (Ctrl) cells normalized to *L28*, n>/=3. Data are displayed as mean +/- SEM, n-numbers represent different animals or independent cell experiments. Statistical analysis was performed with two-tailed unpaired student's t-test. *: *p*-value < 0.05, **: *p*-value< 0.01, ***: *p*-value< 0.001.

## 4.2 Conversions in the mitochondrial intermediate metabolism in Barth Syndrome

Transcriptome analysis is an eminent high throughput method that provides an overview of the transcriptional status of all genes from a sample such as tissue or cells. This enables an easy comparison of genetic alterations and identification of associated metabolic pathways. In order to identify genetic dysregulation in an unbiased approach, transcriptome analysis was performed in collaboration with the group of Prof. Thomas Thum, using cardiac tissue from TAZ deficient mice and WT controls at the age of 10 to 20 weeks. This revealed over 7000 differently regulated genes in the BTHS mouse heart compared to WT. With functional enrichment analysis, including the 262 upregulated coding genes with a fold change higher than 2, the top 30 functions/pathways that are enriched in GO Biological Process were identified. This included the serine synthesis and metabolism, amino acid transport as well as the one-carbon metabolism. A closer examination of the transcriptome data for all enzymes of these pathways revealed a significant upregulation of their genes. Figure 8A represents a schematic overview of the serine synthesis pathway and the one-carbon metabolism. Enzymes whose correspondent genes were increased in the transcriptome analysis are highlighted in red. By assigning the transcriptomic results to single genes, enzymes from the serine pathway and the one-carbon metabolism

were identified as highest upregulated genes in the *Taz*-KD mice including *Mthfd2*, *Phgdh* and *Psat1* (**Figure 8B**).

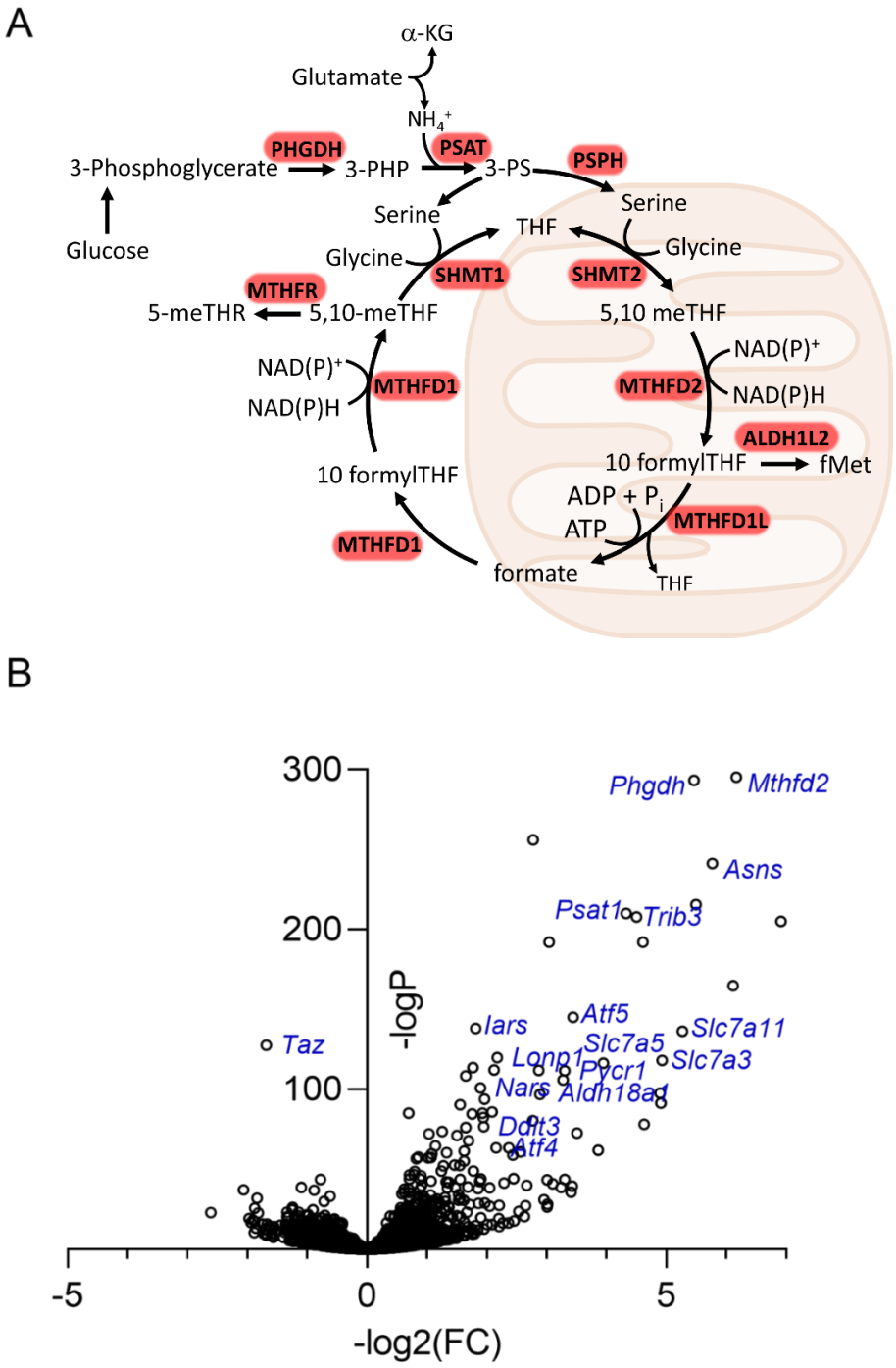


**Figure 8: Transcriptomal analysis of *Taz*-KD cardiac tissue. A)** Scheme of serine and one-carbon metabolism with significantly upregulated genes in the transcriptome analysis of *Taz*-KD hearts highlighted in red. **B)** Volcano plot of log2 fold change versus -log p values of all expressed genes in 10 to 20 weeks old *Taz*-KD heart muscle in comparison with WT. X axis: log2 transformed fold changes. Y-axis: minus log10 transformed p value, n= 5 per genotype. This figures were generated with data

provided by the group of Prof. T Thum. Genes, significantly upregulated in the transcriptome analysis of *Taz*-KD hearts are highlighted in red. 10 formylTHF: 10-Formyltetrahydrofolate; 3-PHP: 3-phosphohydroxypyruvate; 3-PS: 3-phospho-L-serine; 5,10-meTHF: 5,10-methylenetetrahydrofolate; 5-meTHR: 5-methyltetrahydrofolate; ADP: Adenosinediphosphate; $\alpha$-KG: $\alpha$-ketoglutarate; ALDH1L2: mitochondrial 10-formyltetrahydrofolate dehydrogenase; ATP: Adenosine triphosphate; fMet: N-Formylmethionine, MTHFD1: C-1-tetrahydrofolate synthase, cytoplasmic; MTHFD2: bifunctional methylenetetrahydrofolate dehydrogenase/cyclohydrolase, mitochondrial; MTHFD1L: monofunctional C1-tetrahydrofolate synthase, mitochondrial; $NAD(P)^+NAD(P)H^+$: Nicotinamidadenindinukleotid(phosphate) oxidized/reduced; $NH_4^+$: ammonium cation; PHGDH: D-3-phosphoglycerate dehydrogenase; $P_i$: inorganic phosphate; PSAT: Phosphoserine aminotransferase; PSPH: Phosphoserine phosphatase; SHMT1/2: Serine hydroxymethyltransferase cytosolic/mitochondrial; THF: tetrahydrofolate.

By qPCR analysis, the results of the transcriptome were replicated and the transcriptional upregulation of a selected set of genes was verified. The mRNA of the first enzyme of the serine synthesis D-3-phosphoglycerate dehydrogenase (*Phgdh*) and also the second enzyme phosphoserine aminotransferase (*Psat1*) were significantly upregulated in whole *Taz*-KD heart tissue (**Figure 9A**). Additionally, Western Blot analysis showed increased protein levels of both enzymes (**Figure 9B, 9C**).

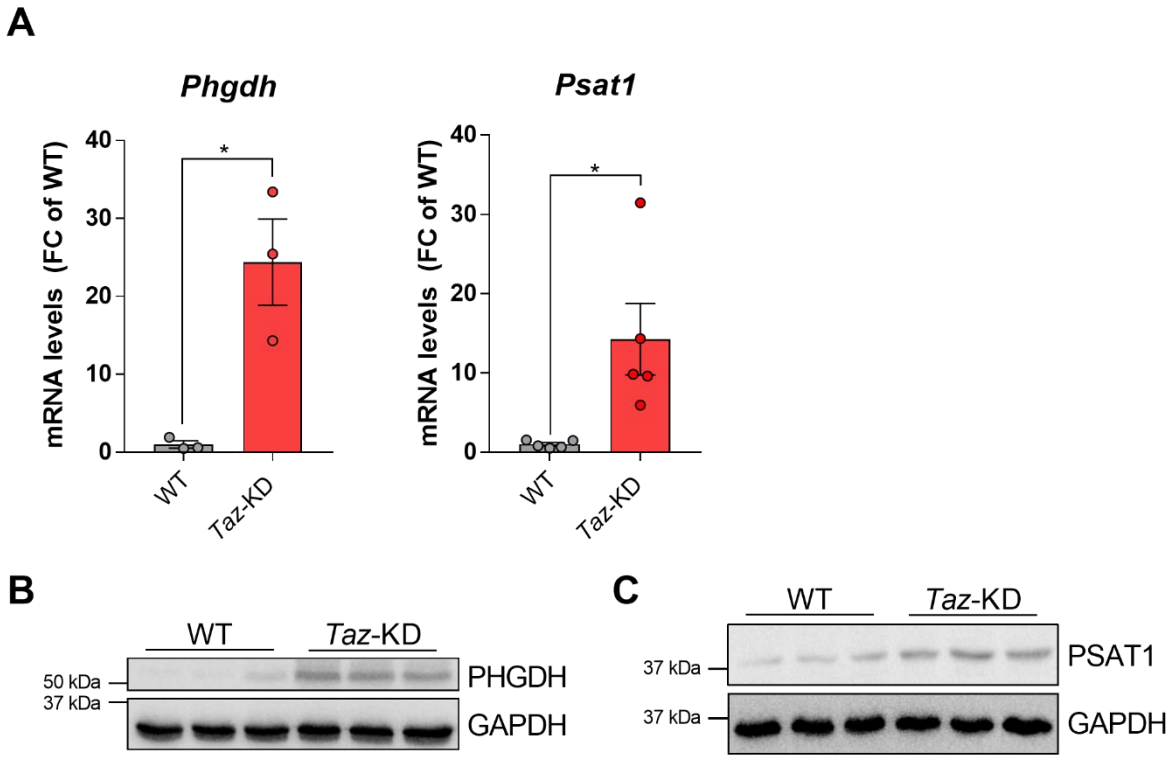


**Figure 9: Regulation of enzymes involved in serine synthesis. A)** mRNA levels of indicated genes in *Taz*-KD mouse heart tissue compared to WT normalized to *Gapdh*, n= 3 for *Phgdh* and n= 5 for *Psat1*. **B)** Western Blot analysis of PHGDH in cardiac tissue from *Taz*-KD mice compared to WT with GAPDH as loading control, n= 3. **C)** Western Blot analysis of PSAT1 in isolated mouse heart mitochondria from *Taz*-KD mice compared to WT with GAPDH as loading control, n= 3. Data are displayed as mean +/- SEM, n-numbers represent individual animals. Statistical analysis was performed with the two-tailed unpaired student's t-test. *: *p*-value < 0.05.

Verification of gene upregulation in the one-carbon metabolism was also done by qPCR. Gene expression of all three enzymes from the mitochondrial branch of the one-carbon metabolism (SHMT2, MTHFD2 and MTHFD1l) were significantly upregulated in the cardiac tissue from *Taz*-KD mice compared to WT (**Figure 10A**). Moreover, the protein levels of SHMT2 and MTHFD2 were also elevated in isolated mitochondria from cardiac tissue of TAZ deficient mice compared to WT (**Figure 10B, 10C**). Interestingly, analysis of the first enzyme of the cytosolic branch in the one-carbon metabolism (Shmt1) showed no upregulation, neither on the mRNA level nor the translated protein (**Figure 10D, 10E**), indicating preferred flux of the one-carbon metabolism into mitochondria.

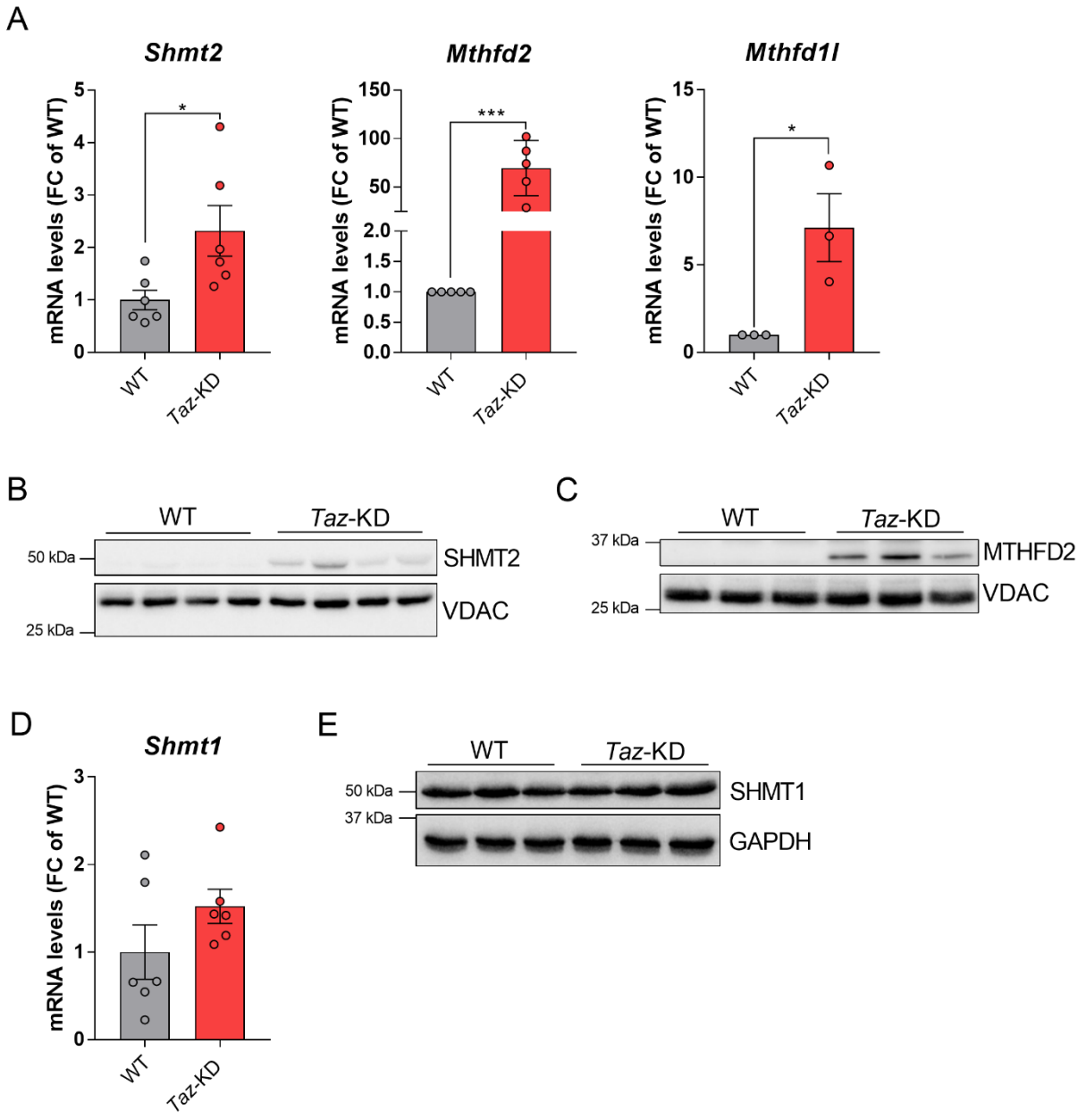


**Figure 10: Regulation of enzymes involved in the one-carbon metabolism. A)** qPCR analysis of mRNA levels of indicated genes in mouse cardiac tissue from *Taz*-KD mice compared to WT normalized to *Gapdh* or *mS12*, n= 6, 5 and 3 respectively. **B)** Western Blot analysis of SHMT2 protein levels in isolated mitochondria from cardiac tissue of WT and *Taz*-KD mice with VDAC as loading control, n= 4. **C)** Western Blot analysis of MTHFD2 in isolated mitochondria from cardiac tissue of *Taz*-KD mice compared to WT with VDAC as loading control, n= 3. **D)** qPCR analysis of mRNA level of *Shmt1* in cardiac tissue from *Taz*-KD mice compared to WT normalized to *Gapdh*, n= 6. **E)** Western Blot analysis of SHMT1 in isolated mitochondria from cardiac tissue lysates of *Taz*-KD mice compared to WT with GAPDH as loading control, n= 3. Data are displayed as mean +/- SEM, n-numbers represent individual animals. Statistical analysis was performed with two-tailed unpaired student's t-test. *: *p*-value < 0.05, ***: *p*-value< 0.001.

Differentiated cardiac myocytes from patient derived iPSCs provide a great opportunity to investigate the metabolic alterations in patient derived cells. In iPSC-derived cardiac myocytes, *MTHFD2* gene expression as well as its protein level were increased in TAZ10 cells compared to healthy control cells (**Figure 11A, 11B**). However, the most precise findings can be obtained by analyzing tissue biopsies from patients. In one BTHS patient myocardial sample, the gene expression of *MTHFD2* was elevated compared to three samples from healthy individuals (**Figure 11C**). Additionally, Western Blot analysis of tissue lysate from the BTHS myocardial sample compared to one healthy donor and two patients with ischemic- or idiopathic dilated cardiomyopathy revealed an increased protein amount of MTHFD2 in the myocardial sample from the BTHS patient (**Figure 11D**).

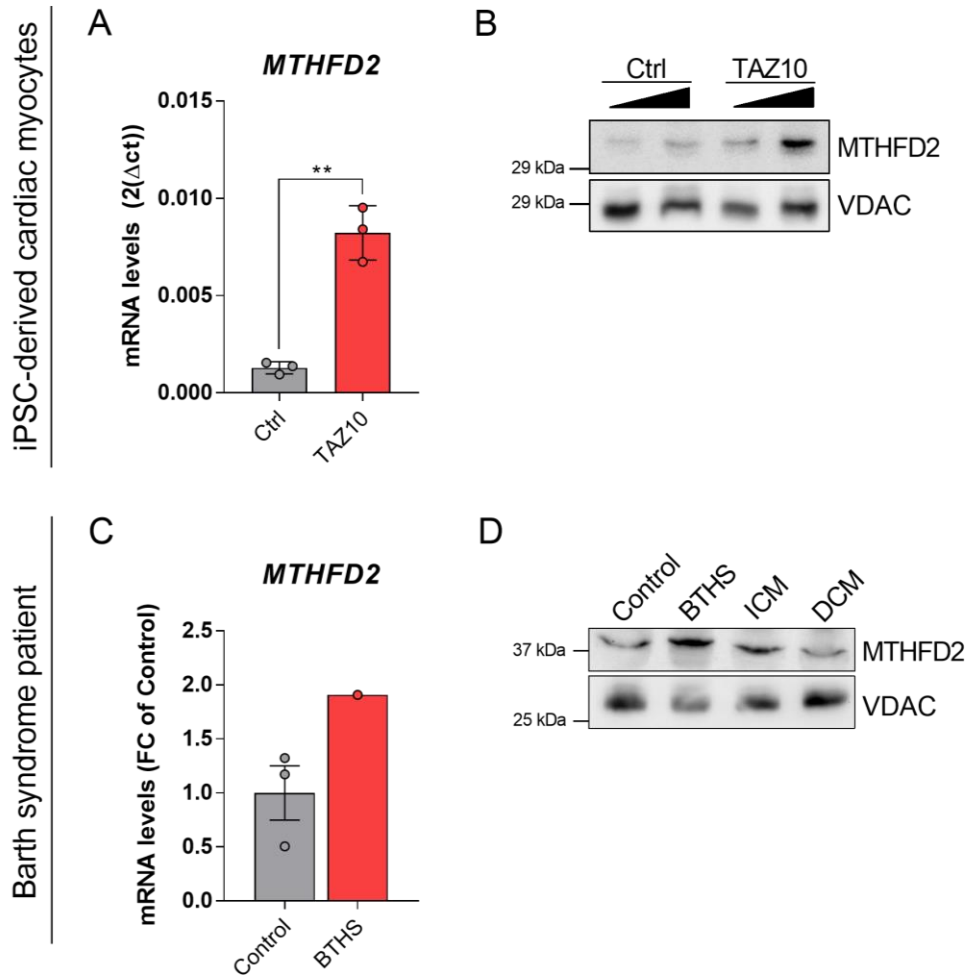


**Figure 11: Regulation of enzymes involved in the one-carbon metabolism in human derived samples. A)** mRNA levels of *MTHFD2* in TAZ10 and control (Ctrl) iPSC-derived cardiac myocytes

normalized to *L28*, n= 3. **B)** Western Blot analysis of MTHFD2 in TAZ10 and control (Ctrl) iPSC-derived cardiac myocytes with VDAC as loading control, n= 1. **C)** mRNA levels of MTHFD2 in cardiac biopsies from Control and BTHS patient tissue normalized to *L28*, n= 3 for Control and n= 1 for BTHS. **D)** Western Blot analysis of cardiac patient biopsies from control, Barth syndrome patient (BTHS), ischemic cardiomyopathy (ICM) and idiopathic dilated cardiomyopathy (DCM) with VDAC as loading control, n= 1. Data are displayed as mean +/- SEM, n-numbers represent technical replicates in panel A and individual samples in all other panels. Statistical analysis was performed with two-tailed unpaired student's t-test. **: *p*-value < 0.01.

## 4.3 The integrated stress response signaling regulates metabolic changes in Barth syndrome

The basic leucine zipper transcription factor ATF4 is a major regulator of the integrated stress response (ISR), a stress-induced signaling pathway. Various studies observed metabolic changes including the serine synthesis pathway, the one-carbon metabolism and amino acid metabolism upon activation of the ISR and ATF4 due to mitochondrial dysfunction [219, 229, 266-268]. Therefore, ATF4 as a transcription factor and the activation of the ISR might play a crucial role in the regulation of the metabolic alterations in BTHS. To verify this hypothesis, Western Blot analysis of lysates from heart tissue of the mouse model were performed and the results confirmed an elevated amount of ATF4 (**Figure 12A**). Asides from that, also the *Atf4* gene expression was increased and additionally, known target genes such as *Chop* and *Gadd45* showed upregulated gene expression in heart tissue of the *Taz*-KD mouse model (**Figure 12C**). The ISR signaling cascade starts with the phosphorylation of eIF2$\alpha$ by different sensor kinases. This phosphorylation regulates the transcription of ATF4. For this reason, Western Blot analysis of eIF2$\alpha$ and its phosphorylated form were performed. These experiments revealed higher levels of phosphorylated eIF2$\alpha$ in cardiac tissue from *Taz*-KD mice compared to WT controls (**Figure 12B**).

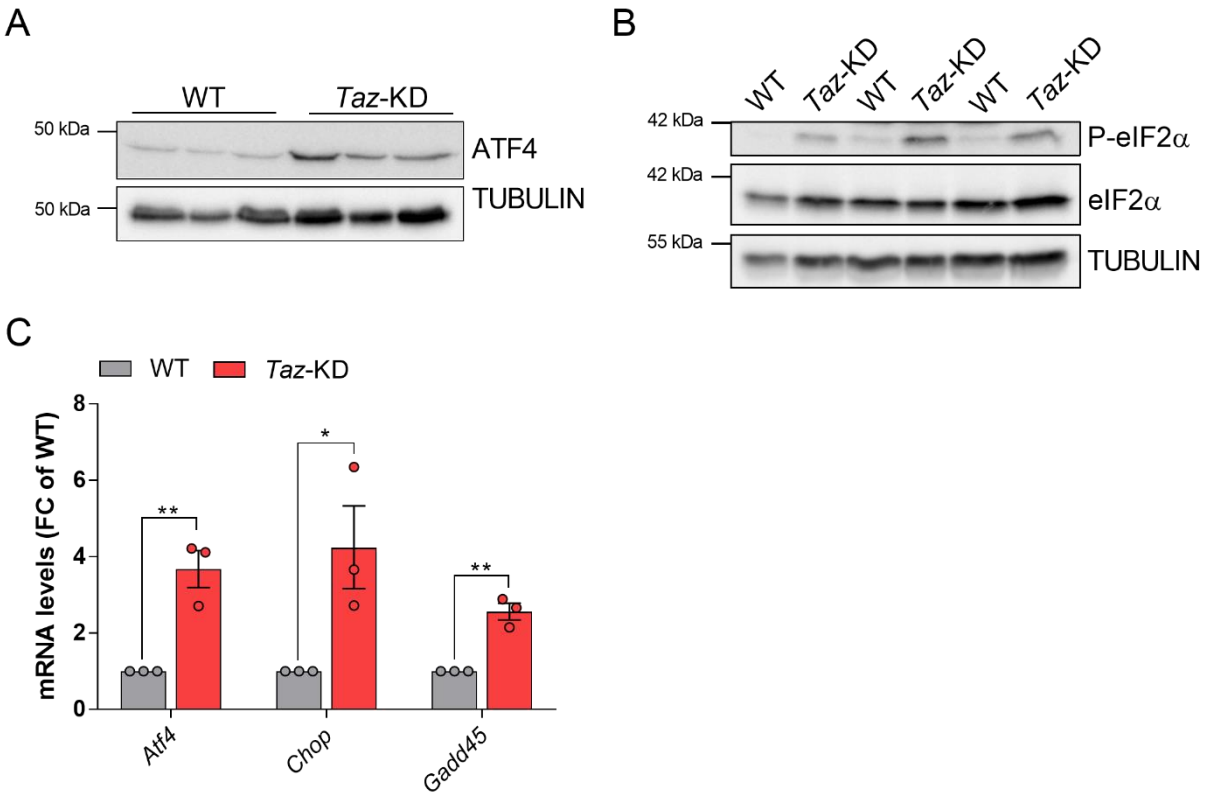


**Figure 12: Activation of the ISR in Barth Syndrome. A)** Western Blot analysis of ATF4 in cardiac lysates from *Taz*-KD mice compared to WT with TUBULIN as loading control, n= 3. **B)** Western Blot analysis of indicated proteins in cardiac lysates from *Taz*-KD and WT mice with TUBULIN as loading control, n= 3. **C)** qPCR analysis of mRNA levels of indicated genes in cardiac tissue from *Taz*-KD mice compared to WT normalized to *Gapdh*, n= 3. Data are displayed as mean +/- SEM, n-numbers represent individual animals. Statistical analysis was performed with two-tailed unpaired student's t-test. *: *p*-value < 0.05, **: *p*-value< 0.01.

Inhibition of ISR signaling might provide novel insights in the mechanistic link between ISR signaling and metabolic remodeling. Immortalized cell lines are a convenient model system for the downregulation of gene expression via small interference RNA and also for the usage of chemical compounds to block signaling pathways. Therefore, we included a previously established MEF cell model that contained a CRISPR/Cas9 mediated knockout of *Tafazzin* (*Taz*$^{KO}$) [150]. In order to find out if this cell model resembles the metabolic changes which were discovered in the mouse model and the human derived samples, gene expression analysis was performed with the same genes. qPCR analysis of *Atf4* and its target *Gadd45* revealed increased mRNA levels in the *Taz*$^{KO}$ cells compared to WT cells (**Figure 13A**). This confirmed activation of the

ISR also in the MEF cell model. Furthermore, elevated mRNA amounts were observed for *Psat1* and *Mthfd2*, genes of the serine synthesis pathway and the one-carbon metabolism (**Figure 13A**). The protein level of PSAT1 was also increased in cell lysates from *Taz*$^{KO}$ cells compared to WT cells (**Figure 13B**). Additionally, elevated activation of the one-carbon metabolism was demonstrated by measuring the formate amount in cell lysates, which was increased in the *Taz*$^{KO}$ cells (**Figure 13C**).

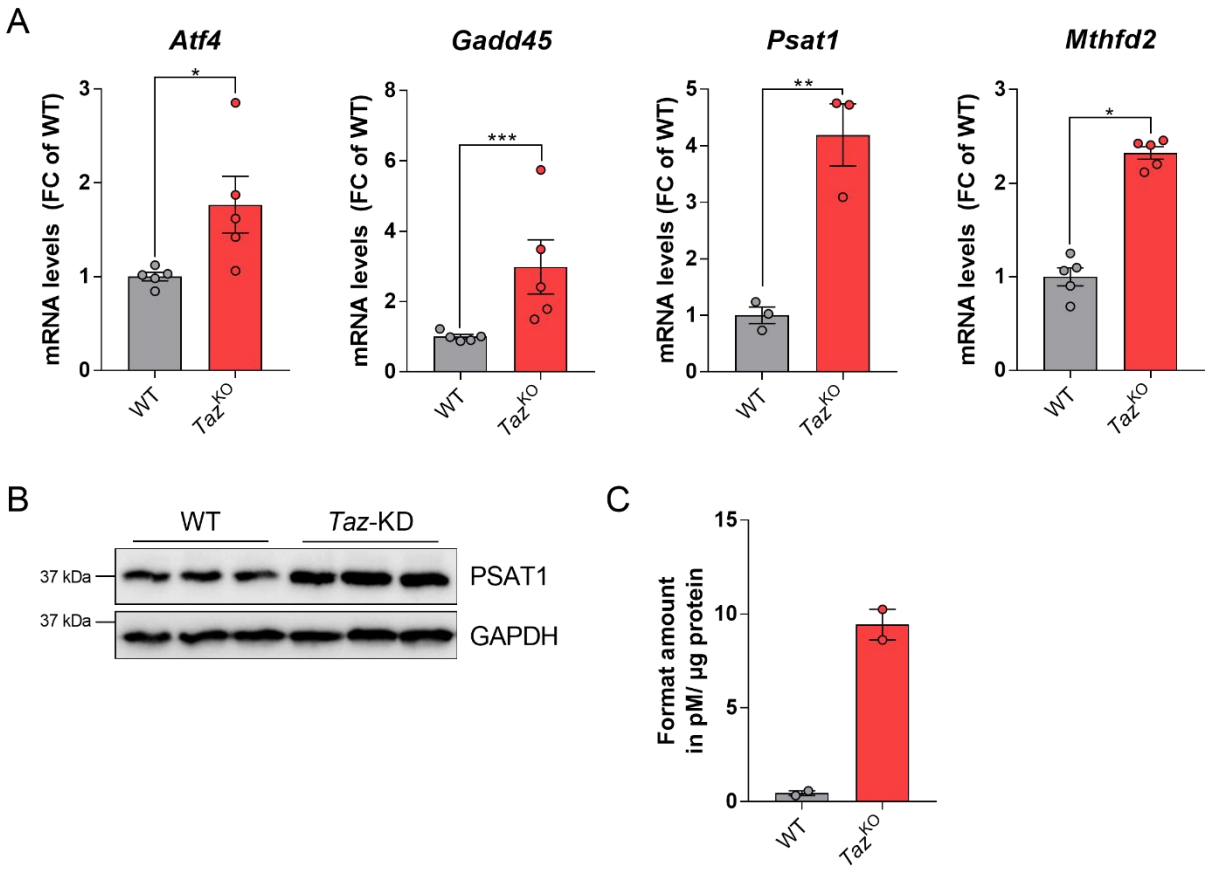


**Figure 13: Recapitulation of the metabolic alterations in TAZ deficient mouse embryonal fibroblasts. A)** qPCR analysis of mRNA levels of indicated genes in *Taz*$^{KO}$ MEF cells compared to WT cells normalized to *mS12*, n= 3 for *Psat1* and n= 5 for all other graphs. **B)** Western Blot analysis of *Taz*$^{KO}$ and WT cell lysates of PSAT1 and GAPDH as loading control, n= 3.**C)** Formate amount in cell lysates from *Taz*$^{KO}$ and WT cell lysates, n= 2. Data are displayed as mean +/- SEM, n-numbers represent individual cell experiments in panels A and B and technical replicates in panel C. Statistical analysis was performed with two-tailed unpaired student's t-test. *: *p*-value < 0.05, **: *p*-value< 0.01, ***: *p*-value <0.001.

In order to test the influence of ATF4 on the regulation of different target genes, a knockdown of *Atf4* was performed using siRNA. Upon successful knockdown of *Atf4*, reduction in gene expression of *Gadd45* and *Mthfd2* was observed in *Taz*$^{KO}$ cells compared to the cells without siRNA (**Figure 14A**). To test whether metabolic gene regulation of MTHFD2 is controlled by GADD45, its gene expression was reduced using siRNA. This revealed that the knockdown *Gadd45* was also able to diminish the overexpression of *Mthfd2* in *Taz*$^{KO}$ cells (**Figure 14B**), which indicates its regulatory role in the elevated *Mthfd2* gene expression.

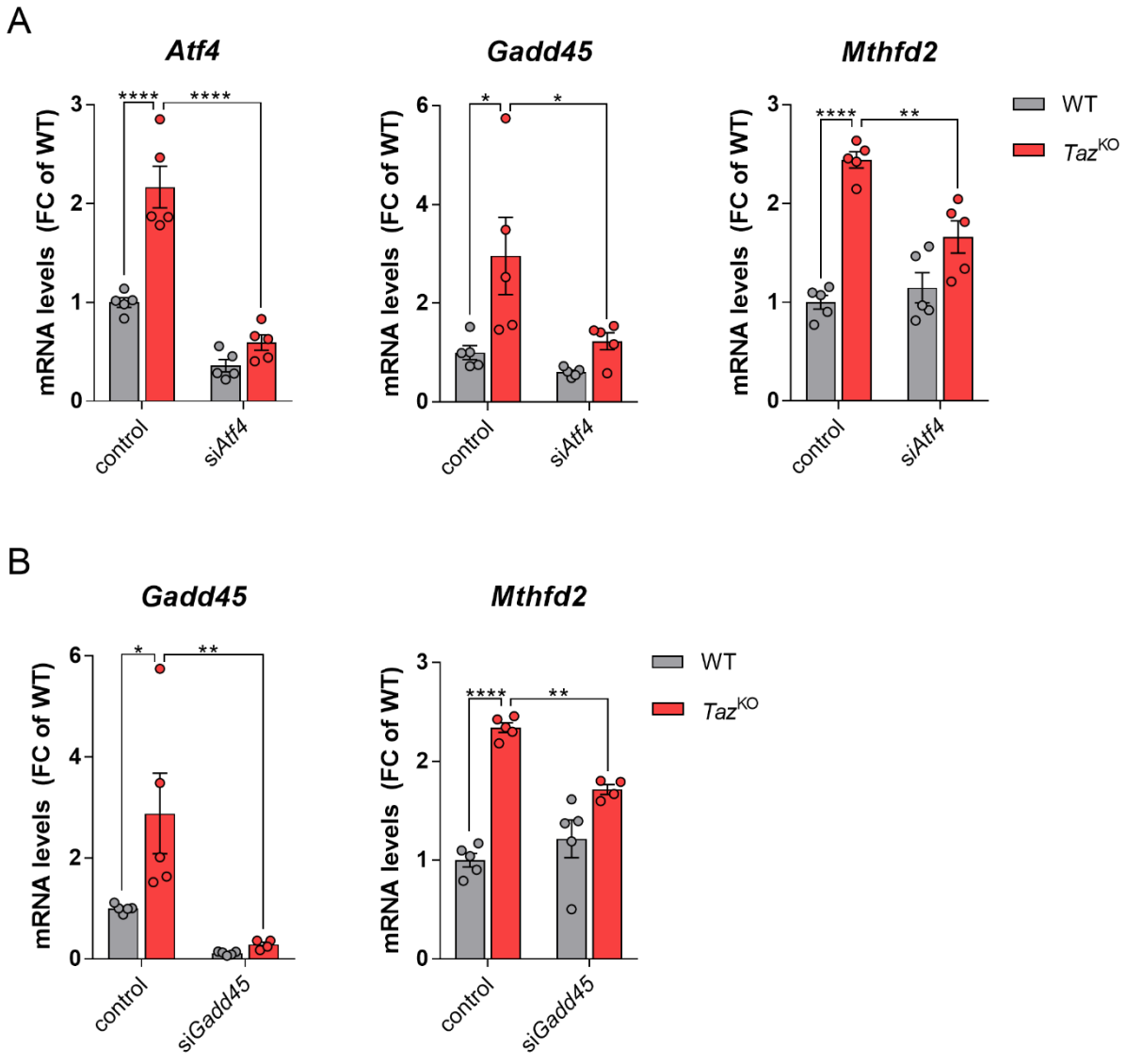


**Figure 14: The integrated stress response regulates metabolic alterations in TAZ deficient mouse embryonal fibroblasts. A)** qPCR analysis of mRNA levels of indicated genes in *Taz*$^{KO}$ MEF cells compared to WT with siRNA mediated knockdown of *Atf4* or control treatment with scrambled RNA

normalized to *mS12*, n= 5. **B)** qPCR analysis of mRNA levels of indicated genes in *Taz*$^{KO}$ MEF cells compared to WT with siRNA mediated knockdown of *Gadd45* or control treatment with scrambled RNA normalized to *mS12*, n= 5. Data are displayed as mean +/- SEM, n-numbers represent individual cell experiments. Statistical analysis was performed with one-way ANOVA followed by Tukey's multiple comparisons test. *: *p*-value < 0.05, **: *p*-value< 0.01, ****: *p*-value< 0.0001.

As a way to achieve information of the regulatory function of the ISR with different unrelated methods and to test a therapeutically usable method, the small compound ISRIB was used to interfere in the ISR signaling. It inhibits phospho-eIF2$\alpha$ activity and therefore represses the upregulation of ATF4 [269]. In general, eIF2$\alpha$ regulation is conducted on protein level, however, ATF is capable to bind the CRE region of its own promoter, regulating *Atf4* gene expression [270]. *Taz*$^{KO}$ cells treated with ISRIB showed a substantial decrease of *Atf4* and *Mthfd2* gene expression compared to the untreated *Taz*$^{KO}$ cells, while the gene expression in WT cells was not changed upon ISRIB administration (**Figure 15A**). Whereas siRNA mediated knockdowns are easy to perform in MEF cells, for iPSC-derived cardiac myocytes the treatment with ISRIB was a more feasible approach to validate the results from the MEF cells. Increased *MTHFD2* gene expression was reduced upon ISRIB treatment in TAZ10 cardiac myocytes compared to the untreated cells, while in control cells, the gene expression of *MTHFD2* was not significantly changed upon ISRIB treatment (**Figure 15B**). As shown in Figure 7H, gene expression of the fatty acid key regulator PPAR$\alpha$ was decreased in cardiac tissue from TAZ deficient mice. This result was verified in iPSC-derived cardiac myocytes. Moreover, the treatment with ISRIB resulted in an elevation of PPAR$\alpha$ gene expression in TAZ10 cells compared to untreated cells (**Figure 15B**).

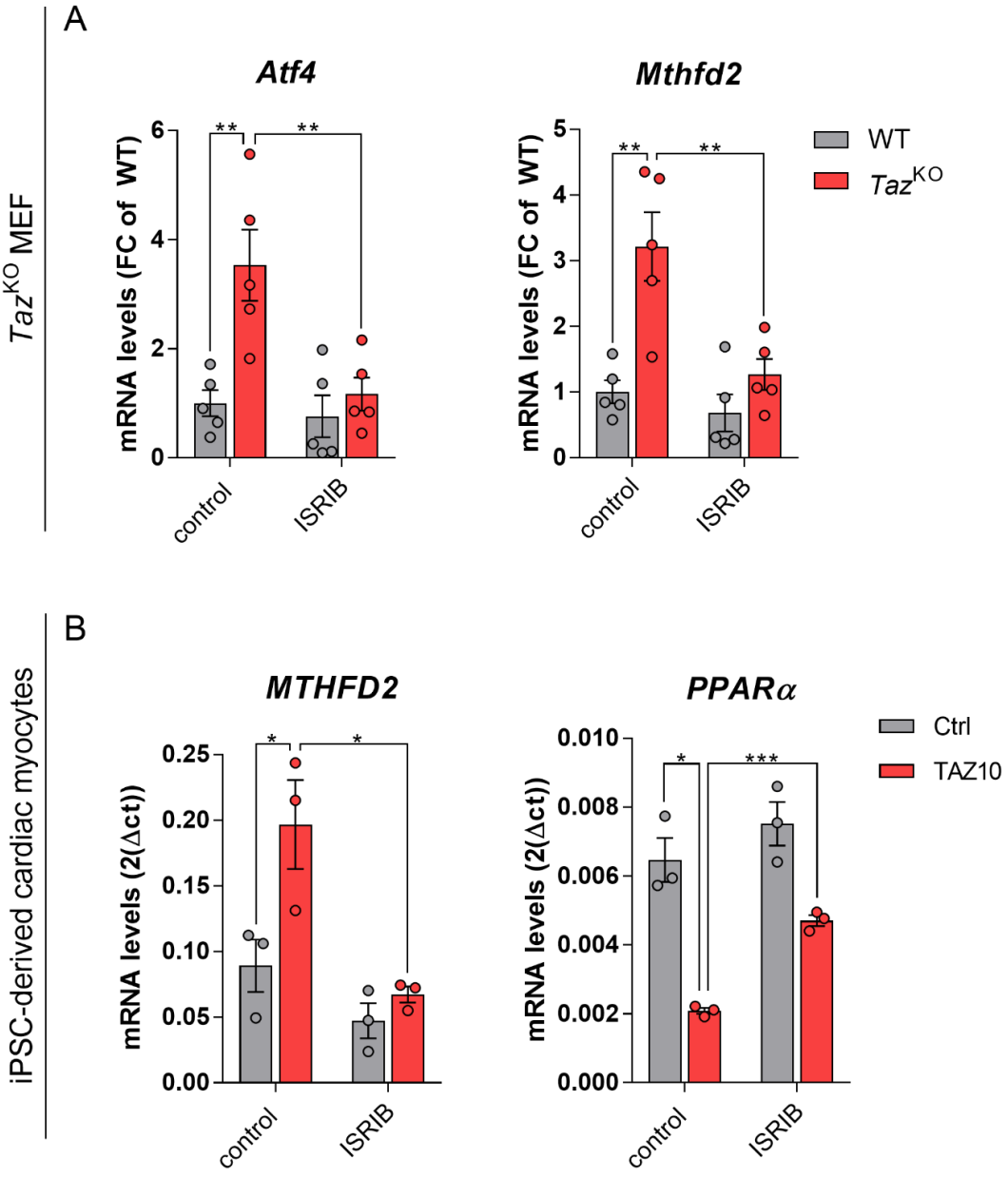


**Figure 15: ISR interference with the small molecule compound ISRIB. A)** qPCR analysis of mRNA levels of indicated genes in *Taz*$^{KO}$ MEF cells compared to WT with or without ISRIB treatment normalized to *mS12*, n= 5. **B)** qPCR analysis of mRNA levels of indicated genes in TAZ10 and control (Ctrl) iPSC-derived cardiac myocytes with or without ISRIB treatment normalized to *L28*, n= 3. Data are displayed as mean +/- SEM, n-numbers represent individual cell experiments in panel A and technical replicates in panel B. Statistical analysis was performed with one-way ANOVA followed by Tukey's multiple comparisons test. *: *p*-value< 0.05, **: *p*-value< 0.01, ***: *p*-value <0.001.

## 4.4 Remodeling of glutamate metabolism in Barth Syndrome

In BTHS, defective fatty acid oxidation and decreased PDH activity lead to the question how the cell is able to maintain its energy supply. Cancer cells are known to exploit amino acid metabolism including glutamine as an energy source to replenish the Krebs cycle via α-KG and for nucleotide synthesis [271, 272]. Hence it was reported that also transporters of amino acids, including the transport of glutamine and glutamate, are upregulated in cancer [273]. It is, however, still unresolved how the BTHS heart is able to meet its energy demand. Altered amino acid metabolism as a result of ISR activation was already shown in mouse models containing deletions of mitochondrial DNA [230, 274]. This lead to the hypothesis that the activated ISR might regulate amino acid metabolism in BTHS. Interestingly, in cardiac tissue from *Taz*-KD mice, gene expression as well as protein levels of the neutral amino acids transporter SLC7A5, which also facilitates the transport of glutamine, were increased compared to WT (**Figure 16A, 16B**). Additionally, gene expression of the sodium-coupled neutral amino acid transporter 1 (*Slc38a1*), which is important for glutamine import, was significantly upregulated in cardiac tissue from *Taz*-KD mice compared to WT (**Figure 16C**). Gene expression analysis via qPCR revealed upregulated gene expression of *Asns* and *Pycr1* in whole heart tissue from *Taz*-KD mice compared to WT (**Figure 16D**). ASNS is a transaminase converting glutamine into glutamate and in parallel produces asparagine from aspartate [275], while PYCR1 uses glutamate to produce proline [276]. Additionally, aldehyde dehydrogenase 18 family member A1 (*Aldh18a1*), which also forms proline from glutamate [277], displays increased gene expression and protein levels (P5CS) in *Taz*-KD mouse heart tissue compared to WT (**Figure 16E, 16F**). Elevated gene expression of *SLC7A5*, *ASNS* and *ALDH18A1* was also verified in iPSC-derived cardiac myocytes from a BTHS patient (**Figure 16G, 16H, 16I**). Furthermore, the treatment with ISRIB significantly diminished the gene overexpression of *ASNS* and *ALDH18A1* in TAZ10 cells compared to untreated TAZ10 cells (**Figure 16H, 16I**), suggesting a regulatory role of the ISR in the amino acid metabolism.

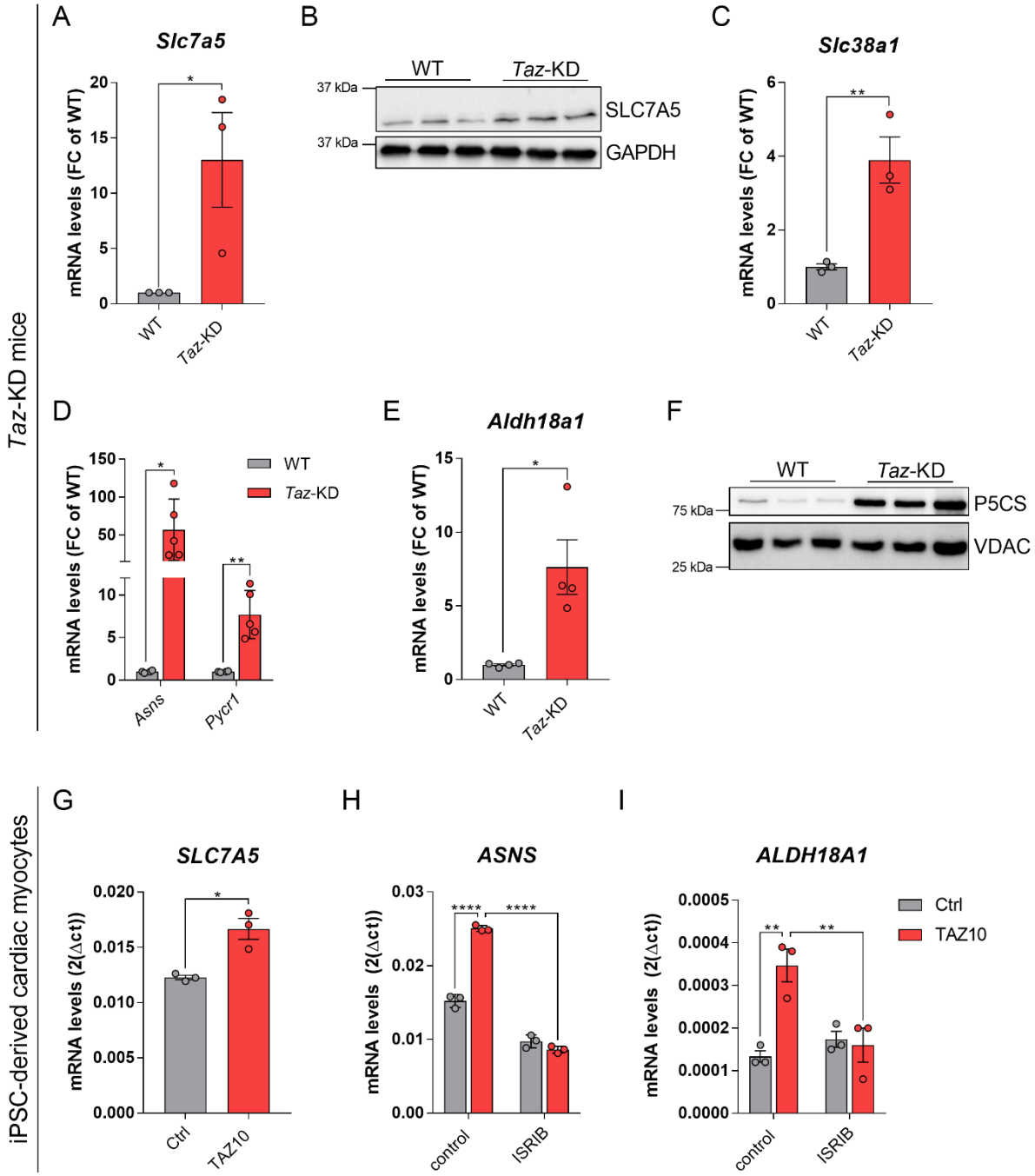


**Figure 16: Glutamate metabolism is elevated in Barth Syndrome. A)** qPCR analysis of *Slc7a5* mRNA in cardiac tissue of *Taz*-KD mice compared to WT normalized to *Gapdh*, n= 3. **B)** Western Blot analysis of SLC7A5 in *Taz*-KD cardiac mouse tissue lysates compared to WT with GAPDH as loading control, n= 3. **C)** qPCR analysis of mRNA levels of *Slc38a1* in cardiac tissue from *Taz*-KD mice compared to WT normalized to *mS12*, n= 3. **D)** qPCR analysis of mRNA levels of indicated genes in cardiac tissue from *Taz*-KD mice compared to WT normalized to *Gapdh*, n= 5. **E)** qPCR analysis of mRNA levels of *Aldh18a1* in cardiac tissue from *Taz*-KD mice compared to WT normalized to *Gapdh*, n= 4. **F)** Western Blot analysis of protein level in cardiac tissue of *Taz*-KD and WT mice with VDAC as loading control, n= 3. **G)** qPCR analysis of *SLC7A5* mRNA in TAZ10 iPSC-derived cardiac myocytes

compared to control (Ctrl) normalized to *L28*, n= 3. **H)** qPCR analysis of *ASNS* mRNA levels in TAZ10 and control (Ctrl) iPSC-derived cardiac myocytes treated with or without ISRIB normalized to *ACTIN*, n= 3. **I)** qPCR analysis of mRNA levels of *ALDH18A1* in TAZ10 compared to control (Ctrl) iPSC-derived cardiac myocytes with or without ISRIB treatment normalized to *L28*, n= 3 Data are displayed as mean +/- SEM, n-numbers represent individual animals in panel A-F, and technical replicates in panel G-I. Statistical analysis was performed with two-tailed unpaired student's t-test in panel A, C, E and G and by one- way ANOVA followed by Tuckey´s multi comparisons test in panel D, H and I. *: *p*-value < 0.05, **: *p*-value< 0.01, ****: *p*-value< 0.0001.

For the purpose of disclosing the function of elevated glutamate metabolism in BTHS, different cellular processes needed to be examined, as glutamate serves many different pathways. In mitochondrial ROS homeostasis, for example, glutamate plays a crucial role as one of the key amino acids in the synthesis of the antioxidant GSH. In addition to glutamate, GSH consists of cysteine and glycine [278, 279]. Cysteine can be produced *de novo* via the trans-sulfuration pathway, or alternatively, its cellular levels are maintained by the import of the oxidized form cystine in exchange for glutamate via the so-called system xCT, which consists of the SLC7A11 transporter together with SLC3A2. Therefore, glutamate is not only used for GSH synthesis itself, but also contributes to cystine uptake via the xCT system [280]. The mRNA levels of *Slc7a11* were elevated in *Taz*-KD mouse cardiac tissue compared to WT (**Figure 17A**). Testing the hypothesis of increased cystine uptake in collaboration with the group of Prof. Takahiro Higuchi, $^{18}$F-5-fluoroaminosuberic acid (18F-FASu) was used *in vivo* to examine the xCT system activity [281]. The cardiac uptake of this tracer was increased in 34 weeks old *Taz*-KD mice compared to WT mice (**Figure 17B**). This tracer was also tested in the MEF cell model, and increased uptake was observed in the *Taz*$^{KO}$ cells (**Figure 17C**). Moreover, an experiment following the glutamate uptake itself by using $H^3$-glutamate was also performed in collaboration with the group of Prof. Takahiro Higuchi. The results showed increased glutamate uptake in the *Taz*$^{KO}$ cells and this effect diminished upon ISRIB treatment (**Figure 17D**). As in the mouse model, qPCR analysis of *Slc7a11* in the MEF cells revealed elevated gene expression in TAZ deficient cells compared to WT, and by blocking the ISR signaling with a knockdown of the transcription factor ATF4, the increased mRNA amount declined in *Taz*$^{KO}$ cells (**Figure 17E**). The same effect was observed in iPSC-derived cardiac myocytes, where *SLC7A11* gene expression was increased in TAZ10 cells compared to the control and ISRIB treatment reduced the mRNA amount (**Figure 17F**). Interestingly, *SLC7A11*

mRNA levels were also elevated in a myocardial sample from one BTHS patient compared to two healthy donor controls (**Figure 17G**). These data indicate that elevated system xCT expression is not only present in the different model systems but also in BTHS patients, and uptake of cystine is increased *in vivo* in the *Taz*-KD mouse model. Moreover, this elevated activity is under the control of ISR signaling.

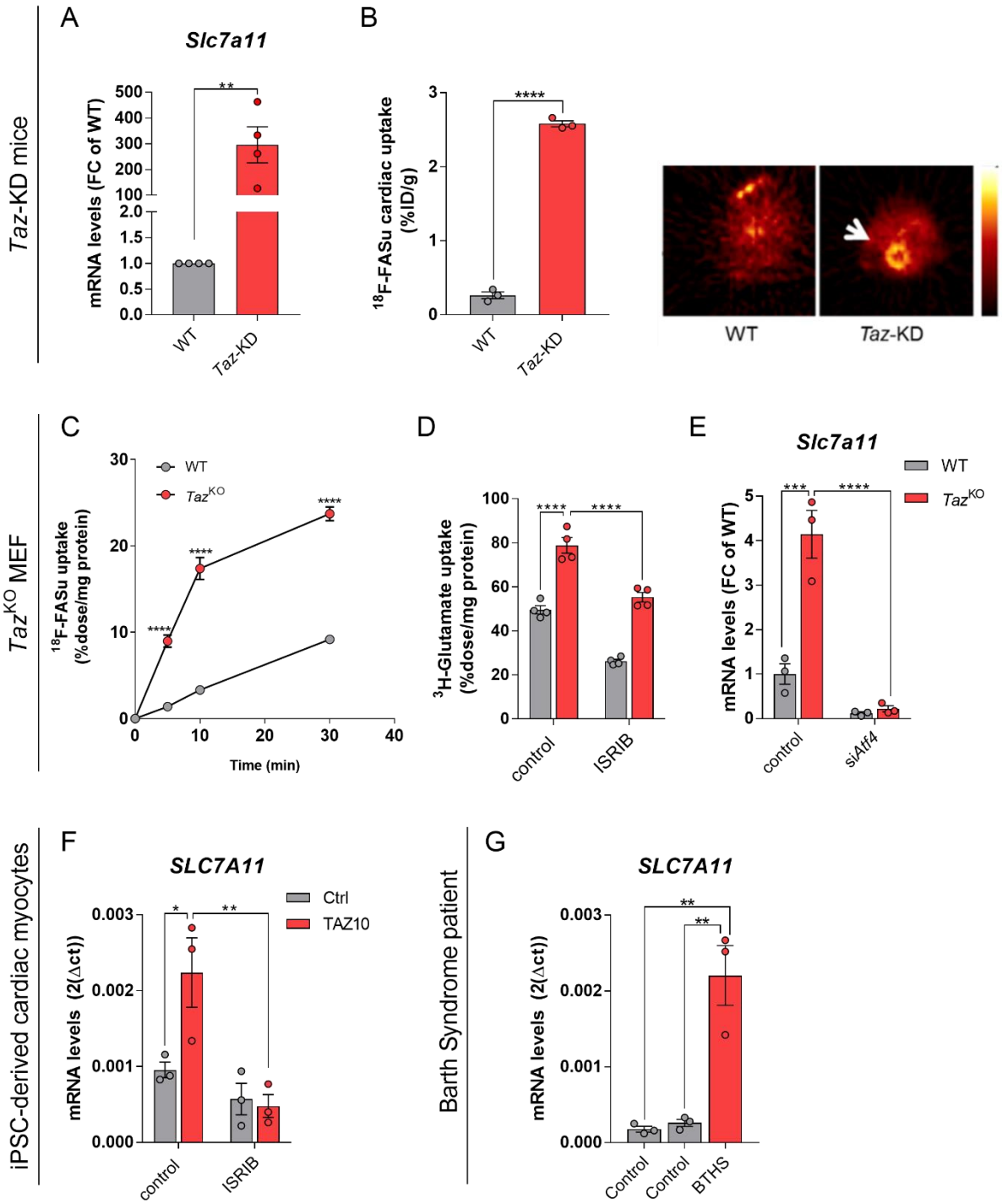

**Figure 17: Elevated activity of the xCT system in Barth Syndrome is dependent on the ISR. A)** qPCR analysis of *Slc7a11* mRNA levels in cardiac tissue from *Taz*-KD mice compared to WT normalized to *Gapdh*, n= 3. **B)** Quantification of $^{18}$F-FASu incorporation into heart of 34 weeks old *Taz*-KD and WT mice (left, n= 3) with representative picture of its visualization by PET-CT scan (right). **C)** $^{18}$F-FASu uptake into *Taz*$^{KO}$ MEF cells compared to WT cells measured by scintillation counting, n= 4. **D)** $^{3}$H-Glutamate tracing in *Taz*$^{KO}$ and WT MEF cells with or without ISRIB treatment, n= 4. **E)** qPCR analysis of *Slc7a11* mRNA levels in *Taz*$^{KO}$ MEF cells compared to WT with siRNA mediated knockdown of *Atf4* or addition of scrambled RNA as control normalized to *Gapdh*, n= 3. **F)** qPCR analysis of *SLC7A11* mRNA level in TAZ10 and control (Ctrl) iPSC-derived cardiac myocytes with or without ISRIB treatment normalized to *L28*, n= 3. **G)** qPCR analysis of *SLC7A11* mRNA in cardiac patient biopsies from two different controls and one BTHS sample normalized to *L28*, n= 3. Results in panels B-D were provided by the group of Prof. T. Higuchi. Data are displayed as mean +/- SEM, n-numbers represent individual animals in panels A and B, individual cell experiments in panels C-E and technical replicates in panels F and G. Statistical analysis for panels A-C and G was performed with two-tailed unpaired student's t-test. For panels D, E and F one-way ANOVA followed by Tukey´s multi comparisons test was performed. *: *p*-value < 0.05, **: *p*-value< 0.01, ***: *p*-value <0.001, ****: *p*-value <0.0001

As a way to test if increased cystine uptake is also accompanied with elevations in the GSH biosynthesis pathway, metabolomic analyses were performed. Metabolomic analysis with mass spectrometry is a precise technique to determine the abundance of metabolites in a biological sample. For this purpose, the sample gets ionized and the mass-to-charge ratio of the ions allows the identification of different molecules. Incubation of cells with labeled substrate even allows to follow the flux of the substrate and its incorporation into different metabolites. In collaboration with Dr. Werner Schmitz mass spectrometry analysis of MEF cell samples, which were incubated with $^{13}C_6$-labeled glucose for 24h, were performed. Considering the natural pattern of the metabolites without carbon incorporation from the labeled glucose, levels of the intermediates of the GSH biosynthesis pathway cystathionine and glutamylcysteine, but also GSH and GSSG levels were elevated in *Taz*$^{KO}$ cells compared to WT (**Figure 18A**). Increased total GSH amount in *Taz*$^{KO}$ MEF cells was additionally confirmed performing an enzymatic GSH assay (**Figure 18B**). To test the hypothesis of increased GSH in mice, different enzymes that are involved in GSH synthesis, were analyzed. The gene expression of the enzyme Cystathione gamma-lyase (*Cth*), which catalyzes the last step of the trans-sulfuration pathway to produce L-cysteine from L-methionine, was significantly increased in *Taz*-KD cardiac tissue compared to WT (**Figure 18C**). Also, the gene expression of the glutathione synthetase (*Gss*), which

produces GSH by using gamma-glutamylcysteine and glycine, was increased in cardiac tissue from *Taz*-KD mice (**Figure 18C**). However, the protein amount of GSS in cardiac tissue from *Taz*-KD mice varies between different biological samples (**Figure 18D**). No significant difference in the amount of total GSH was observed in cardiac tissue from *Taz*-KD and WT mice after its measurement with the enzymatic GSH assay, possibly due to increased flux rates (**Figure 18E**). A trend to elevated gene expression of the predicted mitochondrial glutathione transporter *Slc25a39* in cardiac tissue from *Taz*-KD mice supports increased GSH metabolism in TAZ deficient cells (**Figure 18F**).

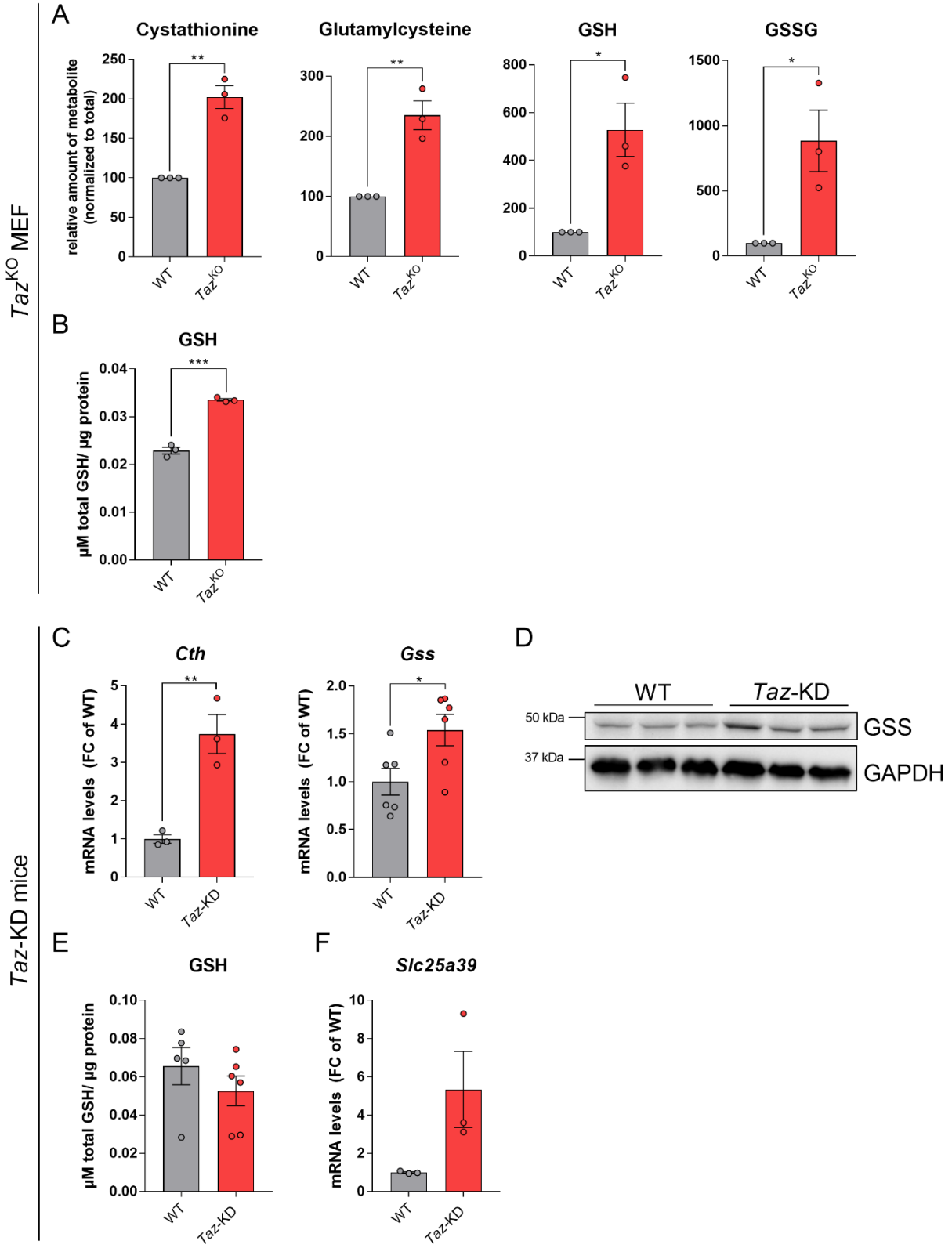


**Figure 18: Metabolic rewiring supports glutathione synthesis in Barth Syndrome. A)** Intermediates of GSH biosynthesis and GSH levels in *Taz*$^{KO}$ MEF cells compared to WT, analyzed by mass-spectrometry, n= 3, Data were provided by Dr. W. Schmitz. **B)** GSH amount in *Taz*$^{KO}$ MEF cells compared to WT, n= 3. **C)** qPCR analysis of mRNA levels of indicated genes in cardiac tissue from *Taz*-

KD mice compared to WT normalized to *mS12*, n= 3 and 6 respectively. **D)** Western Blot analysis of GSS protein levels of cardiac tissue lysates from *Taz*-KD mice compared to WT with GAPDH as loading control, n= 3. **E)** Total GSH amount in mouse cardiac tissue from *Taz*-KD mice compared to WT, n= 5. **F)** qPCR analysis of *Slc25a39* mRNA levels in cardiac tissue from *Taz*-KD mice compared to WT normalized to *mS12*, n= 3. Data are displayed as mean +/- SEM, n-numbers represent individual cell experiments in A and B and individual animals in C-F. Statistical analysis was performed with two-tailed unpaired student's t-test. *: *p*-value < 0.05, **: *p*-value< 0.01, ***: *p*-value <0.001.

In section 4.1, it is shown that in BTHS, the typical energy production from fatty acid in cardiac myocytes was impaired, whereas uptake of glucose into the heart was increased (**Figure 5**). Considering the previous depicted results of elevated glutamate metabolism in BTHS, glutamate might play a role in the energy production in BTHS as well. Glutamine is converted into glutamate by glutaminases, e.g., GLS1, and then further into $\alpha$-KG by different deaminases and transaminases such as GPT2. Gene expression as well as protein levels of GPT2 were increased in heart tissue from *Taz*-KD mice compared to WT mice (**Figure 19A, 19B**) and also the protein level of GAC (a splice variant of GLS1) was higher in the *Taz*-KD mice (**Figure 19B**). The benefit of high glutamate metabolism became apparent with analyzing the oxygen consumption rate of isolated mitochondria from *Taz*-KD and WT mouse cardiac tissue, which was performed by Edoardo Bertero, PhD. *Taz*-KD mouse heart tissue showed a significantly better state 3 respiration with glutamate and malate as substrates compared to mitochondria from WT mice (**Figure 19C**), which is in contrast to the defective fatty acid supported respiration described above (**Figure 6A**).

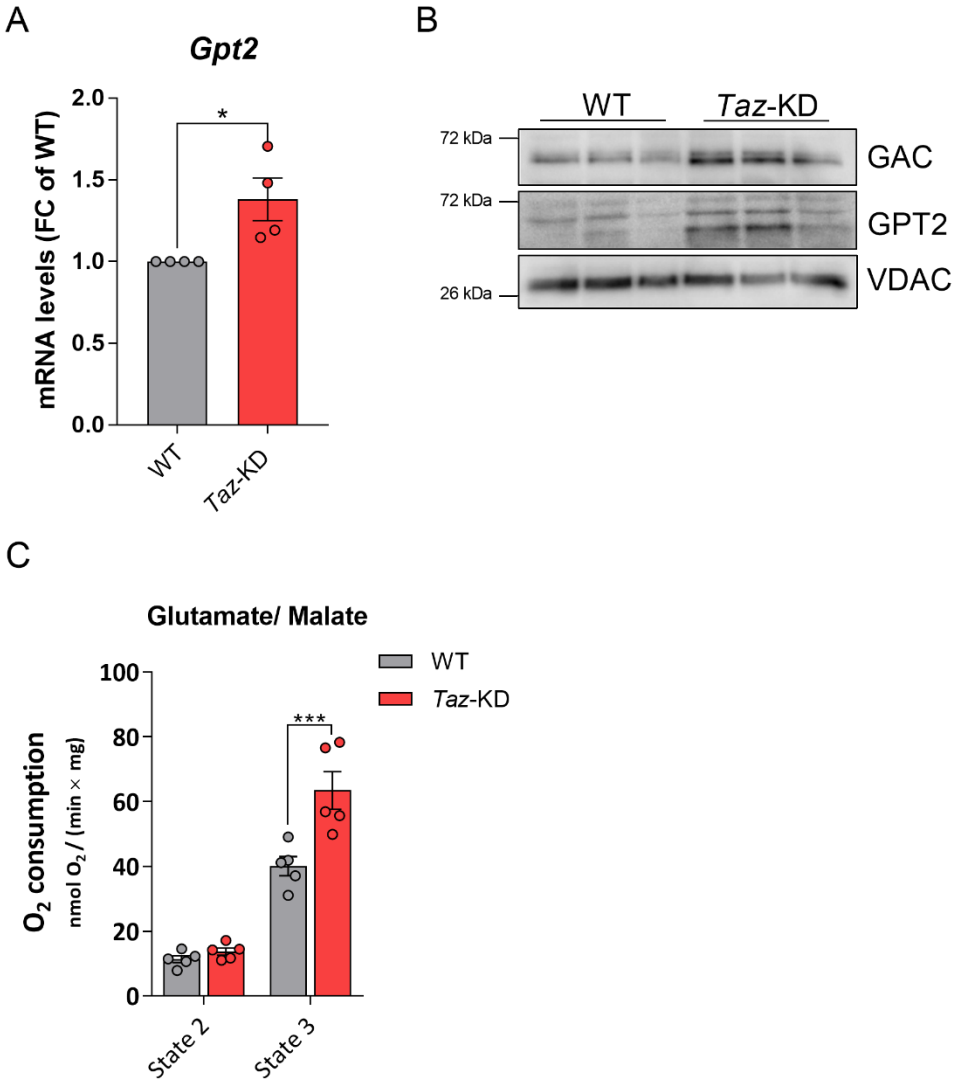


**Figure 19: Glutamate metabolism supports Krebs cycle and respiration in Barth Syndrome. A)** qPCR analysis of *Gpt2* mRNA levels in cardiac tissue from *Taz*-KD mice compared to WT normalized to *Gapdh*, n= 4. **B)** Western Blot analysis of indicated proteins in cardiac lysates from *Taz*-KD and WT mice with VDAC as loading control, n= 3. **C)** Oxygen consumption rate of isolated heart mitochondria from *Taz*-KD mice and WT induced by administration Glutamate/malate. Respiration is measured in absence (State 2) and presence (State3) of ADP, n= 5. Data were provided by Edoardo Bertero, PhD. Data are displayed as mean +/- SEM, n-numbers represent individual animals. For statistical analysis two-tailed unpaired student´s t-test was performed in panel A and 2-way ANOVA followed by Sidak´s multiple comparisons test was performed for panel C. Statistics for panel C were performed by Edoardo Bertero, PhD. *: *p*-value < 0.05, ***: *p*-value <0.001.

# 5. Discussion

## 5.1 Metabolic switch from fatty acid oxidation to glycolysis in Barth Syndrome

To cover the high ATP turnover of cardiac muscle, the adult heart relies mainly on fatty acid oxidation for ATP production. A recent study with young adult BTHS patients reported an increase in glucose utilization in the myocardium in connection with decreased fatty acid metabolism [255]. These data coincide with the *in vivo* findings in the *Taz*-KD mouse model, where fatty acid metabolism in the heart was significantly decreased whereas the glucose uptake was elevated. Respiration defects on different fatty acids were identified in cardiac mitochondria from *Taz*-KD mice, while respiration on pyruvate and malate was unchanged. To identify a possible cause of impaired fatty acid uptake, mechanisms of the fatty acid import into mitochondria and the β-oxidation were closer examined. Reduced protein levels as well as gene expression of enzymes from the carnitine shuttle system were observed in cardiac tissue from *Taz*-KD mice and iPSC-derived cardiac myocytes from one BTHS patient. Deficiencies of these proteins have already been reported to cause cardiomyopathy and arrhythmias in newborns and young infants [282-284], which suggests that the reduced fatty acid oxidation might be conductive to the cardiac phenotype in BTHS. Transcriptional regulation of the genes could be the cause of reduced production of the proteins that are necessary for fatty acid metabolism. However, CL is known to be crucial for correct incorporation and function of many protein complexes in the mitochondria. Diminished amounts of CL in BTHS alters the lipid composition of the membrane bilayer and therefore, might affect the proper incorporation of newly synthesized proteins into the mitochondrial membrane, leading to a high turnover of these proteins. Consequently, the reduced gene expression could be a secondary effect to the impaired incorporation of these proteins. This negative feedback loop probably helps the cell to save energy as the production of the proteins by gene expression and translation cannot repair the actual issue that the proteins are not properly incorporated into the membrane. As a recent study in BTHS patients demonstrated a defect in fatty acid oxidation upstream of β-oxidation cycle [285], we investigated fatty acid transport into mitochondria. In addition to the different membrane bound proteins, fatty acids need carnitine to be able to cross the membranes. Interestingly, protein levels of the first enzyme of carnitine

synthesis were reduced together with a significant reduction in mRNA levels in *Taz*-KD cardiac tissue. This finding supports the hypothesis of defective fatty acid uptake into mitochondria in TAZ deficient cells. Moreover, some patients exhibit carnitine deficiency, and reduced carnitine itself is also known to contribute to cardiomyopathy [135, 286, 287]. Lower carnitine levels were also measured in our laboratory in iPSC-derived cardiac myocytes from BTHS patients (data not shown). An experiment performed in our laboratory during the preparation of this study, using Bodipy labeled fatty acids administered to iPSC-derived cardiac myocytes from a BTHS patient and control, showed the formation of lipid droplets which were taken up by mitochondria in the control cells under starvation. The iPSC-derived cardiac myocytes from the BTHS patient however, still had more lipid droplets in the cytosol after starvation, suggesting a defect in the uptake of fatty acids into mitochondria (data not shown). A possible upstream mechanism of the altered fatty acid metabolism might be the reduction of the key transcription factors of fatty acid metabolism PPAR$\alpha$ and PGC1$\alpha$ in *Taz*-KD cardiac tissue. Their reduction could be causative for subsequent down regulation of gene expression of the proteins from the carnitine shuttle. The variety of defects in the fatty acid metabolism and the substrate switch to glucose might implement that this is a compensatory mechanism of the affected cells. However, even though the increased glucose uptake was confirmed with PET-CT scans, the mitochondrial respiration based on pyruvate and malate as substrates does not increase in *Taz*-KD and therefore does not compensate the defective respiration on fatty acids. The enzyme pyruvate dehydrogenase (PDH) is the linking enzyme bringing pyruvate produced in the glycolysis into the Krebs cycle [288]. A reduced activity of PDH has already been reported in Taz-KO C2C12 myoblast cell models [123, 289], and preliminary data from the working group not shown in this thesis confirm these findings in the *Taz*-KD mouse model. PDH activity is regulated via phosphorylation. De-phosphorylation leads to activation of the enzyme and is catalyzed by the $Ca^{2+}$ sensitive PDH phosphatase [290]. Bertero et al. demonstrated reduction in the MCU complex in BTHS and therefore impaired $Ca^{2+}$ handling [128], which consequently could contribute to the decreased PDH activity. Performing respiration measurements with isolated mitochondria limits the explanatory power as the measurements are not performed in a cellular context and the regulation of PDH activity via the $Ca^{2+}$ signaling is absent. This might explain the unchanged respiration in *Taz*-KD and WT mitochondria with pyruvate and malate addition. Diakos et al. showed in heart failure patients with left

ventricular assist device (LVAD) implant that LVAD unloading activated glycolysis, the produced pyruvate however, did not fuel into the TCA cycle for oxidation and the mitochondrial oxidative functional capacity was not improved after LVAD [291]. Moreover, amino acid levels after LVAD unloading were elevated and could be evidence for a compensatory mechanism and an alternative pathway of anaplerosis fueling into the TCA cycle for energy production [291]. In an ongoing experiment in our lab, no evidence of an increased flux of labelled glucose into the TCA cycle was found *in vitro* (MEF and iPSC-CM) and *in vivo* in the *Taz*-KD mouse model (data not shown). In summary, fatty acid oxidation is reduced in BTHS hearts, and glycolysis and glucose oxidation cannot compensate for this defect.

## 5.2 Activation of the integrated stress response causes metabolic remodeling in Barth Syndrome

Increased ROS levels are often associated with dysfunctional mitochondria [292, 293]. The absence of ROS in the BTHS mouse contrasting the more oxidized redox state under elevated workload conditions lead to the hypothesis that compensatory mechanisms might be responsible for the prevention of oxidative stress. Transcriptome analysis revealed over 7000 de-regulated genes, and among these, a high enrichment of genes engaged in serine biosynthesis and one-carbon metabolism could be observed. The data from transcriptome analyses were confirmed with qPCRs in different model systems, and increased formate levels measured in *Taz*$^{KO}$ MEF cell lysates supports the hypothesis that the whole one-carbon metabolism is elevated in BTHS. Noticeably, the first enzyme of the mitochondrial one-carbon metabolism branch showed elevated protein amounts in *Taz*-KD cardiac tissue, whereas the protein amount of the cytosolic branch is unchanged. This implies a preferential flux of serine into mitochondria instead of the cytosolic part. The most elevated gene expressed in *Taz*-KD cardiac tissue according to the transcriptome data belongs to one-carbon metabolism and is interestingly (in addition to the mouse model) also highly upregulated in TAZ10 iPSC-derived cardiac myocytes and in the heart biopsy from a BTHS patient, both on gene expression as well as protein level. This suggests the same regulation of the metabolism in the human disease as observed in the mouse model. Interestingly, the protein analysis of MHTFD2 in patient biopsies showed elevated levels only in BTHS, but not in ICM or DCM, which suggests that upregulation of the one-carbon metabolism is (at least to this degree) a rather specific response in

BTHS cardiomyopathy rather than in other forms of heart failure. While it was previously reported that in patients with advanced heart failure, elevated flux through the serine synthesis pathway and one-carbon metabolism [294] and reduced catalytic activity of MTHFR, an enzyme at the cytosolic part of the one-carbon metabolism, is related to higher risk of ischemic heart disease and stroke [295], these data do not allow any conclusion about whether such upregulation plays an adaptive or maladaptive role. In contrast, patients with advanced heart failure who responded to LVAD implantation for mechanical unloading had increased enzyme expressions of one-carbon metabolism compared to unresponsive patients, while serine and glycine levels were reduced [294]. In this case, increased one-carbon metabolism seems to be linked to cardiac recovery [296]. An early study from 1993 described the relation of the format production deriving from serine, which is dependent on respiration [297]. The $NAD^+$/NADH ratio in mitochondria is sustained by calcium mediated regulation of mitochondrial metabolism, which is impaired in TAZ deficient cells [128, 152]. As MTHFD2 activity also produces NADH, this might be a compensatory effect of restoring the $NAD^+$/NADH balance and would link the increased one-carbon metabolism to the dysfunction in mitochondrial respiration in BTHS. Additionally, it has been reported that increased SHMT2 activity is critical to maintain mitochondrial redox balance in cancer cells [298], which could also be beneficial for the anti-oxidative capacity in BTHS.

The exact reason for elevated one-carbon metabolism and its consequences for the cell, however, are not fully uncovered yet. Another remaining question is the regulatory mechanism that alters the metabolism in BTHS. In the transcriptome analysis from the *Taz*-KD cardiac tissue, many upregulated genes are known to be regulated by ATF4, which is a central transcription factor of the ISR pathway [225]. Examination of this pathway in the model systems for BTHS showed activation of the ISR upon mitochondrial defects in the heart. Auto-phosphorylation of so far unidentified sensor kinases due to different stress factors leads to phosphorylation of eIF2$\alpha$, which is increased on protein levels in *Taz*-KD heart tissue. Elevated activity of the ISR pathway has already been described in several studies of heart failure models [225, 299, 300]. Yao et al. showed increased signaling through the ISR in different models of heart failure by analyzing typical kinases and transcription factors of the signaling pathway including the phosphorylation of PERK and eIF2$\alpha$ as well as levels of ATF4 and CHOP [301]. They induced cardiac hypertrophy by transverse aortic constriction (TAC) surgery and isoproterenol application in mice, but also analyzed samples from patients

with dilated cardiomyopathy. All proteins mentioned above exhibited elevated levels on Western Blot analysis of cardiac protein extracts, confirming elevated ISR activity [301]. Zhu et al. demonstrated that induced mitochondrial stress due to the knockout of the mitochondrial protein tyrosine phosphatase mitochondrial 1 (PTPMT1) activated the stress signaling along the eIF2α-ATF4 axis and elevated the gene expression from enzymes of the one-carbon metabolism [296]. Moreover, they showed that blocking eIF2α phosphorylation negatively affected the survival [296]. PTPMT1 is an important enzyme in the CL biosynthesis pathway, and its knockout leads to a significant decrease in CL amount [28, 29]. Double mutant mice including *Ptpmt1* knockout and an eIF2α mutation died at time point E13.5 of embryonal development, whereas mice containing only the *Ptpmt1* knockout survived, although with abnormal cardiac morphology [296]. ISR activation occurs under many different conditions, and it can also be induced by mitochondrial dysfunction, as reported in a mouse model of familial progressive external ophthalmoplegia, where mutations in the Twinkle gene cause deletions in mitochondrial DNA leading to the disease [229, 302, 303]. The ISR can be activated by many different triggers and so far, four sensor kinases were identified in this signaling axis.

Different experiments were performed in our lab to identify a possible relation between ROS and ISR induction, but no evidence was obtained that ROS is triggering the elevated ISR in BTHS (data not shown.) Preliminary data from the working group not shown in this thesis suggest an activation of PERK in the *Taz*-KD mouse model due to increased levels of phosphorylated PERK. A typical trigger of PERK phosphorylation is the unfolded protein response, but also deranged membrane lipid composition might activate the ER stress response via PERK [304]. Sohn et al. used a new murine model of BTHS neutropenia and discovered higher expression of ATF4 and CHOP in TAZ deficient cells that suggests increased ER stress [305]. Additionally, those cells were more sensitive to apoptosis. They hypothesize that CL depletion and accumulated MLCL in TAZ deficient cells hinders the normal lipid crosstalk of mitochondria with the ER, causing aggregation of unwanted lipids in the ER. This malfunction in lipid metabolism could result in ER stress and the activation of apoptotic pathways [305]. PERK induced stress signaling has been observed to be beneficial in heart failure [306] but there are also reports of contradicting results suggesting a maladaptive role of the PERK-eIF2α-ATF4 signaling axis leading to apoptosis and causing damage in myocardial ischemia–reperfusion injury [307, 308].

However, it cannot be definitely excluded that also the other kinases are involved in the stress signaling in BTHS. HRI was already reported to be a potential activator of ISR by mitochondrial dysfunction [296, 309]. In the study of Zhu et al., mitochondrial stress was simulated with *Ptpmt1* knockout mice and creating double knockouts with the sensor kinases GCN2 and HRI allowed the identification of the kinase that activated the ISR in this model system [296]. Levels of p-eIF2$\alpha$ and ATF4 were still increased in the GCN2 double knockout, while the effect was abolished in the HRI double knockout. This lead to the conclusion that HRI was responsible for ISR activation in this mouse model [296].

Recently, different studies showed a connection of mitochondrial dysfunction and ISR activation through the OMA1-HRI-Dele1 axis [228, 309, 310]. Preliminary results suggest an activation of ISR through Dele1 in BTHS, as the siRNA mediated knockdown of Dele1 in TAZ deficient cells reduced the phosphorylation of eIF2a, which was increased in cells with scrambled RNA. Moreover, ongoing experiments measuring ROS in these cells showed increased ROS in TAZ deficient cells treated with siRNA against Dele1 compared to scrambled RNA (data not shown). This would denote the ISR to be an adaptive mechanism for TAZ deficient cells that helps to combat excessive mitochondrial ROS and prevent damage to the cell.

Activation of the ISR by GCN2 upon mitochondrial defects has been reported also [292, 293]. GCN2 is known to induce the ISR by sensing amino acid limitation [206]. Interestingly, Ranea-Robles et al. linked the activation of the ISR in the heart to malfunctioning amino acid metabolism, which is caused by dysfunctional long-chain fatty acid oxidation [311]. Amino acid deprivation would suggest ISR activation by GCN2, this was however not verified in the study [311]. In the BTHS model systems, altered amino acid metabolism and defects in fatty acid oxidation were also observed, which would suggest an ISR activation through GCN2. However, the usage of currently available antibodies for the kinases of the ISR pathway did not allow a robust statement about their phosphorylation status in cardiac tissue and therefore, the concrete identification of the sensor kinase in BTHS was not possible.

Taken the literature into account, it seems that active ISR signaling can be beneficial for the cell, but also causing damage through apoptosis. There is no consistent effect of ISR signaling on the cardiac phenotype, even in similar disease models such as myocardial ischemia/reperfusion injury, different studies reported damage caused by ISR signaling, while others observed cardioprotection upon acute ISR signaling [308,

312]. In the different BTHS model systems, increased ISR activity was verified and additionally, its regulatory function for the metabolic alterations could be shown by blocking the signaling with two independent approaches. Hence, it is still not finally resolved, if the activation of the ISR signaling is beneficial for the heart or maladaptive in BTHS and can only be tested by a (cardiac specific) knockout of ATF4 in the BTHS mouse model, which is currently ongoing in our lab, but beyond the scope of this study. As discussed above, the increased glucose uptake does not compensate for the oxidative phosphorylation defects by fueling into the Krebs cycle via pyruvate due to reduced PDH activity. Upregulation of the ISR and consequently other metabolic pathways, such as serine synthesis and one-carbon metabolism, might be a beneficial adaption of the cell to reasonable use the augmented glucose to its advantage by supporting other important mechanisms such as anti-oxidation and providing reduction equivalents for oxidative phosphorylation.

## 5.3 Remodeling of the mitochondrial metabolism supports glutathione synthesis and anaplerosis

The typical substrates for energy production in the heart are fatty acids. The BTHS phenotype includes a defect in fatty acid metabolism, while glucose uptake in the heart is increased. Elevated glucose levels, however, are not compensating for the energy deficit evolving from impaired fatty acid metabolism. Though surprisingly, amino acid metabolism was rewired, which is uncommon in the heart. This applies especially for glutamate metabolism, which was altered in the experimental models. Analysis of typical glutamate transporters and enzymes included in glutamate conversion showed elevated expression in TAZ deficient cells from the murine model and iPSC-derived cardiac myocytes. Increased glutamate uptake was validated in TAZ deficient MEF cells using $^{3}$H-Glutamate. Moreover, ISR signaling was identified as the regulatory mechanism for the altered glutamate metabolism. In mouse models with respiratory chain defects, it was previously shown that besides CHOP, PSAT and MTHFD2, also enzymes of amino acid metabolism, such as ASNS and PYCR1, are highly expressed as a stress response. Both ASNS and PYCR1 utilize glutamate and showed elevated gene expression in TAZ deficient cells. The elevated PYCR1 expression described above might be a response to increased glutamine metabolism, as it is needed to convert glutamine into proline. Additionally, elevated gene expression and protein levels of the first enzyme of proline synthesis (gene: *Aldh18a1*, protein P5CS) argues

for a higher amino acid turnover and proline production. Elevated proline levels have already been reported in BTHS patients [257, 313], and the results from experiments with patient derived iPSC cardiac myocytes support the hypothesis of altered amino acid metabolism including glutamate and proline in BTHS patients.

An additional pivotal role of glutamate is its contribution to the biosynthesis of GSH, which is an important antioxidant in mitochondria. In the development of the BTHS phenotype, the role of ROS emission is still extensively debated without a clear result of the effect of ROS to the pathophysiology [155, 164]. In a previous study from our group, no elevated levels of superoxide or $H_2O_2$ were reported in the *Taz*-KD mouse model [128]. This may be explained by an elevated detoxification via $H_2O_2$-eliminating catalase and GPX1. Activation of the serine pathway and the associated one-carbon metabolism plays an essential role in the biosynthesis of GSH, which is an important substrate for the GPX1-mediated ROS detoxification. Besides glutamate, cysteine is a rate limiting amino acid required for GSH biosynthesis. Although the trans-sulfuration pathway can supplement cysteine by synthesis from homocysteine and serine, elevated GSH production requires cystine - the oxidized form of cysteine - uptake via the system xCT transporter in many tissues [314]. This system was also upregulated in the different BTHS model systems and *in vivo* experiments verified its increased activity in the heart of *Taz*-KD mice. Furthermore, the results supported the hypothesis that the active ISR signaling is responsible for those metabolic changes. Blocking of ISR signaling diminished the overexpression of Slc7a11. Different studies in mice and rats observed reduced cardiac injury by overexpressed *Slc7a11* leading to elevated GSH levels and preventing cardiac ferroptosis [315, 316]. Oxidative stress is a widely reported factor involved in heart failure development [317-320], and Dhalla et al. reported a reduction of the GSH/GSSG ratio developed in heart failure [321]. Indeed, GSH is suggested to play an important role in cardiac abnormalities [322-324]. The effect of GSH on immaculate cardiac function is also evident in the study of Damy et al., who demonstrated a correlation of the severity of cardiac disease in patients with the GSH content in atrial tissue [322]. GSH levels were significantly reduced in patients ranked in the New York Heart Association (NYHA) class IV compared to asymptomatic patients in class NYHA class I. Furthermore, association of antioxidant deficit with heart failure caused by myocardial infarction supports the indispensable role of GSH in the heart [325]. Different studies reported cardioprotective effects by enhancing anti-oxidative enzymes such as superoxide dismutase and glutathione peroxidase [326-

328]. The results in the BTHS models revealed elevated levels of the glutathione precursors cystathionine and glutamylcysteine, that argue for an increased glutathione synthesis with precursors derived from the trans-sulfuration pathway. In addition, the elevated xCT system contributes for elevated cysteine by importing cystine. Increased import of cystine could be responsible for its decreased circulating amount in BTHS patients [257]. In parallel, glutamate is exported by xCT. This might explain the high glutamate uptake into the cell through other transporters. Their upregulation compensates for the lack of glutamate which arises due to the glutamate export via the xCT system. Considering these results, accumulation of GSH in BTHS cells would be expected. This was indeed observed in the TAZ deficient cell model, but was not the case in cardiac tissue from the *Taz*-KD mouse.

This could be due to and rapid GSH turnover in the heart of *Taz*-KD mice by increased levels of GPX1 [128], which prevents the accumulation of GSH. Comparing the results to the reports from the literature about the beneficial effect of GSH for cardiac function, it seems that the ISR signaling upregulates the glutamate metabolism in favor of GSH to hinder the accumulation of harmful ROS. In this case, the stress response would be an adaption of the cell to increase its chance of cardiac tissue survival.

Besides the synthesis of GSH, glutamate can also be converted into $\alpha$-KG and thereby fuel into the Krebs cycle as an anaplerotic substrate. Additional data from *in vivo* labeled glutamine infusion performed in collaboration with the group of Prof. Joshua Rabinowitz (Princeton University, USA) showed alterations in Krebs cycle metabolites, which especially supported the hypothesis of increased glutamate flux into $\alpha$-KG (**Figure 20**).

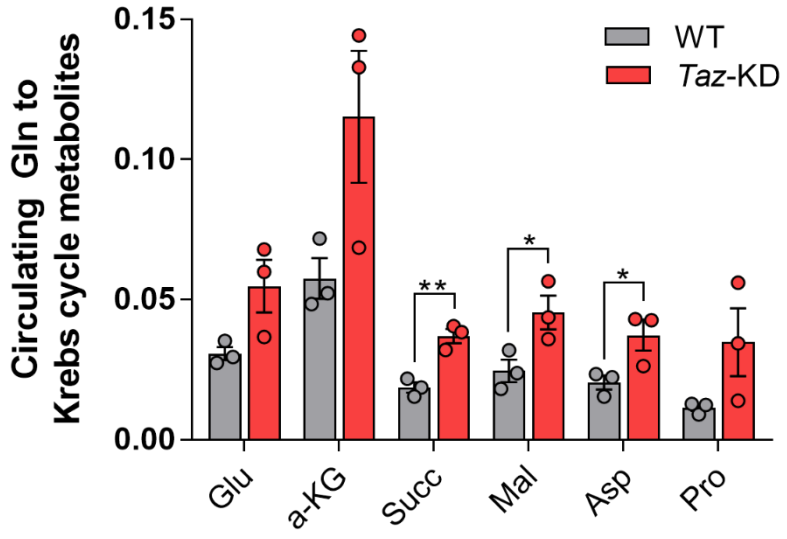


**Figure 20: Cardiac Krebs cycle metabolites labeling from [U-$^{13}$C, $^{15}$N] glutamine (Gln) infusion in 10 to 11 weeks old *Taz*-KD mice compared to WT.** Metabolite enrichment was normalized to the enrichment of tissue [U-$^{13}$C, $^{15}$N] glutamine. n=3 individual animals. Statistical analysis was performed using two-tailed unpaired student´s t-test. *: *p*-value < 0.05, **: *p*-value< 0.01. Data were provided by the group of Prof. J. Rabinowitz. Glu= glucose, a-KG= $\alpha$-ketoglutarate, Succ= succinate, Mal= malate, Asp= Aspartate, Pro= proline.

In agreement with these *in vivo* data, also in isolated cardiac mitochondria *in vitro*, respiration was nearly twice as high in *Taz*-KD compared to WT mitochondria when glutamate and malate were used as substrates. The recently described loss of the MCU complex in BTHS impairs the proper function of the Krebs cycle, due to defective $Ca^{2+}$ induced stimulation of rate-limiting enzymes of the Krebs cycle [128]. By directly fueling $\alpha$-KG into the Krebs cycle, two of the $Ca^{2+}$ stimulated enzymes are bypassed, which might result in the better respiration on glutamate. Therefore, the defects in fatty acid supported respiration and also the Krebs cycle defect not only led to increased glucose uptake, but also amino acids are utilized for energy production in BTHS to countervail the energy deficit. Under physiological conditions, amino acids serve in anabolic pathways as a substrate for protein synthesis and have only limited contribution to energy conversion in the healthy heart. In heart failure, under conditions of low oxygen tension, however, a role of amino acids for anaplerosis of the Krebs cycle has already been reported [329, 330]. Glutamine is a conditionally essential amino acid, whose demand exceeds biosynthesis during physiological stress and infancy and is used as an anaplerotic substrate in the Krebs cycle during myocardial

anoxia and ischemia [331-333]. It has been observed that BTHS patients show preferences for salty and strong flavored food [334]. Glutamate is known to intensify these flavors [335], so one could hypothesize that the body of BTHS patients reacts to the energy deficit caused by impaired fatty acid oxidation and requests for glutamate supplementation itself. Certain diets might promote the wellbeing of BTHS patients, and to monitor the nutrition uptake and growth of patients, growth charts have been published to help determine a normal growth for boys with the disease [137]. Protein supplementation together with resistance exercise training was reported to improve skeletal muscle strength and the overall quality of life in BTHS patients [336].

## 5.4 Outlook

This thesis extensively dealt with the metabolic alterations in BTHS and gives new insight into the metabolic changes that arise from mitochondrial dysfunction due to loss of Tafazzin function. A variety of experimental models enabled the investigation of novel signaling pathways *in vitro* and *in vivo* in TAZ deficient mice and MEF cells as well as human cardiac myocytes derived from BTHS patient stem cells and additionally cardiac tissue from one BTHS patient. In summary, the ISR signaling along the eIF2$\alpha$-ATF4 axis was identified as a central regulator in BTHS cardiomyopathy. This aggravates the activity of *de novo* serine biosynthesis, one-carbon metabolism and the system xCT to maintain glutathione synthesis for ROS elimination, which is accompanied by remodeled GSH metabolism, to support GSH synthesis, but also Krebs cycle anaplerosis. The results of this work provide important new insights into metabolic rewiring in BTHS cardiomyopathy that may serve to develop new therapies to improve mitochondrial and thereby, cardiac function in these patients.

It would be of great interest to decipher the molecular triggers that provoke the metabolic rewiring including the identification of the responsible kinase(s) that activate(s) ISR signaling. Knockdown experiments of the different kinases in TAZ deficient cell models via siRNA or with specific inhibitors might help to answer this open question. Furthermore, genetic modification of cells via CRISPR/Cas9 creating a stable knockout of the gene of the different kinases would be a feasible approach. MEF cell experiments with silencing the ISR signaling already allowed key insights into the relation between the ISR activity and the extensive metabolic changes in TAZ deficient cells. However, for a better understanding of the purpose of the increased ISR, *in vivo* approaches would help to reveal whether it is a compensatory mechanism, triggered

by mitochondrial dysfunction, or rather a maladaptive process. Taking into account the experimental procedures of blocking the ISR *in vitro*, increased ISR could not be unambiguously classified as adaptive or maladaptive. Cellular survival and proliferation did not change by interrupting the ISR. *In vivo* studies with the *Taz*-KD mouse model should supposedly reveal clearer results. However, first approaches with ISRIB treatment in *Taz*-KD mice that are not reported in this thesis did not show the same effects in gene regulation as in the MEF cells and also the obvious phenotype of the mice did not change. This could be due to problems in the drug stability or bioavailability in the mice. Therefore, a genetic approach by introducing an *Atf4* knockout or knockdown into the *Taz*-KD mice could be a more efficient way to silence the ISR. A systemic *Atf4* knockout in mice results in many severe defects, including developmental and metabolic defects, which leads to a very short viability of these mice after birth [337, 338]. Hence, introducing a cardiac specific *Atf4* knockout would make a reasonable approach to investigate the effect of ATF4 on the cardiac phenotype in BTHS. As a way to verify the central role of ATF4 in the development of the metabolic phenotype in BTHS, different experiments could be performed. In a first approach, the actual loss of ATF4 in cardiac tissue should be checked by analyzing the mRNA transcription of *Atf4* but also the reduction of the protein. Then, the different pathways, that were shown to be affected by ISR signaling and ATF4 *in vitro*, should be examined *in vivo* including serine synthesis, one-carbon metabolism and glutamate metabolism. As in the *in vitro* experiments, typical enzymes of these pathways can be analyzed in cardiac tissue and compared to *Taz*-KD without *Atf4* knockout as a control to show the relation of ATF4 and the regulation of the metabolic alterations. Lastly, the examination of cardiac function would be possible in the mouse model using echocardiography. This would provide new insights in the role of ATF4 in the development of the functional cardiac phenotype in BTHS *in vivo*, which was not possible with the *in vitro* experiments so far.

Many results from this thesis argue for a strong alteration in glutamate metabolism fueling into GSH production in BTHS. It appears that the metabolism changed to elevated usage of glutamate is an adaptive process to support ATP and GSH production and thereby, cellular function. Pharmacological inhibition of the xCT system with, for instance, erastin [339] could reveal the necessity of this regulation and also if it is a compensatory alteration that has positive effects on the cell. In a first approach, this could be performed *in vitro* with the different TAZ deficient cell models available.

Furthermore, flux analysis with $^{13}C_5$ labeled glutamine could provide more insights which pathways, besides GSH synthesis and the Krebs cycle, are taking advantage of the increased glutamate metabolism. Even though increased ROS was not detected in the *Taz*-KD mouse [128], it would be valuable to know if there is still some ROS damage occurring. Ahola et al. demonstrate in their study that elevated ISR signaling is a protective regulation in mitochondrial cardiomyopathy, and inhibition of the ISR causes defects in ROS defense mechanisms and increased lipid peroxidation, which ultimately results in ferroptosis [228]. To interrogate lipid peroxidation in hearts could reveal if ROS can be eliminated effectively before causing any damage. This could be obtained by either performing commercially available lipid peroxidation kits, Western Blot analysis detecting typical products of lipid peroxidation, such as 4-HNE or measurements with the commercially available oxidation-sensitive C11-Bodipy [340].
Preliminary data with differentiated cardiac myocytes from patient-derived iPS cells already gave a hint that the metabolic remodeling also takes place in BTHS patients, and that this is regulated by the ISR. The amount of experiments would need to be extended to get robust results. Furthermore, one could conduct the experiments with iPS cells from different patients to cover different mutations in TAZ. There are different severe phenotypes in patients, so it would be interesting to know if the metabolic remodeling is similar in the different cases, or if it is present to a different extent, dependent on the mutation in the *TAZ* gene. The CRISPR/Cas9 technology might be a possible approach to introduce an ATF4 knockout into the iPS cells for extensive studies, which would provide a more stable model system than using inhibitors, where the efficacy of the signaling inhibition could be variable between independent experiments due to, for example, different stocks of inhibitor and its storage time.
Even though this work highly focused on the ISR and highlights its central role as a regulatory mechanism in BTHS, it would be worth the effort to closer examine other stress signaling pathways. Activation of the AMPK pathway was already reported in TAZ deficient cells [147, 148]. AMPK activation upon mitochondrial dysfunction was also shown by Zhao et al. using a loss-of-function mutation in ETC complex III. Here they demonstrated that activation of this signaling helped with cell survival [341]. The AMPK signaling pathway has been also widely discussed in the cardiac field. During cardiac ischemia, AMPK is activated and induces glucose uptake, glycogenesis and fatty acid oxidation, which possibly protects against ischemic reperfusion injury [342-347]. Different studies also report a regulator role of the AMPK in cardiac protein

synthesis linked to hypertrophy, attenuating hypertrophy development upon AMPK activation [348, 349]. Moreover, AMPK is known to be phosphorylated by the Calmodulin-dependent protein kinase kinase-β (CaMKKβ), which is $Ca^{2+}$ sensitive [350, 351]. $Ca^{2+}$ signaling is impaired in BTHS [128], so this could influence the AMPK pathway. The mTOR signaling is reportedly another pathway playing an important regulatory role in cardiac development and function. Cardiac inhibition of mTOR results in mitochondrial and metabolic defects, cardiac dysfunction to the point of heart failure and postnatal fatality [352-354]. However, selective inhibition of mTOR was shown to be beneficial under certain conditions such as cardiac stress due to pressure overload or genetic cardiomyopathies, where the inhibition of mTOR prevents cardiac hypertrophy [355-359]. Zhang et al. recently reported a hyperactivation of the mTOR pathway upon TAZ deficiency, and its inhibition positively affected the mitochondrial dysfunction and the cardiac phenotype [360]. However, preliminary results from our group gave no evidence of elevated mTOR activation in the *Taz*-KD mouse model so far (data not shown). Concerning the different stress signaling pathways, it would be very interesting if those pathways act together in favor of the cardiac phenotype in BTHS, or if they countervail to reduce each other's effects.

The ultimate goal of research in the medical field is to understand the pathophysiology of diseases and ultimately provide therapeutic opportunities to either heal the diseases or, more likely in genetic disorders, to mitigate symptoms to improve quality of life for the patients. Amino acids and in particular, glutamate was revealed to play a significant role in the metabolic remodeling in BTHS cardiomyopathy. If restoring the fatty acid oxidation as a typical energy provider in the heart is not possible, enhancing alternative mechanisms would be reasonable. So far, the results argue for cell function improvement upon altered glutamate metabolism. It would be interesting to see if glutamate enriched diets help patients to improve their energetic deficit in cardiac and/or skeletal muscle. This hypothesis would be supported by the displayed restored mitochondrial function upon glutamate addition. As glutamate is partially used for GSH synthesis, maybe also the addition of GSH precursors, such as N-acetylcystein (NAC) could be beneficial for the BTHS phenotype. The supplementation of NAC had already been reported to be profitable for the cardiac function after myocardial infarction [361-363], which might prevent the transition into heart failure. First *in vitro* experiments could be performed using NAC supplementation in the cell culture medium. As this is already an approved drug used in other diseases, later approaches in *Taz*-KD mice

could depict its effects on BTHS in *in vivo* experiments. Taken together, this thesis provides a solid foundation of metabolic changes in BTHS and opens new avenues to develop novel treatments that eventually should improve cardiac function and outcome of patients with the orphaned disease BTHS.

# 6. Bibliography


1. Atlante, A. and D. Valenti, *Mitochondria Have Made a Long Evolutionary Path from Ancient Bacteria Immigrants within Eukaryotic Cells to Essential Cellular Hosts and Key Players in Human Health and Disease.* Curr Issues Mol Biol, 2023. **45**(5): p. 4451-4479.
2. O'Rourke, B., *From bioblasts to mitochondria: ever expanding roles of mitochondria in cell physiology.* Front Physiol, 2010. **1**: p. 7.
3. Wallin, I.E., *Symbionticism and the Origin of Species*. 1927, Baltimore: Williams & Wilkins Co.
4. Copeland, D.E. and A.J. Dalton, *An association between mitochondria and the endoplasmic reticulum in cells of the pseudobranch gland of a teleost.* J Biophys Biochem Cytol, 1959. **5**(3): p. 393-6.
5. Achleitner, G., et al., *Association between the endoplasmic reticulum and mitochondria of yeast facilitates interorganelle transport of phospholipids through membrane contact.* Eur J Biochem, 1999. **264**(2): p. 545-53.
6. Sugiura, A., et al., *Newly born peroxisomes are a hybrid of mitochondrial and ER-derived pre-peroxisomes.* Nature, 2017. **542**(7640): p. 251-254.
7. Sjostrand, F.S., *Electron microscopy of mitochondria and cytoplasmic double membranes.* Nature, 1953. **171**(4340): p. 30-2.
8. Harner, M., et al., *The mitochondrial contact site complex, a determinant of mitochondrial architecture.* Embo j, 2011. **30**(21): p. 4356-70.
9. Kühlbrandt, W., *Structure and function of mitochondrial membrane protein complexes.* BMC Biol, 2015. **13**: p. 89.
10. Slater, E.C.C., K. W. , *The calcium content of isolated heart-muscle sarcosomes.* Biochemical Journal, 1953. **54**: p. xxii.
11. Jiang, D., L. Zhao, and D.E. Clapham, *Genome-wide RNAi screen identifies Letm1 as a mitochondrial Ca2+/H+ antiporter.* Science, 2009. **326**(5949): p. 144-7.
12. Perocchi, F., et al., *MICU1 encodes a mitochondrial EF hand protein required for Ca(2+) uptake.* Nature, 2010. **467**(7313): p. 291-6.
13. Loschen, G., L. Flohé, and B. Chance, *Respiratory chain linked H(2)O(2) production in pigeon heart mitochondria.* FEBS Lett, 1971. **18**(2): p. 261-264.
14. Loschen, G.A., A.; Richter, C.; Flohé, L., *Superoxide radicals as precursors of mitochondrial hydrogen peroxide.* FEBS Lett, 1974. **42**: p. 68-72.
15. Fang, J., H.S. Wong, and M.D. Brand, *Production of superoxide and hydrogen peroxide in the mitochondrial matrix is dominated by site I(Q) of complex I in diverse cell lines.* Redox Biol, 2020. **37**: p. 101722.
16. McCord, J.M.K., B.B. Jr.; Fridovich, I. , *An enzyme-based theory of obligate anaerobiosis: the physiological function of superoxide dismutase.* Proc Natl Acad Sci USA, 1971. **68**(5): p. 1024-1027.
17. He, L., et al., *Antioxidants Maintain Cellular Redox Homeostasis by Elimination of Reactive Oxygen Species.* Cell Physiol Biochem, 2017. **44**(2): p. 532-553.
18. Zhang, Q., et al., *Circulating mitochondrial DAMPs cause inflammatory responses to injury.* Nature, 2010. **464**(7285): p. 104-7.
19. Marques, P.E., et al., *Chemokines and mitochondrial products activate neutrophils to amplify organ injury during mouse acute liver failure.* Hepatology, 2012. **56**(5): p. 1971-82.

20. Chen, H., et al., *Mitofusins Mfn1 and Mfn2 coordinately regulate mitochondrial fusion and are essential for embryonic development.* J Cell Biol, 2003. **160**(2): p. 189-200.
21. Olichon, A., et al., *Loss of OPA1 perturbates the mitochondrial inner membrane structure and integrity, leading to cytochrome c release and apoptosis.* J Biol Chem, 2003. **278**(10): p. 7743-6.
22. Smirnova, E., et al., *A human dynamin-related protein controls the distribution of mitochondria.* J Cell Biol, 1998. **143**(2): p. 351-8.
23. Pangborn, M.C., *Isolation and purification of a serologically active phosphollipid from beef heart.* Journal of Biological Chemistry, 1942. **143**(1): p. 247-256.
24. Pangborn, M.C., *A simplified preparation of cardiolipin, with note on purification of lecithin for serologic use.* J Biol Chem, 1945. **161**: p. 71-82.
25. Daum, G., *Lipids of mitochondria.* Biochim Biophys Acta, 1985. **822**(1): p. 1-42.
26. Potting, C., et al., *TRIAP1/PRELI complexes prevent apoptosis by mediating intramitochondrial transport of phosphatidic acid.* Cell Metab, 2013. **18**(2): p. 287-95.
27. Jiao, H., Y. Yin, and Z. Liu, *Structures of the Mitochondrial CDP-DAG Synthase Tam41 Suggest a Potential Lipid Substrate Pathway from Membrane to the Active Site.* Structure, 2019. **27**(8): p. 1258-1269.e4.
28. Zhang, J., et al., *Mitochondrial phosphatase PTPMT1 is essential for cardiolipin biosynthesis.* Cell Metab, 2011. **13**(6): p. 690-700.
29. Xiao, J., et al., *Structural and functional analysis of PTPMT1, a phosphatase required for cardiolipin synthesis.* Proc Natl Acad Sci U S A, 2011. **108**(29): p. 11860-5.
30. Chen, D., X.Y. Zhang, and Y. Shi, *Identification and functional characterization of hCLS1, a human cardiolipin synthase localized in mitochondria.* Biochem J, 2006. **398**(2): p. 169-76.
31. Houtkooper, R.H., et al., *Cardiolipin and monolysocardiolipin analysis in fibroblasts, lymphocytes, and tissues using high-performance liquid chromatography-mass spectrometry as a diagnostic test for Barth syndrome.* Anal Biochem, 2009. **387**(2): p. 230-7.
32. Buckland, A.G., A.R. Kinkaid, and D.C. Wilton, *Cardiolipin hydrolysis by human phospholipases A2. The multiple enzymatic activities of human cytosolic phospholipase A2.* Biochim Biophys Acta, 1998. **1390**(1): p. 65-72.
33. Hsu, Y.H., et al., *Assessing phospholipase A2 activity toward cardiolipin by mass spectrometry.* PLoS One, 2013. **8**(3): p. e59267.
34. Dennis, E.A., et al., *Phospholipase A2 enzymes: physical structure, biological function, disease implication, chemical inhibition, and therapeutic intervention.* Chem Rev, 2011. **111**(10): p. 6130-85.
35. Taylor, W.A. and G.M. Hatch, *Identification of the human mitochondrial linoleoyl-coenzyme A monolysocardiolipin acyltransferase (MLCL AT-1).* J Biol Chem, 2009. **284**(44): p. 30360-71.
36. Cao, J., et al., *A novel cardiolipin-remodeling pathway revealed by a gene encoding an endoplasmic reticulum-associated acyl-CoA:lysocardiolipin acyltransferase (ALCAT1) in mouse.* J Biol Chem, 2004. **279**(30): p. 31727-34.
37. Bione, S., et al., *A novel X-linked gene, G4.5. is responsible for Barth syndrome.* Nat Genet, 1996. **12**(4): p. 385-9.
38. Xu, Y., et al., *The enzymatic function of tafazzin.* J Biol Chem, 2006. **281**(51): p. 39217-24.

39. Barth, P.G., et al., *An X-linked mitochondrial disease affecting cardiac muscle, skeletal muscle and neutrophil leucocytes.* J Neurol Sci, 1983. **62**(1-3): p. 327-55.
40. Lecocq, J. and C.E. Ballou, *ON THE STRUCTURE OF CARDIOLIPIN.* Biochemistry, 1964. **3**: p. 976-80.
41. Oemer, G., et al., *Phospholipid Acyl Chain Diversity Controls the Tissue-Specific Assembly of Mitochondrial Cardiolipins.* Cell Rep, 2020. **30**(12): p. 4281-4291.e4.
42. Schägger, H. and K. Pfeiffer, *Supercomplexes in the respiratory chains of yeast and mammalian mitochondria.* Embo j, 2000. **19**(8): p. 1777-83.
43. Carroll, J., et al., *Bovine complex I is a complex of 45 different subunits.* J Biol Chem, 2006. **281**(43): p. 32724-7.
44. Guénebaut, V., et al., *Three-dimensional structure of NADH-dehydrogenase from Neurospora crassa by electron microscopy and conical tilt reconstruction.* J Mol Biol, 1997. **265**(4): p. 409-18.
45. Guénebaut, V., et al., *Consistent structure between bacterial and mitochondrial NADH:ubiquinone oxidoreductase (complex I).* J Mol Biol, 1998. **276**(1): p. 105-12.
46. Radermacher, M., et al., *The three-dimensional structure of complex I from Yarrowia lipolytica: a highly dynamic enzyme.* J Struct Biol, 2006. **154**(3): p. 269-79.
47. Clason, T., et al., *The structure of eukaryotic and prokaryotic complex I.* J Struct Biol, 2010. **169**(1): p. 81-8.
48. Morgan, D.J. and L.A. Sazanov, *Three-dimensional structure of respiratory complex I from Escherichia coli in ice in the presence of nucleotides.* Biochim Biophys Acta, 2008. **1777**(7-8): p. 711-8.
49. Baradaran, R., et al., *Crystal structure of the entire respiratory complex I.* Nature, 2013. **494**(7438): p. 443-8.
50. Wikström, M., *Two protons are pumped from the mitochondrial matrix per electron transferred between NADH and ubiquinone.* FEBS Lett, 1984. **169**(2): p. 300-4.
51. Galkin, A.S., V.G. Grivennikova, and A.D. Vinogradov, *-->H+/2e- stoichiometry in NADH-quinone reductase reactions catalyzed by bovine heart submitochondrial particles.* FEBS Lett, 1999. **451**(2): p. 157-61.
52. Galkin, A., S. Dröse, and U. Brandt, *The proton pumping stoichiometry of purified mitochondrial complex I reconstituted into proteoliposomes.* Biochim Biophys Acta, 2006. **1757**(12): p. 1575-81.
53. Sun, F., et al., *Crystal structure of mitochondrial respiratory membrane protein complex II.* Cell, 2005. **121**(7): p. 1043-57.
54. Hägerhäll, C., *Succinate: quinone oxidoreductases. Variations on a conserved theme.* Biochim Biophys Acta, 1997. **1320**(2): p. 107-41.
55. Mitchell, P., *Coupling of Phosphorylation to Electron and Hydrogen Transfer by a Chemi-Osmotic type of Mechanism.* Nature, 1961. **191**(4784): p. 144-148.
56. Fry, M. and D.E. Green, *Cardiolipin requirement for electron transfer in complex I and III of the mitochondrial respiratory chain.* J Biol Chem, 1981. **256**(4): p. 1874-80.
57. McKenzie, M., et al., *Mitochondrial respiratory chain supercomplexes are destabilized in Barth Syndrome patients.* J Mol Biol, 2006. **361**(3): p. 462-9.
58. Dudek, J., et al., *Cardiolipin deficiency affects respiratory chain function and organization in an induced pluripotent stem cell model of Barth syndrome.* Stem Cell Res, 2013. **11**(2): p. 806-19.

59. Sedlák, E. and N.C. Robinson, *Phospholipase A(2) digestion of cardiolipin bound to bovine cytochrome c oxidase alters both activity and quaternary structure.* Biochemistry, 1999. **38**(45): p. 14966-72.
60. Sedlák, E., et al., *The kinetic stability of cytochrome C oxidase: effect of bound phospholipid and dimerization.* Biophys J, 2014. **107**(12): p. 2941-2949.
61. Sedlák, E. and N.C. Robinson, *Destabilization of the Quaternary Structure of Bovine Heart Cytochrome c Oxidase upon Removal of Tightly Bound Cardiolipin.* Biochemistry, 2015. **54**(36): p. 5569-77.
62. Fry, M., G.A. Blondin, and D.E. Green, *The localization of tightly bound cardiolipin in cytochrome oxidase.* J Biol Chem, 1980. **255**(20): p. 9967-70.
63. Liko, I., et al., *Dimer interface of bovine cytochrome c oxidase is influenced by local posttranslational modifications and lipid binding.* Proc Natl Acad Sci U S A, 2016. **113**(29): p. 8230-5.
64. Gomez, B., Jr. and N.C. Robinson, *Phospholipase digestion of bound cardiolipin reversibly inactivates bovine cytochrome bc1.* Biochemistry, 1999. **38**(28): p. 9031-8.
65. Schägger, H., et al., *Phospholipid specificity of bovine heart bc1 complex.* Eur J Biochem, 1990. **190**(1): p. 123-30.
66. Schwall, C.T., V.L. Greenwood, and N.N. Alder, *The stability and activity of respiratory Complex II is cardiolipin-dependent.* Biochim Biophys Acta, 2012. **1817**(9): p. 1588-96.
67. Jussupow, A., A. Di Luca, and V.R.I. Kaila, *How cardiolipin modulates the dynamics of respiratory complex I.* Sci Adv, 2019. **5**(3): p. eaav1850.
68. Schäfer, E., et al., *Three-dimensional structure of the respiratory chain supercomplex I1III2IV1 from bovine heart mitochondria.* Biochemistry, 2007. **46**(44): p. 12579-85.
69. Dudkina, N.V., et al., *Interaction of complexes I, III, and IV within the bovine respirasome by single particle cryoelectron tomography.* Proc Natl Acad Sci U S A, 2011. **108**(37): p. 15196-200.
70. Althoff, T., et al., *Arrangement of electron transport chain components in bovine mitochondrial supercomplex I1III2IV1.* Embo j, 2011. **30**(22): p. 4652-64.
71. Wu, M., et al., *Structure of Mammalian Respiratory Supercomplex I(1)III(2)IV(1).* Cell, 2016. **167**(6): p. 1598-1609.e10.
72. Gu, J., et al., *The architecture of the mammalian respirasome.* Nature, 2016. **537**(7622): p. 639-643.
73. Lobo-Jarne, T. and C. Ugalde, *Respiratory chain supercomplexes: Structures, function and biogenesis.* Semin Cell Dev Biol, 2018. **76**: p. 179-190.
74. Dudek, J., et al., *Cardiac-specific succinate dehydrogenase deficiency in Barth syndrome.* EMBO Mol Med, 2016. **8**(2): p. 139-54.
75. Lange, C., et al., *Specific roles of protein-phospholipid interactions in the yeast cytochrome bc1 complex structure.* Embo j, 2001. **20**(23): p. 6591-600.
76. Pöyry, S., et al., *Atomistic simulations indicate cardiolipin to have an integral role in the structure of the cytochrome bc1 complex.* Biochim Biophys Acta, 2013. **1827**(6): p. 769-78.
77. Musatov, A. and N.C. Robinson, *Bound cardiolipin is essential for cytochrome c oxidase proton translocation.* Biochimie, 2014. **105**: p. 159-64.
78. Quinlan, C.L., et al., *Sites of reactive oxygen species generation by mitochondria oxidizing different substrates.* Redox Biol, 2013. **1**(1): p. 304-12.
79. Chen, Q., et al., *Production of reactive oxygen species by mitochondria: central role of complex III.* J Biol Chem, 2003. **278**(38): p. 36027-31.

80. Liu, Y., G. Fiskum, and D. Schubert, *Generation of reactive oxygen species by the mitochondrial electron transport chain.* J Neurochem, 2002. **80**(5): p. 780-7.
81. Kudin, A.P., et al., *Characterization of superoxide-producing sites in isolated brain mitochondria.* J Biol Chem, 2004. **279**(6): p. 4127-35.
82. Treberg, J.R., C.L. Quinlan, and M.D. Brand, *Evidence for two sites of superoxide production by mitochondrial NADH-ubiquinone oxidoreductase (complex I).* J Biol Chem, 2011. **286**(31): p. 27103-10.
83. Turrens, J.F., A. Alexandre, and A.L. Lehninger, *Ubisemiquinone is the electron donor for superoxide formation by complex III of heart mitochondria.* Arch Biochem Biophys, 1985. **237**(2): p. 408-14.
84. Muller, F., A.R. Crofts, and D.M. Kramer, *Multiple Q-cycle bypass reactions at the Qo site of the cytochrome bc1 complex.* Biochemistry, 2002. **41**(25): p. 7866-74.
85. Starkov, A.A., et al., *Mitochondrial alpha-ketoglutarate dehydrogenase complex generates reactive oxygen species.* J Neurosci, 2004. **24**(36): p. 7779-88.
86. Fisher-Wellman, K.H., et al., *Mitochondrial glutathione depletion reveals a novel role for the pyruvate dehydrogenase complex as a key H2O2-emitting source under conditions of nutrient overload.* Free Radic Biol Med, 2013. **65**: p. 1201-1208.
87. Wagner, M., et al., *Selective NADH communication from α-ketoglutarate dehydrogenase to mitochondrial transhydrogenase prevents reactive oxygen species formation under reducing conditions in the heart.* Basic Res Cardiol, 2020. **115**(5): p. 53.
88. Fridovich, I., *Superoxide radical and superoxide dismutases.* Annu Rev Biochem, 1995. **64**: p. 97-112.
89. Arai, M., et al., *Mitochondrial phospholipid hydroperoxide glutathione peroxidase plays a major role in preventing oxidative injury to cells.* J Biol Chem, 1999. **274**(8): p. 4924-33.
90. Wiswedel, I., et al., *Degradation of phospholipids by oxidative stress--exceptional significance of cardiolipin.* Free Radic Res, 2010. **44**(2): p. 135-45.
91. Paradies, G., et al., *Lipid peroxidation and alterations to oxidative metabolism in mitochondria isolated from rat heart subjected to ischemia and reperfusion.* Free Radic Biol Med, 1999. **27**(1-2): p. 42-50.
92. Paradies, G., et al., *Reactive oxygen species affect mitochondrial electron transport complex I activity through oxidative cardiolipin damage.* Gene, 2002. **286**(1): p. 135-41.
93. Paradies, G., et al., *Decrease in mitochondrial complex I activity in ischemic/reperfused rat heart: involvement of reactive oxygen species and cardiolipin.* Circ Res, 2004. **94**(1): p. 53-9.
94. Petrosillo, G., et al., *Mitochondrial dysfunction associated with cardiac ischemia/reperfusion can be attenuated by oxygen tension control. Role of oxygen-free radicals and cardiolipin.* Biochim Biophys Acta, 2005. **1710**(2-3): p. 78-86.
95. Petrosillo, G., et al., *Mitochondrial complex I dysfunction in rat heart with aging: critical role of reactive oxygen species and cardiolipin.* Free Radic Biol Med, 2009. **46**(1): p. 88-94.
96. Shi, Y., et al., *Comparative studies of oxidative stress and mitochondrial function in aging.* Integr Comp Biol, 2010. **50**(5): p. 869-79.
97. Li, J., et al., *Cardiolipin remodeling by ALCAT1 links oxidative stress and mitochondrial dysfunction to obesity.* Cell Metab, 2010. **12**(2): p. 154-65.

98. Nomura, K., et al., *Mitochondrial phospholipid hydroperoxide glutathione peroxidase inhibits the release of cytochrome c from mitochondria by suppressing the peroxidation of cardiolipin in hypoglycaemia-induced apoptosis.* Biochem J, 2000. **351**(Pt 1): p. 183-93.
99. Kagan, V.E., et al., *Cytochrome c acts as a cardiolipin oxygenase required for release of proapoptotic factors.* Nat Chem Biol, 2005. **1**(4): p. 223-32.
100. Jiang, J., et al., *Interplay between bax, reactive oxygen species production, and cardiolipin oxidation during apoptosis.* Biochem Biophys Res Commun, 2008. **368**(1): p. 145-50.
101. Ockner, R.K., et al., *A binding protein for fatty acids in cytosol of intestinal mucosa, liver, myocardium, and other tissues.* Science, 1972. **177**(4043): p. 56-8.
102. Bayrhuber, M., et al., *Structure of the human voltage-dependent anion channel.* Proc Natl Acad Sci U S A, 2008. **105**(40): p. 15370-5.
103. Coe, N.R., et al., *The fatty acid transport protein (FATP1) is a very long chain acyl-CoA synthetase.* J Biol Chem, 1999. **274**(51): p. 36300-4.
104. Pande, S.V., *A mitochondrial carnitine acylcarnitine translocase system.* Proc Natl Acad Sci U S A, 1975. **72**(3): p. 883-7.
105. Ramsay, R.R. and P.K. Tubbs, *The mechanism of fatty acid uptake by heart mitochondria: an acylcarnitine-carnitine exchange.* FEBS Lett, 1975. **54**(1): p. 21-5.
106. Beyer, K. and M. Klingenberg, *ADP/ATP carrier protein from beef heart mitochondria has high amounts of tightly bound cardiolipin, as revealed by 31P nuclear magnetic resonance.* Biochemistry, 1985. **24**(15): p. 3821-6.
107. Hoffmann, B., et al., *The reconstituted ADP/ATP carrier activity has an absolute requirement for cardiolipin as shown in cysteine mutants.* J Biol Chem, 1994. **269**(3): p. 1940-4.
108. Claypool, S.M., *Cardiolipin, a critical determinant of mitochondrial carrier protein assembly and function.* Biochim Biophys Acta, 2009. **1788**(10): p. 2059-68.
109. Murthy, M.S. and S.V. Pande, *Malonyl-CoA binding site and the overt carnitine palmitoyltransferase activity reside on the opposite sides of the outer mitochondrial membrane.* Proc Natl Acad Sci U S A, 1987. **84**(2): p. 378-82.
110. Meinhardt, B., et al., *Cardiolipin Stabilizes and Increases Catalytic Efficiency of Carnitine Palmitoyltransferase II and Its Variants S113L, P50H, and Y479F.* Int J Mol Sci, 2021. **22**(9).
111. Aoyama, T., et al., *Purification of human very-long-chain acyl-coenzyme A dehydrogenase and characterization of its deficiency in seven patients.* J Clin Invest, 1995. **95**(6): p. 2465-73.
112. Zhang, Y., et al., *SIRT3 and SIRT5 regulate the enzyme activity and cardiolipin binding of very long-chain acyl-CoA dehydrogenase.* PLoS One, 2015. **10**(3): p. e0122297.
113. Xiong, D., et al., *Cardiac-specific VLCAD deficiency induces dilated cardiomyopathy and cold intolerance.* Am J Physiol Heart Circ Physiol, 2014. **306**(3): p. H326-38.
114. Houten, S.M. and R.J. Wanders, *A general introduction to the biochemistry of mitochondrial fatty acid β-oxidation.* J Inherit Metab Dis, 2010. **33**(5): p. 469-77.
115. Francy, C.A., et al., *Cryo-EM Studies of Drp1 Reveal Cardiolipin Interactions that Activate the Helical Oligomer.* Sci Rep, 2017. **7**(1): p. 10744.
116. Ban, T., et al., *Molecular basis of selective mitochondrial fusion by heterotypic action between OPA1 and cardiolipin.* Nat Cell Biol, 2017. **19**(7): p. 856-863.

117. DeVay, R.M., et al., *Coassembly of Mgm1 isoforms requires cardiolipin and mediates mitochondrial inner membrane fusion.* J Cell Biol, 2009. **186**(6): p. 793-803.
118. Bustillo-Zabalbeitia, I., et al., *Specific interaction with cardiolipin triggers functional activation of Dynamin-Related Protein 1.* PLoS One, 2014. **9**(7): p. e102738.
119. Rampelt, H., et al., *Assembly of the Mitochondrial Cristae Organizer Mic10 Is Regulated by Mic26-Mic27 Antagonism and Cardiolipin.* J Mol Biol, 2018. **430**(13): p. 1883-1890.
120. Ikon, N. and R.O. Ryan, *Cardiolipin and mitochondrial cristae organization.* Biochim Biophys Acta Biomembr, 2017. **1859**(6): p. 1156-1163.
121. Ugarte-Uribe, B., et al., *Drp1 polymerization stabilizes curved tubular membranes similar to those of constricted mitochondria.* J Cell Sci, 2018. **132**(4).
122. Malhotra, K., et al., *Cardiolipin mediates membrane and channel interactions of the mitochondrial TIM23 protein import complex receptor Tim50.* Sci Adv, 2017. **3**(9): p. e1700532.
123. Li, Y., et al., *Cardiolipin-induced activation of pyruvate dehydrogenase links mitochondrial lipid biosynthesis to TCA cycle function.* J Biol Chem, 2019. **294**(30): p. 11568-11578.
124. Paradies, G., et al., *Age-dependent decline in the cytochrome c oxidase activity in rat heart mitochondria: role of cardiolipin.* FEBS Lett, 1997. **406**(1-2): p. 136-8.
125. Liu, X., et al., *Induction of apoptotic program in cell-free extracts: requirement for dATP and cytochrome c.* Cell, 1996. **86**(1): p. 147-57.
126. Sorice, M., et al., *Cardiolipin and its metabolites move from mitochondria to other cellular membranes during death receptor-mediated apoptosis.* Cell Death Differ, 2004. **11**(10): p. 1133-45.
127. Lovell, J.F., et al., *Membrane binding by tBid initiates an ordered series of events culminating in membrane permeabilization by Bax.* Cell, 2008. **135**(6): p. 1074-84.
128. Bertero, E., et al., *Loss of Mitochondrial Ca(2+) Uniporter Limits Inotropic Reserve and Provides Trigger and Substrate for Arrhythmias in Barth Syndrome Cardiomyopathy.* Circulation, 2021. **144**(21): p. 1694-1713.
129. Steward, C.G., et al., *Barth syndrome: an X-linked cause of fetal cardiomyopathy and stillbirth.* Prenat Diagn, 2010. **30**(10): p. 970-6.
130. Barth, P.G., et al., *X-linked cardioskeletal myopathy and neutropenia (Barth syndrome): respiratory-chain abnormalities in cultured fibroblasts.* J Inherit Metab Dis, 1996. **19**(2): p. 157-60.
131. Lu, Y.W., et al., *Defining functional classes of Barth syndrome mutation in humans.* Hum Mol Genet, 2016. **25**(9): p. 1754-70.
132. Johnston, J., et al., *Mutation characterization and genotype-phenotype correlation in Barth syndrome.* Am J Hum Genet, 1997. **61**(5): p. 1053-8.
133. Cardonick, E.H., et al., *Prenatal clinical expression of 3-methylglutaconic aciduria: Barth syndrome.* Prenat Diagn, 1997. **17**(10): p. 983-8.
134. Adès, L.C., et al., *Barth syndrome: clinical features and confirmation of gene localisation to distal Xq28.* Am J Med Genet, 1993. **45**(3): p. 327-34.
135. Christodoulou, J., et al., *Barth syndrome: clinical observations and genetic linkage studies.* Am J Med Genet, 1994. **50**(3): p. 255-64.
136. Cosson, L., et al., *Barth syndrome in a female patient.* Mol Genet Metab, 2012. **106**(1): p. 115-20.

137. Roberts, A.E., et al., *The Barth Syndrome Registry: distinguishing disease characteristics and growth data from a longitudinal study.* Am J Med Genet A, 2012. **158a**(11): p. 2726-32.
138. Spencer, C.T., et al., *Cardiac and clinical phenotype in Barth syndrome.* Pediatrics, 2006. **118**(2): p. e337-46.
139. Spencer, C.T., et al., *Impaired cardiac reserve and severely diminished skeletal muscle $O_2$ utilization mediate exercise intolerance in Barth syndrome.* Am J Physiol Heart Circ Physiol, 2011. **301**(5): p. H2122-9.
140. Thompson, W.R., et al., *New targets for monitoring and therapy in Barth syndrome.* Genet Med, 2016. **18**(10): p. 1001-10.
141. Kelley, R.I., et al., *X-linked dilated cardiomyopathy with neutropenia, growth retardation, and 3-methylglutaconic aciduria.* J Pediatr, 1991. **119**(5): p. 738-47.
142. Baban, A., et al., *Delayed appearance of 3-methylglutaconic aciduria in neonates with early onset metabolic cardiomyopathies: A potential pitfall for the diagnosis.* Am J Med Genet A, 2020. **182**(1): p. 64-70.
143. Schmidt, M.R., et al., *Barth syndrome without 3-methylglutaconic aciduria.* Acta Paediatr, 2004. **93**(3): p. 419-21.
144. Duran, M., et al., *Inherited 3-methylglutaconic aciduria in two brothers--another defect of leucine metabolism.* J Pediatr, 1982. **101**(4): p. 551-4.
145. Ensenauer, R., et al., *3-Methylglutaconyl-CoA hydratase deficiency: a new patient with speech retardation as the leading sign.* J Inherit Metab Dis, 2000. **23**(4): p. 341-4.
146. Hastings, R., et al., *Dysmorphology of Barth syndrome.* Clin Dysmorphol, 2009. **18**(4): p. 185-7.
147. He, Q., *Tafazzin knockdown causes hypertrophy of neonatal ventricular myocytes.* Am J Physiol Heart Circ Physiol, 2010. **299**(1): p. H210-6.
148. He, Q., et al., *Tafazzin knockdown interrupts cell cycle progression in cultured neonatal ventricular fibroblasts.* Am J Physiol Heart Circ Physiol, 2013. **305**(9): p. H1332-43.
149. Lou, W., et al., *Loss of tafazzin results in decreased myoblast differentiation in C2C12 cells: A myoblast model of Barth syndrome and cardiolipin deficiency.* Biochim Biophys Acta Mol Cell Biol Lipids, 2018. **1863**(8): p. 857-865.
150. Chowdhury, A., et al., *Defective Mitochondrial Cardiolipin Remodeling Dampens HIF-1alpha Expression in Hypoxia.* Cell Rep, 2018. **25**(3): p. 561-570 e6.
151. Hsu, P., et al., *Cardiolipin remodeling by TAZ/tafazzin is selectively required for the initiation of mitophagy.* Autophagy, 2015. **11**(4): p. 643-52.
152. Gonzalvez, F., et al., *Barth syndrome: cellular compensation of mitochondrial dysfunction and apoptosis inhibition due to changes in cardiolipin remodeling linked to tafazzin (TAZ) gene mutation.* Biochim Biophys Acta, 2013. **1832**(8): p. 1194-206.
153. Xu, Y., et al., *Characterization of lymphoblast mitochondria from patients with Barth syndrome.* Laboratory Investigation, 2005. **85**(6): p. 823-830.
154. Chatzispyrou, I.A., et al., *Barth syndrome cells display widespread remodeling of mitochondrial complexes without affecting metabolic flux distribution.* Biochim Biophys Acta Mol Basis Dis, 2018. **1864**(11): p. 3650-3658.
155. Wang, G., et al., *Modeling the mitochondrial cardiomyopathy of Barth syndrome with induced pluripotent stem cell and heart-on-chip technologies.* Nat Med, 2014. **20**(6): p. 616-23.
156. Acehan, D., et al., *Cardiac and skeletal muscle defects in a mouse model of human Barth syndrome.* J Biol Chem, 2011. **286**(2): p. 899-908.

157. Soustek, M.S., et al., *Characterization of a transgenic short hairpin RNA-induced murine model of Tafazzin deficiency.* Hum Gene Ther, 2011. **22**(7): p. 865-71.
158. Mekada, K., et al., *Genetic differences among C57BL/6 substrains.* Exp Anim, 2009. **58**(2): p. 141-9.
159. Kim, J., et al., *Cardiac mitochondrial structure and function in tafazzin-knockdown mice.* Mitochondrion, 2018. **43**: p. 53-62.
160. Phoon, C.K., et al., *Tafazzin knockdown in mice leads to a developmental cardiomyopathy with early diastolic dysfunction preceding myocardial noncompaction.* J Am Heart Assoc, 2012. **1**(2).
161. Kiebish, M.A., et al., *Dysfunctional cardiac mitochondrial bioenergetic, lipidomic, and signaling in a murine model of Barth syndrome.* J Lipid Res, 2013. **54**(5): p. 1312-25.
162. Le, C.H., et al., *Tafazzin deficiency impairs CoA-dependent oxidative metabolism in cardiac mitochondria.* J Biol Chem, 2020. **295**(35): p. 12485-12497.
163. Powers, C., et al., *Diminished Exercise Capacity and Mitochondrial bc1 Complex Deficiency in Tafazzin-Knockdown Mice.* Front Physiol, 2013. **4**: p. 74.
164. Goncalves, R.L.S., et al., *Cardiolipin deficiency in Barth syndrome is not associated with increased superoxide/H2 O2 production in heart and skeletal muscle mitochondria.* FEBS Lett, 2020.
165. Wang, S., et al., *AAV Gene Therapy Prevents and Reverses Heart Failure in a Murine Knockout Model of Barth Syndrome.* Circ Res, 2020. **126**(8): p. 1024-1039.
166. Vaz, F.M., et al., *Only one splice variant of the human TAZ gene encodes a functional protein with a role in cardiolipin metabolism.* J Biol Chem, 2003. **278**(44): p. 43089-94.
167. Gu, Z., et al., *Aberrant cardiolipin metabolism in the yeast taz1 mutant: a model for Barth syndrome.* Mol Microbiol, 2004. **51**(1): p. 149-58.
168. Ye, C., et al., *Deletion of the cardiolipin-specific phospholipase Cld1 rescues growth and life span defects in the tafazzin mutant: implications for Barth syndrome.* J Biol Chem, 2014. **289**(6): p. 3114-25.
169. Baile, M.G., et al., *Unremodeled and remodeled cardiolipin are functionally indistinguishable in yeast.* J Biol Chem, 2014. **289**(3): p. 1768-78.
170. Raja, V. and M.L. Greenberg, *The functions of cardiolipin in cellular metabolism-potential modifiers of the Barth syndrome phenotype.* Chem Phys Lipids, 2014. **179**: p. 49-56.
171. Raja, V., et al., *Loss of Cardiolipin Leads to Perturbation of Acetyl-CoA Synthesis.* J Biol Chem, 2017. **292**(3): p. 1092-1102.
172. Khuchua, Z., et al., *A zebrafish model of human Barth syndrome reveals the essential role of tafazzin in cardiac development and function.* Circ Res, 2006. **99**(2): p. 201-8.
173. Xu, Y., et al., *A Drosophila model of Barth syndrome.* Proc Natl Acad Sci U S A, 2006. **103**(31): p. 11584-8.
174. Damschroder, D., C. Reynolds, and R. Wessells, *Drosophila tafazzin mutants have impaired exercise capacity.* Physiol Rep, 2018. **6**(3).
175. Li, Y., et al., *Favorable outcomes after heart transplantation in Barth syndrome.* J Heart Lung Transplant, 2021. **40**(10): p. 1191-1198.
176. Kantor, P.F., et al., *Presentation, diagnosis, and medical management of heart failure in children: Canadian Cardiovascular Society guidelines.* Can J Cardiol, 2013. **29**(12): p. 1535-52.

177. Cade, W.T., et al., *Endurance Exercise Training in Young Adults with Barth Syndrome: A Pilot Study.* JIMD reports, 2017. **32**: p. 15-24.
178. Steward, C.G., et al., *Neutropenia in Barth syndrome: characteristics, risks, and management.* Curr Opin Hematol, 2019. **26**(1): p. 6-15.
179. Dale, D.C., et al., *A randomized controlled phase III trial of recombinant human granulocyte colony-stimulating factor (filgrastim) for treatment of severe chronic neutropenia.* Blood, 1993. **81**(10): p. 2496-502.
180. Freedman, M.H., et al., *Myelodysplasia syndrome and acute myeloid leukemia in patients with congenital neutropenia receiving G-CSF therapy.* Blood, 2000. **96**(2): p. 429-36.
181. Shiraishi, H., et al., *Efficacy of bezafibrate for preventing myopathic attacks in patients with very long-chain acyl-CoA dehydrogenase deficiency.* Brain Dev, 2021. **43**(2): p. 214-219.
182. Steele, H., et al., *Metabolic effects of bezafibrate in mitochondrial disease.* EMBO Mol Med, 2020. **12**(3): p. e11589.
183. Ørngreen, M.C., et al., *Bezafibrate in skeletal muscle fatty acid oxidation disorders: a randomized clinical trial.* Neurology, 2014. **82**(7): p. 607-13.
184. Bonnefont, J.P., et al., *Long-term follow-up of bezafibrate treatment in patients with the myopathic form of carnitine palmitoyltransferase 2 deficiency.* Clin Pharmacol Ther, 2010. **88**(1): p. 101-8.
185. Huang, Y., et al., *The PPAR pan-agonist bezafibrate ameliorates cardiomyopathy in a mouse model of Barth syndrome.* Orphanet J Rare Dis, 2017. **12**(1): p. 49.
186. Dabner, L., et al., *Treatment of Barth Syndrome by Cardiolipin Manipulation (CARDIOMAN) With Bezafibrate: Protocol for a Randomized Placebo-Controlled Pilot Trial Conducted in the Nationally Commissioned Barth Syndrome Service.* JMIR Res Protoc, 2021. **10**(5): p. e22533.
187. Allen, M.E., et al., *The cardiolipin-binding peptide elamipretide mitigates fragmentation of cristae networks following cardiac ischemia reperfusion in rats.* Commun Biol, 2020. **3**(1): p. 389.
188. Birk, A.V., et al., *The mitochondrial-targeted compound SS-31 re-energizes ischemic mitochondria by interacting with cardiolipin.* J Am Soc Nephrol, 2013. **24**(8): p. 1250-61.
189. Birk, A.V., et al., *Targeting mitochondrial cardiolipin and the cytochrome c/cardiolipin complex to promote electron transport and optimize mitochondrial ATP synthesis.* Br J Pharmacol, 2014. **171**(8): p. 2017-28.
190. Karaa, A., et al., *A randomized crossover trial of elamipretide in adults with primary mitochondrial myopathy.* J Cachexia Sarcopenia Muscle, 2020. **11**(4): p. 909-918.
191. Reid Thompson, W., et al., *A phase 2/3 randomized clinical trial followed by an open-label extension to evaluate the effectiveness of elamipretide in Barth syndrome, a genetic disorder of mitochondrial cardiolipin metabolism.* Genet Med, 2021. **23**(3): p. 471-478.
192. Suzuki-Hatano, S., et al., *AAV-Mediated TAZ Gene Replacement Restores Mitochondrial and Cardioskeletal Function in Barth Syndrome.* Hum Gene Ther, 2019. **30**(2): p. 139-154.
193. Rzymski, T., et al., *Regulation of autophagy by ATF4 in response to severe hypoxia.* Oncogene, 2010. **29**(31): p. 4424-35.
194. Harding, H.P., et al., *An integrated stress response regulates amino acid metabolism and resistance to oxidative stress.* Mol Cell, 2003. **11**(3): p. 619-33.

195. Dever, T.E., et al., *Phosphorylation of initiation factor 2 alpha by protein kinase GCN2 mediates gene-specific translational control of GCN4 in yeast.* Cell, 1992. **68**(3): p. 585-96.
196. Harding, H.P., Y. Zhang, and D. Ron, *Protein translation and folding are coupled by an endoplasmic-reticulum-resident kinase.* Nature, 1999. **397**(6716): p. 271-4.
197. Neerukonda, S.N., et al., *Induction of the unfolded protein response (UPR) during Marek's disease virus (MDV) infection.* Virology, 2018. **522**: p. 1-12.
198. Harding, H.P., et al., *Perk Is Essential for Translational Regulation and Cell Survival during the Unfolded Protein Response.* Molecular Cell, 2000. **5**(5): p. 897-904.
199. Katze, M.G., *Regulation of the interferon-induced PKR: can viruses cope?* Trends Microbiol, 1995. **3**(2): p. 75-8.
200. Cheshire, J.L., B.R. Williams, and A.S. Baldwin, Jr., *Involvement of double-stranded RNA-activated protein kinase in the synergistic activation of nuclear factor-kappaB by tumor necrosis factor-alpha and gamma-interferon in preneuronal cells.* J Biol Chem, 1999. **274**(8): p. 4801-6.
201. Abraham, N., et al., *Characterization of transgenic mice with targeted disruption of the catalytic domain of the double-stranded RNA-dependent protein kinase, PKR.* J Biol Chem, 1999. **274**(9): p. 5953-62.
202. Han, A.P., et al., *Heme-regulated eIF2alpha kinase (HRI) is required for translational regulation and survival of erythroid precursors in iron deficiency.* Embo j, 2001. **20**(23): p. 6909-18.
203. Chefalo, P.J., et al., *Heme-regulated eIF-2alpha kinase purifies as a hemoprotein.* Eur J Biochem, 1998. **258**(2): p. 820-30.
204. McEwen, E., et al., *Heme-regulated inhibitor kinase-mediated phosphorylation of eukaryotic translation initiation factor 2 inhibits translation, induces stress granule formation, and mediates survival upon arsenite exposure.* J Biol Chem, 2005. **280**(17): p. 16925-33.
205. Lu, L., A.P. Han, and J.J. Chen, *Translation initiation control by heme-regulated eukaryotic initiation factor 2alpha kinase in erythroid cells under cytoplasmic stresses.* Mol Cell Biol, 2001. **21**(23): p. 7971-80.
206. Deval, C., et al., *Amino acid limitation regulates the expression of genes involved in several specific biological processes through GCN2-dependent and GCN2-independent pathways.* Febs j, 2009. **276**(3): p. 707-18.
207. Ye, J., et al., *The GCN2-ATF4 pathway is critical for tumour cell survival and proliferation in response to nutrient deprivation.* Embo j, 2010. **29**(12): p. 2082-96.
208. Young, S.K. and R.C. Wek, *Upstream Open Reading Frames Differentially Regulate Gene-specific Translation in the Integrated Stress Response.* J Biol Chem, 2016. **291**(33): p. 16927-35.
209. Harding, H.P., et al., *Regulated translation initiation controls stress-induced gene expression in mammalian cells.* Mol Cell, 2000. **6**(5): p. 1099-108.
210. Vallejo, M., et al., *C/ATF, a member of the activating transcription factor family of DNA-binding proteins, dimerizes with CAAT/enhancer-binding proteins and directs their binding to cAMP response elements.* Proc Natl Acad Sci U S A, 1993. **90**(10): p. 4679-83.
211. Wang, C., et al., *ATF4 regulates lipid metabolism and thermogenesis.* Cell Res, 2010. **20**(2): p. 174-84.
212. Wang, C., et al., *Effects of ATF4 on PGC1α expression in brown adipose tissue and metabolic responses to cold stress.* Metabolism, 2013. **62**(2): p. 282-9.

213. Ebert, S.M., et al., *Identification and Small Molecule Inhibition of an Activating Transcription Factor 4 (ATF4)-dependent Pathway to Age-related Skeletal Muscle Weakness and Atrophy.* J Biol Chem, 2015. **290**(42): p. 25497-511.
214. Fawcett, T.W., et al., *Complexes containing activating transcription factor (ATF)/cAMP-responsive-element-binding protein (CREB) interact with the CCAAT/enhancer-binding protein (C/EBP)-ATF composite site to regulate Gadd153 expression during the stress response.* Biochem J, 1999. **339 ( Pt 1)**(Pt 1): p. 135-41.
215. B'Chir, W., et al., *The eIF2α/ATF4 pathway is essential for stress-induced autophagy gene expression.* Nucleic Acids Res, 2013. **41**(16): p. 7683-99.
216. Averous, J., et al., *Induction of CHOP expression by amino acid limitation requires both ATF4 expression and ATF2 phosphorylation.* J Biol Chem, 2004. **279**(7): p. 5288-97.
217. Siu, F., et al., *ATF4 is a mediator of the nutrient-sensing response pathway that activates the human asparagine synthetase gene.* J Biol Chem, 2002. **277**(27): p. 24120-7.
218. Su, N. and M.S. Kilberg, *C/EBP homology protein (CHOP) interacts with activating transcription factor 4 (ATF4) and negatively regulates the stress-dependent induction of the asparagine synthetase gene.* J Biol Chem, 2008. **283**(50): p. 35106-17.
219. Quirós, P.M., et al., *Multi-omics analysis identifies ATF4 as a key regulator of the mitochondrial stress response in mammals.* J Cell Biol, 2017. **216**(7): p. 2027-2045.
220. Harding, H.P., et al., *Diabetes mellitus and exocrine pancreatic dysfunction in perk-/- mice reveals a role for translational control in secretory cell survival.* Mol Cell, 2001. **7**(6): p. 1153-63.
221. Iida, K., et al., *PERK eIF2 alpha kinase is required to regulate the viability of the exocrine pancreas in mice.* BMC Cell Biol, 2007. **8**: p. 38.
222. Back, S.H., et al., *Translation attenuation through eIF2alpha phosphorylation prevents oxidative stress and maintains the differentiated state in beta cells.* Cell Metab, 2009. **10**(1): p. 13-26.
223. Ma, L., et al., *The human TAZ gene complements mitochondrial dysfunction in the yeast taz1Delta mutant. Implications for Barth syndrome.* J Biol Chem, 2004. **279**(43): p. 44394-9.
224. Yuan, S.H., et al., *Tauopathy-associated PERK alleles are functional hypomorphs that increase neuronal vulnerability to ER stress.* Hum Mol Genet, 2018. **27**(22): p. 3951-3963.
225. Liu, C.L., et al., *Inhibition of serine/threonine protein phosphatase PP1 protects cardiomyocytes from tunicamycin-induced apoptosis and I/R through the upregulation of p-eIF2α.* Int J Mol Med, 2014. **33**(3): p. 499-506.
226. Burda, J., et al., *Phosphorylation of the alpha subunit of initiation factor 2 correlates with the inhibition of translation following transient cerebral ischaemia in the rat.* Biochem J, 1994. **302 ( Pt 2)**(Pt 2): p. 335-8.
227. Vilatoba, M., et al., *Sodium 4-phenylbutyrate protects against liver ischemia reperfusion injury by inhibition of endoplasmic reticulum-stress mediated apoptosis.* Surgery, 2005. **138**(2): p. 342-51.
228. Ahola, S., et al., *OMA1-mediated integrated stress response protects against ferroptosis in mitochondrial cardiomyopathy.* Cell Metab, 2022. **34**(11): p. 1875-1891.e7.
229. Tyynismaa, H., et al., *Mitochondrial myopathy induces a starvation-like response.* Hum Mol Genet, 2010. **19**(20): p. 3948-58.

230. Tyynismaa, H., et al., *Mutant mitochondrial helicase Twinkle causes multiple mtDNA deletions and a late-onset mitochondrial disease in mice.* Proc Natl Acad Sci U S A, 2005. **102**(49): p. 17687-92.
231. Liu, Y., et al., *Reduced endoplasmic reticulum stress might alter the course of heart failure via caspase-12 and JNK pathways.* Can J Cardiol, 2014. **30**(3): p. 368-75.
232. Li, R.J., et al., *Salubrinal protects cardiomyocytes against apoptosis in a rat myocardial infarction model via suppressing the dephosphorylation of eukaryotic translation initiation factor 2α.* Mol Med Rep, 2015. **12**(1): p. 1043-9.
233. Wang, H., et al., *Double-stranded RNA-dependent protein kinase deficiency protects the heart from systolic overload-induced congestive heart failure.* Circulation, 2014. **129**(13): p. 1397-406.
234. Lu, Z., et al., *Loss of the eukaryotic initiation factor 2α kinase general control nonderepressible 2 protects mice from pressure overload-induced congestive heart failure without affecting ventricular hypertrophy.* Hypertension, 2014. **63**(1): p. 128-35.
235. Feng, W., et al., *GCN2 deficiency ameliorates cardiac dysfunction in diabetic mice by reducing lipotoxicity and oxidative stress.* Free Radic Biol Med, 2019. **130**: p. 128-139.
236. Tameire, F., et al., *ATF4 couples MYC-dependent translational activity to bioenergetic demands during tumour progression.* Nat Cell Biol, 2019. **21**(7): p. 889-899.
237. Feng, Y.X., et al., *Cancer-specific PERK signaling drives invasion and metastasis through CREB3L1.* Nat Commun, 2017. **8**(1): p. 1079.
238. Albert, A.E., et al., *Adaptive Protein Translation by the Integrated Stress Response Maintains the Proliferative and Migratory Capacity of Lung Adenocarcinoma Cells.* Mol Cancer Res, 2019. **17**(12): p. 2343-2355.
239. Darini, C., et al., *An integrated stress response via PKR suppresses HER2+ cancers and improves trastuzumab therapy.* Nat Commun, 2019. **10**(1): p. 2139.
240. Pizzolo, F., et al., *Folic acid effects on s-adenosylmethionine, s-adenosylhomocysteine, and DNA methylation in patients with intermediate hyperhomocysteinemia.* J Am Coll Nutr, 2011. **30**(1): p. 11-8.
241. Sae-Lee, C., et al., *Dietary Intervention Modifies DNA Methylation Age Assessed by the Epigenetic Clock.* Mol Nutr Food Res, 2018. **62**(23): p. e1800092.
242. Zheng, Y. and L.C. Cantley, *Toward a better understanding of folate metabolism in health and disease.* J Exp Med, 2019. **216**(2): p. 253-266.
243. Tibbetts, A.S. and D.R. Appling, *Compartmentalization of Mammalian folate-mediated one-carbon metabolism.* Annu Rev Nutr, 2010. **30**: p. 57-81.
244. Garratt, L.C., et al., *Comprehensive metabolic profiling of mono- and polyglutamated folates and their precursors in plant and animal tissue using liquid chromatography/negative ion electrospray ionisation tandem mass spectrometry.* Rapid Commun Mass Spectrom, 2005. **19**(17): p. 2390-8.
245. Fowler, B., *The folate cycle and disease in humans.* Kidney Int Suppl, 2001. **78**: p. S221-9.
246. Ducker, G.S. and J.D. Rabinowitz, *One-Carbon Metabolism in Health and Disease.* Cell Metab, 2017. **25**(1): p. 27-42.
247. Ducker, G.S., et al., *Reversal of Cytosolic One-Carbon Flux Compensates for Loss of the Mitochondrial Folate Pathway.* Cell Metab, 2016. **24**(4): p. 640-641.

248. Shuvalov, O., et al., *One-carbon metabolism and nucleotide biosynthesis as attractive targets for anticancer therapy.* Oncotarget, 2017. **8**(14): p. 23955-23977.
249. Kurniawan, H., T. Kobayashi, and D. Brenner, *The emerging role of one-carbon metabolism in T cells.* Curr Opin Biotechnol, 2021. **68**: p. 193-201.
250. Mentch, S.J., et al., *Histone Methylation Dynamics and Gene Regulation Occur through the Sensing of One-Carbon Metabolism.* Cell Metab, 2015. **22**(5): p. 861-73.
251. Belalcázar, A.D., et al., *Transsulfuration Is a Significant Source of Sulfur for Glutathione Production in Human Mammary Epithelial Cells.* ISRN Biochemistry, 2013. **2013**: p. 637897.
252. Fan, J., et al., *Quantitative flux analysis reveals folate-dependent NADPH production.* Nature, 2014. **510**(7504): p. 298-302.
253. Bashir, A., et al., *Impaired cardiac and skeletal muscle bioenergetics in children, adolescents, and young adults with Barth syndrome.* Physiol Rep, 2017. **5**(3).
254. Cade, W.T., et al., *Blunted fat oxidation upon submaximal exercise is partially compensated by enhanced glucose metabolism in children, adolescents, and young adults with Barth syndrome.* J Inherit Metab Dis, 2019. **42**(3): p. 480-493.
255. Cade, W.T., et al., *Myocardial glucose and fatty acid metabolism is altered and associated with lower cardiac function in young adults with Barth syndrome.* J Nucl Cardiol, 2021. **28**(4): p. 1649-1659.
256. Saric, A., et al., *Barth Syndrome: From Mitochondrial Dysfunctions Associated with Aberrant Production of Reactive Oxygen Species to Pluripotent Stem Cell Studies.* Front Genet, 2015. **6**: p. 359.
257. Vernon, H.J., et al., *Clinical laboratory studies in Barth Syndrome.* Mol Genet Metab, 2014. **112**(2): p. 143-7.
258. Maack, C., et al., *Endogenous activation of mitochondrial KATP channels protects human failing myocardium from hydroxyl radical-induced stunning.* Circ Res, 2009. **105**(8): p. 811-7.
259. Hohl, M., et al., *HDAC4 controls histone methylation in response to elevated cardiac load.* J Clin Invest, 2013. **123**(3): p. 1359-70.
260. Fatica, E.M., et al., *Barth Syndrome: Exploring Cardiac Metabolism with Induced Pluripotent Stem Cell-Derived Cardiomyocytes.* Metabolites, 2019. **9**(12).
261. Knapp, F.F., Jr., et al., *Radioiodinated 15-(p-iodophenyl)-3,3-dimethylpentadecanoic acid: a useful new agent to evaluate myocardial fatty acid uptake.* J Nucl Med, 1986. **27**(4): p. 521-31.
262. van de Weijer, T., E.H.M. Paiman, and H.J. Lamb, *Cardiac metabolic imaging: current imaging modalities and future perspectives.* J Appl Physiol (1985), 2018. **124**(1): p. 168-181.
263. DeGrado, T.R., et al., *Synthesis and preliminary evaluation of 18-(18)F-fluoro-4-thia-oleate as a PET probe of fatty acid oxidation.* J Nucl Med, 2010. **51**(8): p. 1310-7.
264. Chance, B. and G.R. Williams, *Respiratory enzymes in oxidative phosphorylation. III. The steady state.* J Biol Chem, 1955. **217**(1): p. 409-27.
265. Steinlechner-Maran, R., et al., *Oxygen dependence of respiration in coupled and uncoupled endothelial cells.* Am J Physiol, 1996. **271**(6 Pt 1): p. C2053-61.
266. Fujita, Y., et al., *CHOP (C/EBP homologous protein) and ASNS (asparagine synthetase) induction in cybrid cells harboring MELAS and NARP mitochondrial DNA mutations.* Mitochondrion, 2007. **7**(1-2): p. 80-8.

267. Bao, X.R., et al., *Mitochondrial dysfunction remodels one-carbon metabolism in human cells.* Elife, 2016. **5**.
268. Celardo, I., et al., *dATF4 regulation of mitochondrial folate-mediated one-carbon metabolism is neuroprotective.* Cell Death Differ, 2017. **24**(4): p. 638-648.
269. Sidrauski, C., et al., *Pharmacological brake-release of mRNA translation enhances cognitive memory.* Elife, 2013. **2**: p. e00498.
270. Cho, H., et al., *Signaling dynamics of palmitate-induced ER stress responses mediated by ATF4 in HepG2 cells.* BMC Syst Biol, 2013. **7**: p. 9.
271. DeBerardinis, R.J. and T. Cheng, *Q's next: the diverse functions of glutamine in metabolism, cell biology and cancer.* Oncogene, 2010. **29**(3): p. 313-24.
272. Yoo, H.C., et al., *Glutamine reliance in cell metabolism.* Exp Mol Med, 2020. **52**(9): p. 1496-1516.
273. Cha, Y.J., E.S. Kim, and J.S. Koo, *Amino Acid Transporters and Glutamine Metabolism in Breast Cancer.* Int J Mol Sci, 2018. **19**(3).
274. Chung, C.Y., et al., *Rewiring cell signalling pathways in pathogenic mtDNA mutations.* Trends Cell Biol, 2022. **32**(5): p. 391-405.
275. Van Heeke, G. and S.M. Schuster, *The N-terminal cysteine of human asparagine synthetase is essential for glutamine-dependent activity.* J Biol Chem, 1989. **264**(33): p. 19475-7.
276. Adams, E. and L. Frank, *Metabolism of proline and the hydroxyprolines.* Annu Rev Biochem, 1980. **49**: p. 1005-61.
277. Pérez-Arellano, I., et al., *Pyrroline-5-carboxylate synthase and proline biosynthesis: from osmotolerance to rare metabolic disease.* Protein Sci, 2010. **19**(3): p. 372-82.
278. Lu, S.C., *Regulation of glutathione synthesis.* Mol Aspects Med, 2009. **30**(1-2): p. 42-59.
279. Wu, G., et al., *Glutathione metabolism and its implications for health.* J Nutr, 2004. **134**(3): p. 489-92.
280. Sato, H., et al., *Cloning and expression of a plasma membrane cystine/glutamate exchange transporter composed of two distinct proteins.* J Biol Chem, 1999. **274**(17): p. 11455-8.
281. Yang, H., et al., *(18)F-5-Fluoroaminosuberic Acid as a Potential Tracer to Gauge Oxidative Stress in Breast Cancer Models.* J Nucl Med, 2017. **58**(3): p. 367-373.
282. Longo, N., C. Amat di San Filippo, and M. Pasquali, *Disorders of carnitine transport and the carnitine cycle.* Am J Med Genet C Semin Med Genet, 2006. **142c**(2): p. 77-85.
283. Bertrand, C., et al., *Very long chain acyl-CoA dehydrogenase deficiency: identification of a new inborn error of mitochondrial fatty acid oxidation in fibroblasts.* Biochim Biophys Acta, 1993. **1180**(3): p. 327-9.
284. Spiekerkoetter, U., et al., *Cardiomyopathy and pericardial effusion in infancy point to a fatty acid b-oxidation defect after exclusion of an underlying infection.* Pediatr Cardiol, 2003. **24**(3): p. 295-7.
285. Chatfield, K.C., et al., *Long-chain fatty acid oxidation and respiratory complex I deficiencies distinguish Barth Syndrome from idiopathic pediatric cardiomyopathy.* J Inherit Metab Dis, 2022. **45**(1): p. 111-124.
286. Magoulas, P.L. and A.W. El-Hattab, *Systemic primary carnitine deficiency: an overview of clinical manifestations, diagnosis, and management.* Orphanet J Rare Dis, 2012. **7**: p. 68.
287. Shibbani, K., et al., *Primary carnitine deficiency: novel mutations and insights into the cardiac phenotype.* Clin Genet, 2014. **85**(2): p. 127-37.

288. Patel, M.S., et al., *The pyruvate dehydrogenase complexes: structure-based function and regulation.* J Biol Chem, 2014. **289**(24): p. 16615-23.
289. Greenwell, A.A., et al., *Barth syndrome-related cardiomyopathy is associated with a reduction in myocardial glucose oxidation.* Am J Physiol Heart Circ Physiol, 2021. **320**(6): p. H2255-h2269.
290. Huang, B., et al., *Isoenzymes of pyruvate dehydrogenase phosphatase. DNA-derived amino acid sequences, expression, and regulation.* J Biol Chem, 1998. **273**(28): p. 17680-8.
291. Diakos, N.A., et al., *Evidence of Glycolysis Up-Regulation and Pyruvate Mitochondrial Oxidation Mismatch During Mechanical Unloading of the Failing Human Heart: Implications for Cardiac Reloading and Conditioning.* JACC Basic Transl Sci, 2016. **1**(6): p. 432-444.
292. Leadsham, J.E., et al., *Loss of cytochrome c oxidase promotes RAS-dependent ROS production from the ER resident NADPH oxidase, Yno1p, in yeast.* Cell Metab, 2013. **18**(2): p. 279-86.
293. Yi, D.G., S. Hong, and W.K. Huh, *Mitochondrial dysfunction reduces yeast replicative lifespan by elevating RAS-dependent ROS production by the ER-localized NADPH oxidase Yno1.* PLoS One, 2018. **13**(6): p. e0198619.
294. Badolia, R., et al., *The Role of Nonglycolytic Glucose Metabolism in Myocardial Recovery Upon Mechanical Unloading and Circulatory Support in Chronic Heart Failure.* Circulation, 2020. **142**(3): p. 259-274.
295. Casas, J.P., et al., *Homocysteine and stroke: evidence on a causal link from mendelian randomisation.* Lancet, 2005. **365**(9455): p. 224-32.
296. Zhu, S., et al., *Mitochondrial Stress Induces an HRI-eIF2α Pathway Protective for Cardiomyopathy.* Circulation, 2022. **146**(13): p. 1028-1031.
297. García-Martínez, L.F. and D.R. Appling, *Characterization of the folate-dependent mitochondrial oxidation of carbon 3 of serine.* Biochemistry, 1993. **32**(17): p. 4671-6.
298. Ye, J., et al., *Serine catabolism regulates mitochondrial redox control during hypoxia.* Cancer Discov, 2014. **4**(12): p. 1406-17.
299. Huang, M.L., et al., *Molecular and functional alterations in a mouse cardiac model of Friedreich ataxia: activation of the integrated stress response, eIF2α phosphorylation, and the induction of downstream targets.* Am J Pathol, 2013. **183**(3): p. 745-57.
300. Castillero, E., et al., *Activin type II receptor ligand signaling inhibition after experimental ischemic heart failure attenuates cardiac remodeling and prevents fibrosis.* Am J Physiol Heart Circ Physiol, 2020. **318**(2): p. H378-h390.
301. Yao, Y., et al., *A non-canonical pathway regulates ER stress signaling and blocks ER stress-induced apoptosis and heart failure.* Nat Commun, 2017. **8**(1): p. 133.
302. Nikkanen, J., et al., *Mitochondrial DNA Replication Defects Disturb Cellular dNTP Pools and Remodel One-Carbon Metabolism.* Cell Metab, 2016. **23**(4): p. 635-48.
303. Khan, N.A., et al., *mTORC1 Regulates Mitochondrial Integrated Stress Response and Mitochondrial Myopathy Progression.* Cell Metab, 2017. **26**(2): p. 419-428.e5.
304. Volmer, R., K. van der Ploeg, and D. Ron, *Membrane lipid saturation activates endoplasmic reticulum unfolded protein response transducers through their transmembrane domains.* Proc Natl Acad Sci U S A, 2013. **110**(12): p. 4628-33.

305. Sohn, J., et al., *A new murine model of Barth syndrome neutropenia links TAFAZZIN deficiency to increased ER stress-induced apoptosis.* Blood Adv, 2022. **6**(8): p. 2557-2577.
306. Liu, X., et al., *Endoplasmic reticulum stress sensor protein kinase R-like endoplasmic reticulum kinase (PERK) protects against pressure overload-induced heart failure and lung remodeling.* Hypertension, 2014. **64**(4): p. 738-44.
307. Yu, L., et al., *Melatonin reduces PERK-eIF2α-ATF4-mediated endoplasmic reticulum stress during myocardial ischemia-reperfusion injury: role of RISK and SAFE pathways interaction.* Apoptosis, 2016. **21**(7): p. 809-24.
308. Yu, L., et al., *Reduced silent information regulator 1 signaling exacerbates myocardial ischemia-reperfusion injury in type 2 diabetic rats and the protective effect of melatonin.* J Pineal Res, 2015. **59**(3): p. 376-90.
309. Guo, X., et al., *Mitochondrial stress is relayed to the cytosol by an OMA1-DELE1-HRI pathway.* Nature, 2020. **579**(7799): p. 427-432.
310. Fessler, E., et al., *A pathway coordinated by DELE1 relays mitochondrial stress to the cytosol.* Nature, 2020. **579**(7799): p. 433-437.
311. Ranea-Robles, P., et al., *A mitochondrial long-chain fatty acid oxidation defect leads to transfer RNA uncharging and activation of the integrated stress response in the mouse heart.* Cardiovasc Res, 2022. **118**(16): p. 3198-3210.
312. Zhang, G., et al., *Integrated Stress Response Couples Mitochondrial Protein Translation With Oxidative Stress Control.* Circulation, 2021. **144**(18): p. 1500-1515.
313. Sandlers, Y., et al., *Metabolomics Reveals New Mechanisms for Pathogenesis in Barth Syndrome and Introduces Novel Roles for Cardiolipin in Cellular Function.* PLoS One, 2016. **11**(3): p. e0151802.
314. Stipanuk, M.H., *Sulfur amino acid metabolism: pathways for production and removal of homocysteine and cysteine.* Annu Rev Nutr, 2004. **24**: p. 539-77.
315. Fang, X., et al., *Loss of Cardiac Ferritin H Facilitates Cardiomyopathy via Slc7a11-Mediated Ferroptosis.* Circ Res, 2020. **127**(4): p. 486-501.
316. Zhang, X., et al., *SLC7A11/xCT Prevents Cardiac Hypertrophy by Inhibiting Ferroptosis.* Cardiovasc Drugs Ther, 2022. **36**(3): p. 437-447.
317. Belch, J.J., et al., *Oxygen free radicals and congestive heart failure.* Br Heart J, 1991. **65**(5): p. 245-8.
318. Mollnau, H., et al., *Mechanisms of increased vascular superoxide production in an experimental model of idiopathic dilated cardiomyopathy.* Arterioscler Thromb Vasc Biol, 2005. **25**(12): p. 2554-9.
319. Tsutsui, H., S. Kinugawa, and S. Matsushima, *Oxidative stress and heart failure.* Am J Physiol Heart Circ Physiol, 2011. **301**(6): p. H2181-90.
320. Shah, A.K., et al., *Oxidative Stress as A Mechanism for Functional Alterations in Cardiac Hypertrophy and Heart Failure.* Antioxidants (Basel), 2021. **10**(6).
321. Dhalla, A.K., M.F. Hill, and P.K. Singal, *Role of oxidative stress in transition of hypertrophy to heart failure.* J Am Coll Cardiol, 1996. **28**(2): p. 506-14.
322. Damy, T., et al., *Glutathione deficiency in cardiac patients is related to the functional status and structural cardiac abnormalities.* PLoS One, 2009. **4**(3): p. e4871.
323. Ardanaz, N., et al., *Lack of glutathione peroxidase 1 accelerates cardiac-specific hypertrophy and dysfunction in angiotensin II hypertension.* Hypertension, 2010. **55**(1): p. 116-23.

324. Watanabe, Y., et al., *Chronic depletion of glutathione exacerbates ventricular remodelling and dysfunction in the pressure-overloaded heart.* Cardiovasc Res, 2013. **97**(2): p. 282-92.
325. Hill, M.F. and P.K. Singal, *Antioxidant and oxidative stress changes during heart failure subsequent to myocardial infarction in rats.* Am J Pathol, 1996. **148**(1): p. 291-300.
326. Yoshida, T., et al., *Transgenic mice overexpressing glutathione peroxidase are resistant to myocardial ischemia reperfusion injury.* J Mol Cell Cardiol, 1996. **28**(8): p. 1759-67.
327. Shiomi, T., et al., *Overexpression of glutathione peroxidase prevents left ventricular remodeling and failure after myocardial infarction in mice.* Circulation, 2004. **109**(4): p. 544-9.
328. van Deel, E.D., et al., *Extracellular superoxide dismutase protects the heart against oxidative stress and hypertrophy after myocardial infarction.* Free Radic Biol Med, 2008. **44**(7): p. 1305-13.
329. Cohen, D.M., et al., *Glutamine cycling in isolated working rat heart.* Am J Physiol Endocrinol Metab, 2003. **285**(6): p. E1312-6.
330. Drake, K.J., et al., *Amino acids as metabolic substrates during cardiac ischemia.* Exp Biol Med (Maywood), 2012. **237**(12): p. 1369-78.
331. Boelens, P.G., et al., *Intestinal renal metabolism of L-citrulline and L-arginine following enteral or parenteral infusion of L-alanyl-L-[2,15N]glutamine or L-[2,15N]glutamine in mice.* Am J Physiol Gastrointest Liver Physiol, 2005. **289**(4): p. G679-85.
332. Taegtmeyer, H., *Metabolic responses to cardiac hypoxia. Increased production of succinate by rabbit papillary muscles.* Circ Res, 1978. **43**(5): p. 808-15.
333. Wischmeyer, P.E., et al., *Glutamine preserves cardiomyocyte viability and enhances recovery of contractile function after ischemia-reperfusion injury.* JPEN J Parenter Enteral Nutr, 2003. **27**(2): p. 116-22.
334. Reynolds, S., C.M. Kreider, and R. Bendixen, *A mixed-methods investigation of sensory response patterns in Barth syndrome: a clinical phenotype?* Am J Med Genet A, 2012. **158a**(7): p. 1647-53.
335. Chung, Y., et al., *Effect of Monosodium Glutamate on Salt and Sugar Content Reduction in Cooked Foods for the Sensory Characteristics and Consumer Acceptability.* Foods, 2022. **11**(16).
336. Bohnert, K.L., et al., *Resistance exercise training with protein supplementation improves skeletal muscle strength and improves quality of life in late adolescents and young adults with Barth syndrome: A pilot study.* JIMD Rep, 2021. **62**(1): p. 74-84.
337. Masuoka, H.C. and T.M. Townes, *Targeted disruption of the activating transcription factor 4 gene results in severe fetal anemia in mice.* Blood, 2002. **99**(3): p. 736-45.
338. Yoshizawa, T., et al., *The transcription factor ATF4 regulates glucose metabolism in mice through its expression in osteoblasts.* J Clin Invest, 2009. **119**(9): p. 2807-17.
339. Dixon, S.J., et al., *Ferroptosis: an iron-dependent form of nonapoptotic cell death.* Cell, 2012. **149**(5): p. 1060-72.
340. Drummen, G.P., et al., *C11-BODIPY(581/591), an oxidation-sensitive fluorescent lipid peroxidation probe: (micro)spectroscopic characterization and validation of methodology.* Free Radic Biol Med, 2002. **33**(4): p. 473-90.
341. Zhao, B., et al., *Mitochondrial dysfunction activates the AMPK signaling and autophagy to promote cell survival.* Genes Dis, 2016. **3**(1): p. 82-87.

342. Kudo, N., et al., *High rates of fatty acid oxidation during reperfusion of ischemic hearts are associated with a decrease in malonyl-CoA levels due to an increase in 5'-AMP-activated protein kinase inhibition of acetyl-CoA carboxylase.* J Biol Chem, 1995. **270**(29): p. 17513-20.
343. Kudo, N., et al., *Characterization of 5'AMP-activated protein kinase activity in the heart and its role in inhibiting acetyl-CoA carboxylase during reperfusion following ischemia.* Biochim Biophys Acta, 1996. **1301**(1-2): p. 67-75.
344. Baron, S.J., et al., *Dual mechanisms regulating AMPK kinase action in the ischemic heart.* Circ Res, 2005. **96**(3): p. 337-45.
345. Russell, R.R., 3rd, et al., *Translocation of myocardial GLUT-4 and increased glucose uptake through activation of AMPK by AICAR.* Am J Physiol, 1999. **277**(2): p. H643-9.
346. Russell, R.R., 3rd, et al., *AMP-activated protein kinase mediates ischemic glucose uptake and prevents postischemic cardiac dysfunction, apoptosis, and injury.* J Clin Invest, 2004. **114**(4): p. 495-503.
347. Shibata, R., et al., *Adiponectin protects against myocardial ischemia-reperfusion injury through AMPK- and COX-2-dependent mechanisms.* Nat Med, 2005. **11**(10): p. 1096-103.
348. Shibata, R., et al., *Adiponectin-mediated modulation of hypertrophic signals in the heart.* Nat Med, 2004. **10**(12): p. 1384-9.
349. Chan, A.Y., et al., *Activation of AMP-activated protein kinase inhibits protein synthesis associated with hypertrophy in the cardiac myocyte.* J Biol Chem, 2004. **279**(31): p. 32771-9.
350. Hurley, R.L., et al., *The Ca2+/calmodulin-dependent protein kinase kinases are AMP-activated protein kinase kinases.* J Biol Chem, 2005. **280**(32): p. 29060-6.
351. Hawley, S.A., et al., *Calmodulin-dependent protein kinase kinase-beta is an alternative upstream kinase for AMP-activated protein kinase.* Cell Metab, 2005. **2**(1): p. 9-19.
352. Zhang, D., et al., *MTORC1 regulates cardiac function and myocyte survival through 4E-BP1 inhibition in mice.* J Clin Invest, 2010. **120**(8): p. 2805-16.
353. Zhu, Y., et al., *Mechanistic target of rapamycin (Mtor) is essential for murine embryonic heart development and growth.* PLoS One, 2013. **8**(1): p. e54221.
354. Shende, P., et al., *Cardiac raptor ablation impairs adaptive hypertrophy, alters metabolic gene expression, and causes heart failure in mice.* Circulation, 2011. **123**(10): p. 1073-82.
355. Shioi, T., et al., *Rapamycin attenuates load-induced cardiac hypertrophy in mice.* Circulation, 2003. **107**(12): p. 1664-70.
356. McMullen, J.R., et al., *Inhibition of mTOR signaling with rapamycin regresses established cardiac hypertrophy induced by pressure overload.* Circulation, 2004. **109**(24): p. 3050-5.
357. Völkers, M., et al., *Pathological hypertrophy amelioration by PRAS40-mediated inhibition of mTORC1.* Proc Natl Acad Sci U S A, 2013. **110**(31): p. 12661-6.
358. Marin, T.M., et al., *Rapamycin reverses hypertrophic cardiomyopathy in a mouse model of LEOPARD syndrome-associated PTPN11 mutation.* J Clin Invest, 2011. **121**(3): p. 1026-43.
359. Ramos, F.J., et al., *Rapamycin reverses elevated mTORC1 signaling in lamin A/C-deficient mice, rescues cardiac and skeletal muscle function, and extends survival.* Sci Transl Med, 2012. **4**(144): p. 144ra103.
360. Zhang, J., et al., *Restoration of mitophagy ameliorates cardiomyopathy in Barth syndrome.* Autophagy, 2022. **18**(9): p. 2134-2149.

361. Sochman, J. and J.H. Peregrin, *Total recovery of left ventricular function after acute myocardial infarction: comprehensive therapy with streptokinase, N-acetylcysteine and percutaneous transluminal coronary angioplasty.* Int J Cardiol, 1992. **35**(1): p. 116-8.
362. Arstall, M.A., et al., *N-acetylcysteine in combination with nitroglycerin and streptokinase for the treatment of evolving acute myocardial infarction. Safety and biochemical effects.* Circulation, 1995. **92**(10): p. 2855-62.
363. Sochman, J., et al., *Infarct Size Limitation: acute N-acetylcysteine defense (ISLAND trial): preliminary analysis and report after the first 30 patients.* Clin Cardiol, 1996. **19**(2): p. 94-100.

# 7. Appendix

## 7.1 Abbreviations

| | |
|---|---|
| ADP | Adenosine diphosphate |
| ATP | Adenosine triphosphate |
| APS | Ammonium Persulfate |
| ATF-4 | Activating transcription factor-4 |
| BTHS | Barth Syndrome |
| BSA | Bovine serum albumin |
| $Ca^{2+}$ | Calcium |
| cDNA | Coding DNA |
| CL | Cardiolipin |
| CRISPR | Clustered regularly interspaced short palindromic repeats |
| Da | Dalton |
| DMEM | Dulbecco's Modified Eagle Medium |
| DMSO | Dimethylsulfoxide |
| DNA | Deoxyribonucleic acid |
| ECL | Enhanced chemiluminescence |
| EDTA | Ethylenediaminetetraacetic acid |
| e.g. | Exempli gratia |
| EGTA | Ethylene glycol tetraacetic acid |
| eIF2α | Eukaryotic translation initiation factor |
| ER | Endoplasmic reticulum |
| Et al. | Et alii |
| ETC | Electron transport chain |
| $FADH_2$ | Flavine adenine dinucleotide, reduced form |
| FCS | Fetal calve serum |
| h | Hours |
| HCl | Hydrogen chloride |
| HFpEF | Heart failure with preserved ejection fraction |
| HEPES | N-2-hydroxyethypiperazine-N'-2-ethanesulfonic acid |
| HRP | Horseradish peroxidase |
| IMM | Inner mitochondrial membrane |

| | |
|---|---|
| IMS | Intermembrane space |
| ISR | Integrated stress response |
| ISRIB | Integrated stress response inhibitor |
| KD | Knockdown |
| KO | Knockout |
| LVEF | Left ventricular ejection fraction |
| mM | Millimol |
| ml | Milliliter |
| M | Mol |
| Min | Minute |
| MLCL | Monolysocardiolipin |
| NADH | Nicotinamide adenine dinucleotide, reduced form |
| OMM | Outer mitochondrial membrane |
| OxPHOS | Oxidative phosphorylation |
| PAGE | Polyacrylamide gel electrophoresis |
| PBS | Phosphate buffered saline |
| PCR | Polymerase chain reaction |
| PMSF | Phenylmethylsulphonylfluorid |
| PSAT | Phosphoserine aminotransferase |
| PSPH | Phosphoserine phosphatase |
| PVDF | Polyvinylidene difluoride |
| RNA | Ribonucleic acid |
| ROS | Reactive oxygen species |
| RT | Room temperature |
| RT-qPCR | Reverse transcription quantitative polymerase chain reaction |
| s | seconds |
| SDS | Sodium dodecyl sulfate |
| siRNA | Small interfering RNA |
| TAC | Transverse aortic constriction |
| TAZ | Tafazzin |
| TBS | Tris buffered saline |
| TEMED | Tetramethylethylenediamine |
| TRIS | Tris(hydroxymethyl)aminomethane |
| WT | Wild-type |

| | |
|---|---|
| µl | Miroliter |
| µM | Micromol |

## 7.2 List of figures

Figure 1: Schematic overview of the electron transport chain at the inner mitochondrial membrane. ....4
Figure 2: Schematic representation of the carnitine shuttle system for fatty acid uptake into mitochondria. ....7
Figure 3: Overview of mitochondrial processes that require cardiolipin for correct function. ....9
Figure 4: Overview of the one-carbon metabolism. ....19
Figure 5: *In vivo* measurement of cardiac glucose and fatty acid uptake. ....48
Figure 6: Defective fatty acid supported respiration in cardiac *Taz*-KD mitochondria. ....50
Figure 7: Altered gene expression and protein levels of fatty acid metabolism enzymes in Barth Syndrome. ....52
Figure 8: Transcriptomal analysis of *Taz*-KD cardiac tissue. ....54
Figure 9: Regulation of enzymes involved in serine synthesis. ....56
Figure 10: Regulation of enzymes involved in the one-carbon metabolism. ....57
Figure 11: Regulation of enzymes involved in the one-carbon metabolism in human derived samples. ....58
Figure 12: Activation of the ISR in Barth Syndrome. ....60
Figure 13: Recapitulation of the metabolic alterations in TAZ deficient mouse embryonal fibroblasts. ....61
Figure 14: The integrated stress response regulates metabolic alterations in TAZ deficient mouse embryonal fibroblasts. ....62
Figure 15: ISR interference with the small molecule compound ISRIB. ....64
Figure 16: Glutamate metabolism is elevated in Barth Syndrome. ....66
Figure 17: Elevated activity of the xCT system in Barth Syndrome is dependent on the ISR. ....69
Figure 18: Metabolic rewiring supports glutathione synthesis in Barth Syndrome. ....71
Figure 19: Glutamate metabolism supports Krebs cycle and respiration in Barth Syndrome. ....73

Figure 20: Cardiac Krebs cycle metabolites labeling from [U-$^{13}$C, $^{15}$N] glutamine (Gln) infusion in 10 to 11 weeks old *Taz*-KD mice compared to WT. .....83

## 7.3 List of tables

Table 1: Chemicals and reagents. .....21
Table 2: Primary and secondary antibodies for Western Blot. .....26
Table 3: Primer sequences for qPCRs with samples from mice. .....27
Table 4: Primer sequences for qPCRs with human derived samples. .....29
Table 5: siRNA sequences for knockdown experiments. .....30
Table 6: Kits. .....30
Table 7: Composition of different buffers and solutions. .....31
Table 8: Composition of different media for MEF cell cultivation. .....33
Table 9: Composition of different media for cultivation of iPS cells and their differentiation into cardiac myocytes . .....33
Table 10: Consumables. .....34
Table 11: Equipment. .....35
Table 12: Softwares. .....36
Table 13: qPCR protocol settings. .....42
Table 14: Polyacrylamide gel recipe for two BioRad mini gels. .....44

## 7.4 Acknowledgement

At first I want to thank Dr. Jan Dudek for the opportunity to work on this project in his Juniorgroup, for all the scientific input, insightful discussions and helpful advice whenever it was needed.

I also want to thank Prof. Christoph Maack for the constructive discussions and the help to understand the medical aspects of the project.

To all my colleagues from the Juniorgroup and the Translational Science I want to say “thank you” for their advises and practical support, especially concerning the work with mice: Christina Wasmus, Manuela Erk, Mehrnoush Gabriel, Berkan Arslan, Edoardo Bertero, Vasco Sequeira, Anton Xu, Michael Kohlhaas, Alexander Nickel, Michelle Hofmann, Annette Berbner, Anja Sauer and Alice Schaaf.

A big thank you to Antonella Cellini and Anna Janz not only for their practical and scientific advises but especially for listening to any problems and their support during stressful phases.

Zum Schluss geht ein großes “Danke” an meine Familie und besonders an Markus für die Unterstützung in den letzten Jahren und die aufbauenden Worte, wenn die Motivation mal gefehlt hat.

## 7.5 Curriculum vitae

## 7.6 Publications in peer reviewed journals

Bertero E, Nickel A, Kohlhaas M, Hohl M, Sequeira V, Brune C, Schwemmlein J, Abeßer M, Schuh K, **Kutschka I**, Carlein C, Münker K, Atighetchi S, Müller A, Kazakov A, Kappl R, Von der Malsburg K, Van der Laan M, Schiuma A, Böhm M, Laufs U, Hoth M, Rehling P, Kuhn M, Dudek J, Von der Malsburg A, Prates Roma L, Maack C.
Loss of Mitochondrial $Ca^{2+}$ Uniporter Limits Inotropic Reserve and Provides Trigger and Substrate for Arrhythmias in Barth Syndrome Cardiomyopathy.
*Circulation*. 2021 Nov 23;144(21)

Dudek J, **Kutschka I**, Maack C.
Metabolic and Redox Regulation of Cardiovascular Stem Cell Biology and Pathology.
*Antioxidants & Redox Signaling*. 2021 Jul 20;35(3)
Review.

Bertero E, **Kutschka I**, Maack C, Dudek J.
Cardiolipin remodeling in Barth syndrome and other hereditary cardiomyopathies.
*Biochimica et Biophysica Acta - Molecular Basis of Disease*. 2020 Aug 1;1866(8).
Review.

Fischer FT, **Kutschka I**, Kunz SN, Grove C, Lochner SJ.
Todesfeststellung und Reanimationsabbruch im Notarztdienst.
*Rechtsmedizin.* 2016 Nov 2, Vol. 26.

## 7.7 Affidavit

I hereby confirm that my thesis entitled "*Activation of the integrated stress response induces remodeling of cardiac metabolism in Barth Syndrome*" is the result of my own work. I did not receive any help or support from commercial consultants. All sources and/or materials applied are listed and specified in the thesis.

Furthermore, I confirm that this thesis has not yet been submitted as part of another examination process neither in identical nor in similar form.

Place, date Signature

## 7.8 Eidesstattliche Erklärung

Hiermit erkläre ich an Eides statt, die Dissertation „*Aktivierung der "Integrated Stress Response" führt zur Umstellung des kardialen Metabolismus im Barth Syndrom*" eigenständig, d.h. insbesondere selbständig und ohne Hilfe eines kommerziellen Promotionsberaters, angefertigt und keine anderen als die von mir angegeben Quellen und Hilfsmittel verwendet zu haben.

Ich erkläre außerdem, dass die Dissertation weder in gleicher noch in ähnlicher Form bereits in einem anderen Prüfungsverfahren vorgelegen hat.

Ort, Datum Unterschrift